

Fundamentals of Radiation Dosimetry
and
Radiological Physics

Alex F Bielajew
The University of Michigan
Department of Nuclear Engineering and Radiological Sciences
2927 Cooley Building (North Campus)
2355 Bonisteel Boulevard
Ann Arbor, Michigan 48109-2104
U. S. A.
Tel: 734 764 6364
Fax: 734 763 4540
email: bielajew@umich.edu

© 2005 Alex F Bielajew

June 21, 2005

Preface

This book arises out of a course I am teaching for a three-credit (42 hour) graduate-level course *Dosimetry Fundamentals* being taught at the Department of Nuclear Engineering and Radiological Sciences at the University of Michigan. It is far from complete.

A formal course in dosimetry usually starts at Chapter 4, Macroscopic Radiation Physics, that describes macroscopic field quantities (primarily fluence). However, this is an approximation (a good one) for rudimentary dosimetry. Underpinning this, however, is the realization that these fields are made up of discrete particles. Therefore, a discussion of microscopic radiation physics should really be the starting point. This material is given in Chapters 1 and 2, couched in the language of Monte Carlo practitioner, who estimates macroscopic quantities, from microscopic calculation. Chapter 3 describes transport of particles through matter, again in a microscopic way.

These first three chapters should be considered pre-requisite material for the following chapters. Perhaps they should be combined into a single chapter with the title “Microscopic radiation physics”. Deep understanding is not required and much of the language is in a form more suitable for Monte Carlo practitioners. Nonetheless, knowledge of this material will aid in the assimilation of the material of the following chapters. The Monte Carlo-specific details should be glossed over if they are unfamiliar. However, the microscopic processes that govern interaction and transport must be understood, at least intuitively, before attempting the later chapters.

Finally, there are many missing figures. This book is far from completion. Anyone volunteering figures for this book will be gratefully acknowledged. Chapters 4–7 were all written up during a very hectic week, from a collection of hand-written notes. There will be spelling and grammatical errors, some mathematics errors, and perhaps a conceptual error or two. I would be grateful if these were pointed out to me.

AFB, June 21, 2005

Contents

1	Photon Monte Carlo Simulation	1
1.1	Basic photon interaction processes	1
1.1.1	Pair production in the nuclear field	2
1.1.2	The Compton interaction (incoherent scattering)	5
1.1.3	Photoelectric interaction	6
1.1.4	Rayleigh (coherent) interaction	9
1.1.5	Relative importance of various processes	10
1.2	Photon transport logic	10
2	Electron Monte Carlo Simulation	21
2.1	Catastrophic interactions	22
2.1.1	Hard bremsstrahlung production	22
2.1.2	Møller (Bhabha) scattering	22
2.1.3	Positron annihilation	23
2.2	Statistically grouped interactions	23
2.2.1	“Continuous” energy loss	23
2.2.2	Multiple scattering	24
2.3	Electron transport “mechanics”	25
2.3.1	Typical electron tracks	25
2.3.2	Typical multiple scattering substeps	25
2.4	Examples of electron transport	26
2.4.1	Effect of physical modeling on a 20 MeV e^- depth-dose curve	26

2.5	Electron transport logic	38
3	Transport in media, interaction models	45
3.1	Interaction probability in an infinite medium	45
3.1.1	Uniform, infinite, homogeneous media	46
3.2	Finite media	47
3.3	Regions of different scattering characteristics	47
3.4	Obtaining μ from microscopic cross sections	50
3.5	Compounds and mixtures	53
3.6	Branching ratios	54
3.7	Other pathlength schemes	54
3.8	Model interactions	55
3.8.1	Isotropic scattering	55
3.8.2	Semi-isotropic or P_1 scattering	55
3.8.3	Rutherfordian scattering	56
3.8.4	Rutherfordian scattering—small angle form	56
4	Macroscopic Radiation Physics	59
4.1	Fluence	59
4.2	Radiation equilibrium	62
4.2.1	Planar fluence	63
4.3	Fluence-related radiometric quantities	65
4.3.1	Energy fluence	65
4.4	Attenuation, radiological pathlength	66
4.4.1	Solid angle subtended by a surface	67
4.4.2	Primary fluence determinations	68
4.4.3	Volumetric symmetry	68
4.5	Fano's theorem	69
5	Photon dose calculation models	77

5.1	Kerma, collision kerma, and dose for photo irradiation	77
5.1.1	Kerma	77
5.1.2	Collision Kerma	80
5.1.3	Dose	83
5.1.4	Comparison of dose deposition models	85
5.1.5	Transient charged particle equilibrium	87
5.1.6	Dose due to scattered photons	89
6	Electron dose calculation models	93
6.1	The microscopic picture of dose deposition	93
6.2	Stopping power	94
6.2.1	Total mass stopping power	94
6.2.2	Restricted mass stopping power	98
6.3	Electron angular scattering	99
6.4	Dose due to electrons from primary photon interaction	100
6.4.1	A practical semi-analytic dose deposition model	101
6.5	The convolution method	105
6.6	Monte Carlo methods	105
7	Ionization chamber-based air kerma standards	111
7.1	Bragg-Gray cavity theory	111
7.1.1	Exposure measurements	112
7.2	Spencer-Attix cavity theory	114
7.3	Modern cavity theory	115
7.4	Interface effects	117
7.5	Saturation corrections	117
7.6	Burlin cavity theory	118
7.7	The dosimetry chain	118

Chapter 1

Photon Monte Carlo Simulation

*“I could have done it in a much more complicated way”
said the red Queen, immensely proud.*

Lewis Carroll

In this chapter we discuss the basic mechanism by which the simulation of photon interaction and transport is undertaken. We start with a review of the basic interaction processes that are involved, some common simplifications and the relative importance of the various processes. We discuss when and how one goes about choosing, by random selection, which process occurs. We discuss the rudimentary geometry involved in the transport and deflection of photons. We conclude with a schematic presentation of the logic flow executed by a typical photon Monte Carlo transport algorithm. This chapter will only sketch the bare minimum required to construct a photon Monte Carlo code. A particularly good reference for a description of basic interaction mechanisms is the excellent book [Eva55] by Robley Evans, *The Atomic Nucleus*. This book should be in the bookshelf of anyone undertaking a career in the radiation sciences. Simpler descriptions of photon interaction processes are useful as well and are included in many common textbooks [JC83, Att86, SF96].

1.1 Basic photon interaction processes

We now give a brief discussion of the photon interaction processes that should be modeled by a photon Monte Carlo code, namely:

- Pair production in the nuclear field
- The Compton interaction (incoherent scattering)

- The photoelectric interaction
- The Rayleigh interaction (coherent scattering)

1.1.1 Pair production in the nuclear field

As seen in Figure 1.1, a photon can interact in the field of a nucleus, annihilate and produce an electron-positron pair. A third body, usually a nucleus, is required to be present to conserve energy and momentum. This interaction scales as Z^2 for different nuclei. Thus, materials containing high atomic number materials more readily convert photons into charged particles than do low atomic number materials. This interaction is the quantum “analog” of the bremsstrahlung interaction, which we will encounter in the next Chapter, *Electron Monte Carlo simulation*. At high energies, greater than 50 MeV or so in all materials, the pair and bremsstrahlung interactions dominate. The pair interaction gives rise to charged particles in the form of electrons and positrons (muons at very high energy) and the bremsstrahlung interaction of the electrons and positrons leads to more photons. Thus there is a “cascade” process that quickly converts high energy electromagnetic particles into copious amounts of lower energy electromagnetic particles. Hence, a high-energy photon or electron beam not only has “high energy”, it is also able to deposit a lot of its energy near one place by virtue of this cascade phenomenon. A picture of this process is given in Figure 1.2.

The high-energy limit of the pair production cross section per nucleus takes the form:

$$\lim_{\alpha \rightarrow \infty} \sigma_{\text{pp}}(\alpha) = \sigma_0^{\text{pp}} Z^2 \left(\ln(2\alpha) - \frac{109}{42} \right), \quad (1.1)$$

where $\alpha = E_\gamma/m_e c^2$, that is, the energy of the photon divided by the rest mass energy¹ of the electron ($0.51099907 \pm 0.00000015$ MeV) and $\sigma_0^{\text{pp}} = 1.80 \times 10^{-27}$ cm²/nucleus. We note that the cross section grows logarithmically with incoming photon energy.

The kinetic energy distribution of the electrons and positrons is remarkably “flat” except near the kinematic extremes of $K_\pm = 0$ and $K_\pm = E_\gamma - 2m_e c^2$. Note as well that the rest-mass energy of the electron-positron pair must be created and so this interaction has a threshold at $E_\gamma = 2m_e c^2$. It is exactly zero below this energy.

Occasionally it is one of the *electrons* in the atomic cloud surrounding the nucleus that interacts with the incoming photon and provides the necessary third body for momentum and energy conservation. This interaction channel is suppressed by a factor of $1/Z$ relative to the nucleus-participating channel as well as additional phase-space and Pauli exclusion differences. In this case, the atomic electron is ejected with two electrons and one positron emitted. This is called “triplet” production. It is common to include the effects of triplet production by “scaling up” the two-body reaction channel and ignoring the 3-body kinematics. This is a good approximation for all but the low- Z atoms.

¹The latest information on particle data is available on the web at: <http://pdg.lbl.gov/pdg.html> This web page is maintained by the Particle Data Group at the Lawrence Berkeley laboratory.

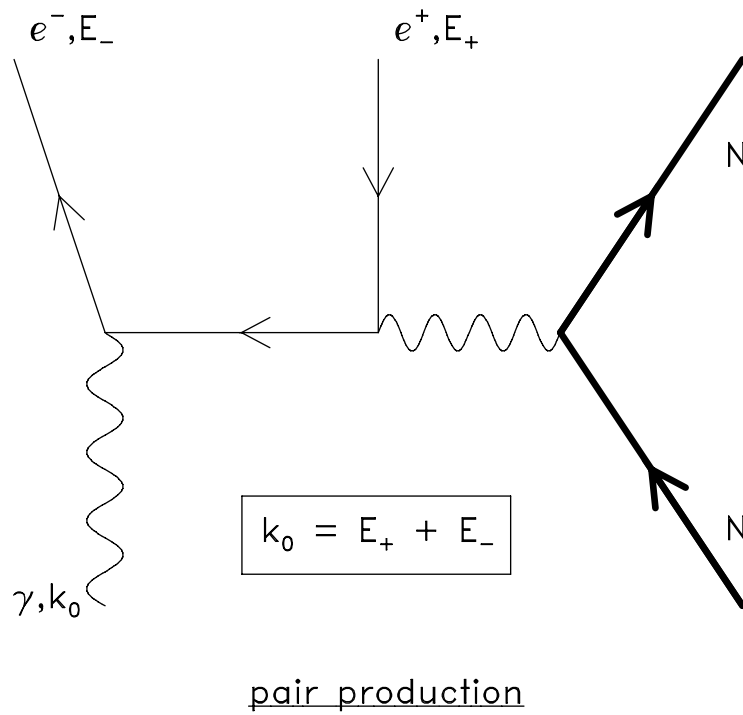


Figure 1.1: The Feynman diagram depicting pair production in the field of a nucleus. Occasionally (suppressed by a factor of $1/Z$), “triplet” production occurs whereby the incoming photon interacts with one of the electrons in the atomic cloud resulting in a final state with two electrons and one positron. (Picture not shown.)

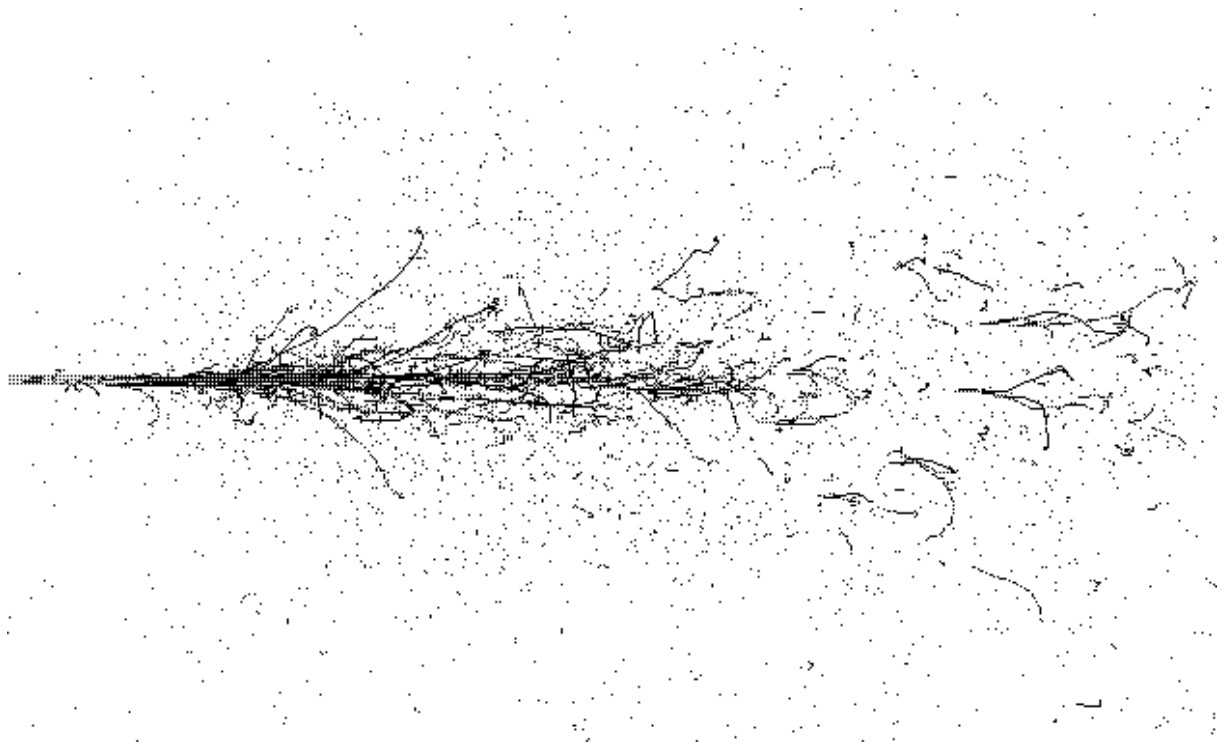


Figure 1.2: A simulation of the cascade resulting from five 1.0 GeV electrons incident from the left on a target. The electrons produce photons which produce electron-positron pairs and so on until the energy of the particles falls below the cascade region. Electron and positron tracks are shown with black lines. Photon tracks are not shown explaining why some electrons and positrons appear to be “disconnected”. This simulation depicted here was produced by the EGS4 code [NHR85, BHNR94] and the system for viewing the trajectories is called EGS_Windows [BW91].

Further reading on the pair production interaction can be found in the reviews by Davies, Bethe, Maximon [DBM54], Motz, Olsen, and Koch [MOK69], and Tsai [Tsa74].

1.1.2 The Compton interaction (incoherent scattering)

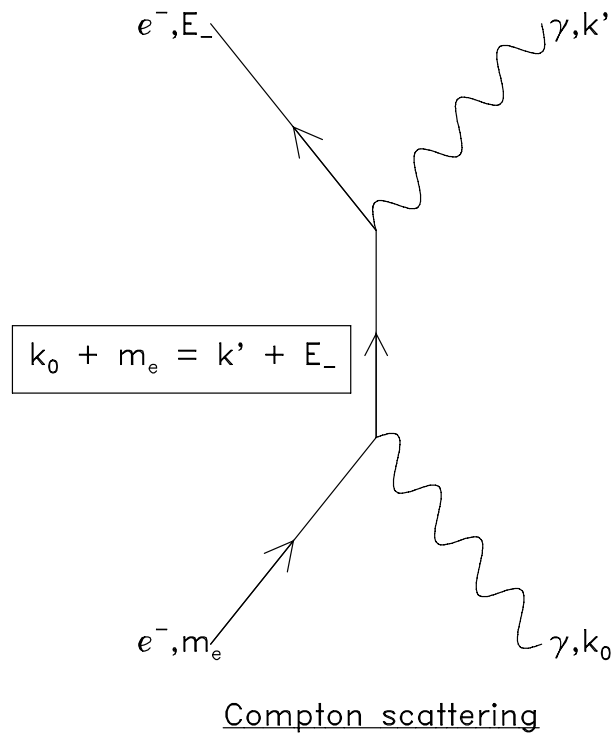


Figure 1.3: The Feynman diagram depicting the Compton interaction in free space. The photon strikes an electron assumed to be “at rest”. The electron is set into motion and the photon recoils with less energy.

The Compton interaction [CA35] is an inelastic “bounce” of a photon from an electron in the atomic shell of a nucleus. It is also known as “incoherent” scattering in recognition of the fact that the recoil photon is reduced in energy. A Feynman diagram depicting this process is

given in Figure 1.3. At large energies, the Compton interaction approaches asymptotically:

$$\lim_{\alpha \rightarrow \infty} \sigma_{\text{inc}}(\alpha) = \sigma_0^{\text{inc}} \frac{Z}{\alpha}, \quad (1.2)$$

where $\sigma_0^{\text{inc}} = 3.33 \times 10^{-25} \text{ cm}^2/\text{nucleus}$. It is proportional to Z (*i.e.* the number of electrons) and falls off as $1/E_\gamma$. Thus, the Compton cross section per unit mass is nearly a constant independent of material and the energy-weighted cross section is nearly a constant independent of energy. Unlike the pair production cross section, the Compton cross section decreases with increased energy.

At low energies, the Compton cross section becomes a constant with energy. That is,

$$\lim_{\alpha \rightarrow 0} \sigma_{\text{inc}}(\alpha) = 2\sigma_0^{\text{inc}} Z. \quad (1.3)$$

This is the classical limit and it corresponds to Thomson scattering, which describes the scattering of light from “free” (unbound) electrons. In almost all applications, the electrons are bound to atoms and this binding has a profound effect on the cross section at low energies. However, above about 100 keV one can consider these bound electrons as “free”, and ignore atomic binding effects. As seen in Figure 1.4, this is a good approximation for photon energies down to 100 of keV or so, for most materials. This lower bound is defined by the K -shell energy although the effects can have influence greatly above it, particularly for the low- Z elements. Below this energy the cross section is depressed since the K -shell electrons are too tightly bound to be liberated by the incoming photon. The unbound Compton differential cross section is taken from the Klein-Nishina cross section [KN29], derived in lowest order Quantum Electrodynamics, without any further approximation.

It is possible to improve the modeling of the Compton interaction. Namito and Hirayama [NH91] have considered the effect of binding for the Compton effect as well as allowing for the transport of polarised photons for both the Compton and Rayleigh interactions.

1.1.3 Photoelectric interaction

The dominant low energy photon process is the photoelectric effect. In this case the photon gets absorbed by an electron of an atom resulting in escape of the electron from the atom and accompanying small energy photons as the electron cloud of the atom settles into its ground state. The theory concerning this phenomenon is not complete and exceedingly complicated. The cross section formulae are usually in the form of numerical fits and take the form:

$$\sigma_{\text{ph}}(E_\gamma) \propto \frac{Z^m}{E_\gamma^n}, \quad (1.4)$$

where the exponent on Z ranges from 4 (low energy, below 100 keV) to 4.6 (high energy, above 500 keV) and the exponent on E_γ ranges from 3 (low energy, below 100 keV) to 1

Effect of binding on Compton cross section

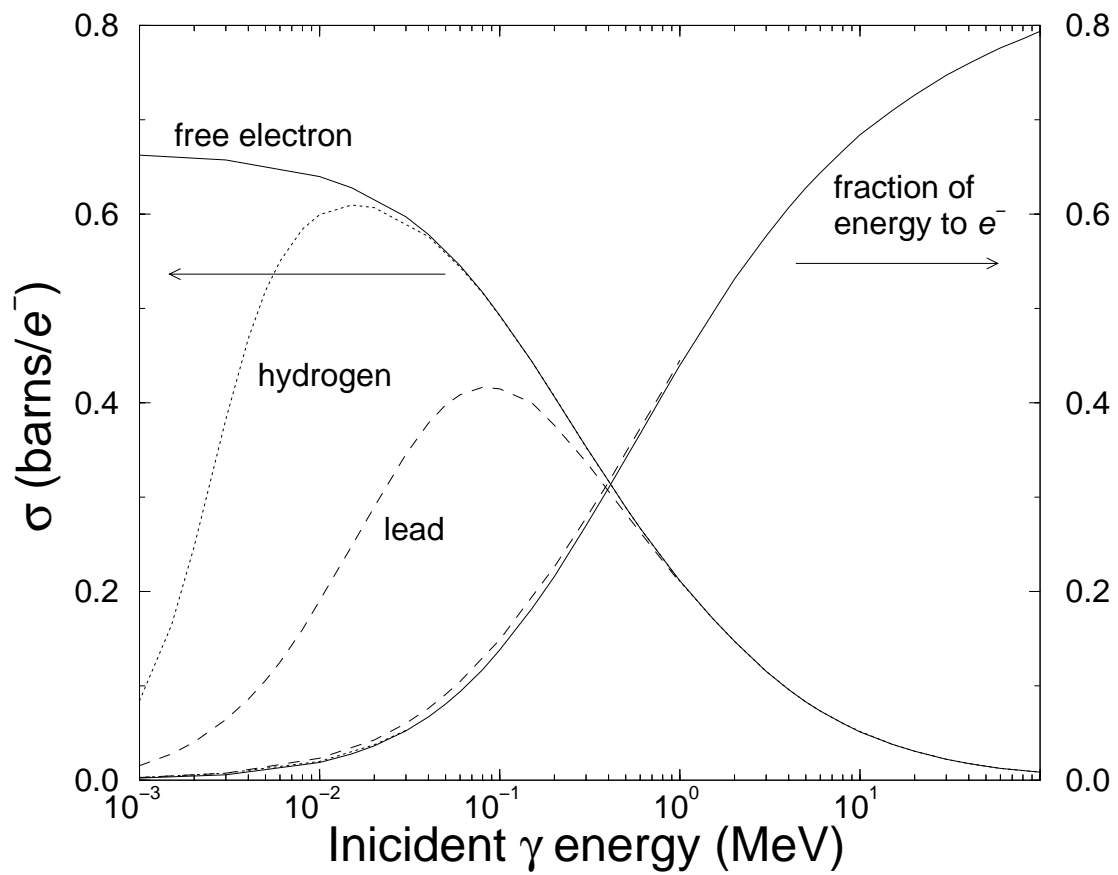


Figure 1.4: The effect of atomic binding on the Compton cross section.

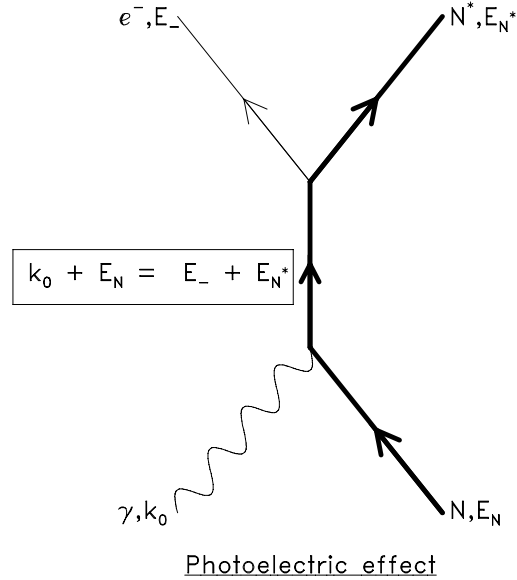


Figure 1.5: Photoelectric effect

(high energy, above 500 keV). Note that the high-energy fall-off is the same as the Compton interaction. However, the high-energy photoelectric cross section is depressed by a factor of about $Z^{3.6}10^{-8}$ relative to the Compton cross section and so is negligible in comparison to the Compton cross section at high energies.

A useful approximation that applies in the regime where the photoelectric effect is dominant is:

$$\sigma_{\text{ph}}(E_\gamma) \propto \frac{Z^4}{E_\gamma^3}, \quad (1.5)$$

which is often employed for simple analytic calculations. However, most Monte Carlo codes employ a table look-up for the photoelectric interaction.

Angular distributions of the photoelectron can be determined according to the theory of Sauter [Sau31]. Although Sauter's theory is relativistic, it appears to work in the non-relativistic regime as well.

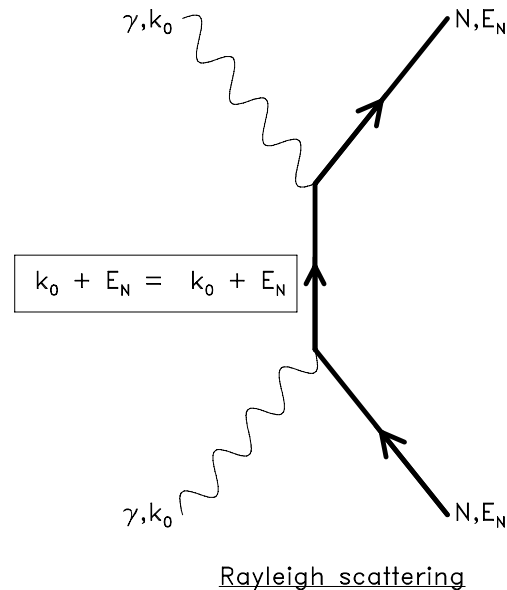


Figure 1.6: Rayleigh scattering

1.1.4 Rayleigh (coherent) interaction

Now we consider the Rayleigh interaction, also known as coherent scattering. In terms of cross section, the Rayleigh cross section is at least an order of magnitude *less* than the photoelectric cross section. However, it is still important! As can be seen from the Feynman diagram in Figure 1.6, the distinguishing feature of this interaction in contrast to the photoelectric interaction is that there is a photon in the final state. Indeed, if low energy photons impinge on an optically thick shield both Compton and Rayleigh scattered photons will emerge from the far side. Moreover, the proportions will be a sensitive function of the incoming energy.

The coherent interaction is an *elastic* (no energy loss) scattering from atoms. It is not good enough to treat molecules as if they are made up of independent atoms. A good demonstration of the importance of molecular structure was demonstrated by Johns and Yaffe [JY83].

The Rayleigh differential cross section has the following form:

$$\sigma_{\text{coh}}(E_\gamma, \Theta) = \frac{r_e^2}{2}(1 + \cos^2 \Theta)[F(q, Z)]^2, \quad (1.6)$$

where r_e is the classical electron radius (2.8179×10^{-13} cm), q is the *momentum-transfer parameter*, $q = (E_\gamma/hc) \sin(\Theta/2)$, and $F(q, Z)$ is the *atomic form factor*. $F(q, Z)$ approaches Z as q goes to zero either by virtue of E_γ going to zero or Θ going to zero. The atomic form factor also falls off rapidly with angle although the Z -dependence increases with angle to approximately $Z^{3/2}$.

The tabulation of the form factors published by Hubbell and Øverbø [HØ79].

1.1.5 Relative importance of various processes

We now consider the relative importance of the various processes involved.

For carbon, a moderately low- Z material, the relative strengths of the photon interactions versus energy is shown in Figure 1.7. For this material we note three distinct regions of single interaction dominance: photoelectric below 20 keV, pair above 30 MeV and Compton in between. The almost order of magnitude depression of the Rayleigh and triplet contributions is some justification for the relatively crude approximations we have discussed. For lead, shown in Figure 1.8, there are several differences and many similarities. The same comment about the relative unimportance of the Rayleigh and triplet cross sections applies. The “Compton dominance” section is much smaller, now extending only from 700 keV to 4 MeV. We also note quite a complicated structure below about 90 keV, the K -shell binding energy of the lead atom. Below this threshold, atomic structure effects become very important.

Finally, we consider the total cross section versus energy for the materials hydrogen, water and lead, shown in Figure 1.9. The total cross section is plotted in the units cm^2/g . The Compton dominance regions are equivalent except for a relative $\overline{A/Z}$ factor. At high energy the Z^2 dependence of pair production is evident in the lead. At lower energies the Z^n ($n > 4$) dependence of the photoelectric cross section is quite evident.

1.2 Photon transport logic

We now discuss a simplified version of photon transport logic. It is simplified by ignoring electron creation and considering that the transport occurs in only a single volume element and a single medium.

This photon transport logic is schematised in Figure 1.10. Imagine that an initial photon’s parameters are present at the top of an array called **STACK**. **STACK** is an array that retains particle phase space characteristics for processing. We also imagine that there is a photon

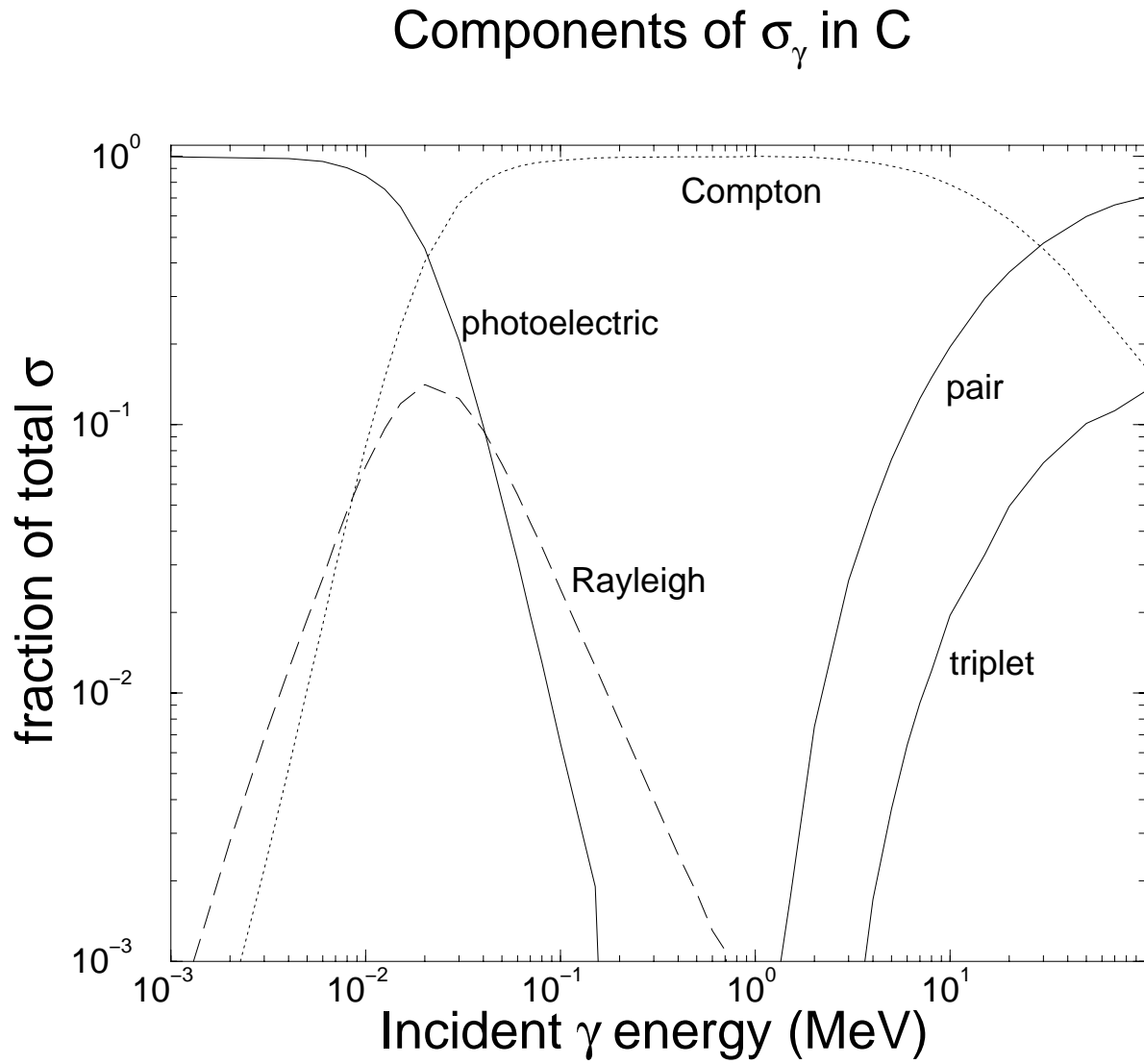


Figure 1.7: Components of the photon cross section in Carbon.

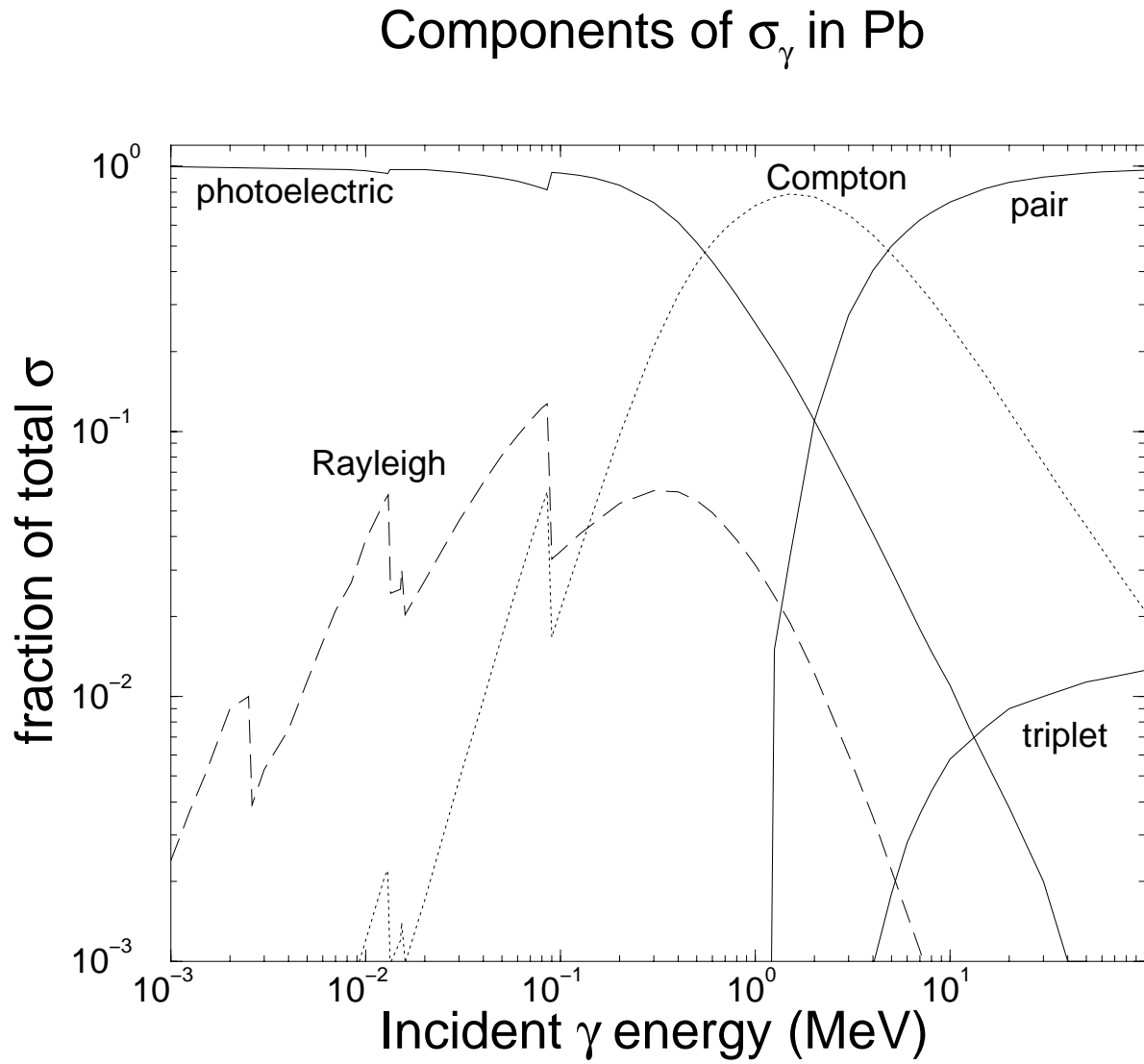
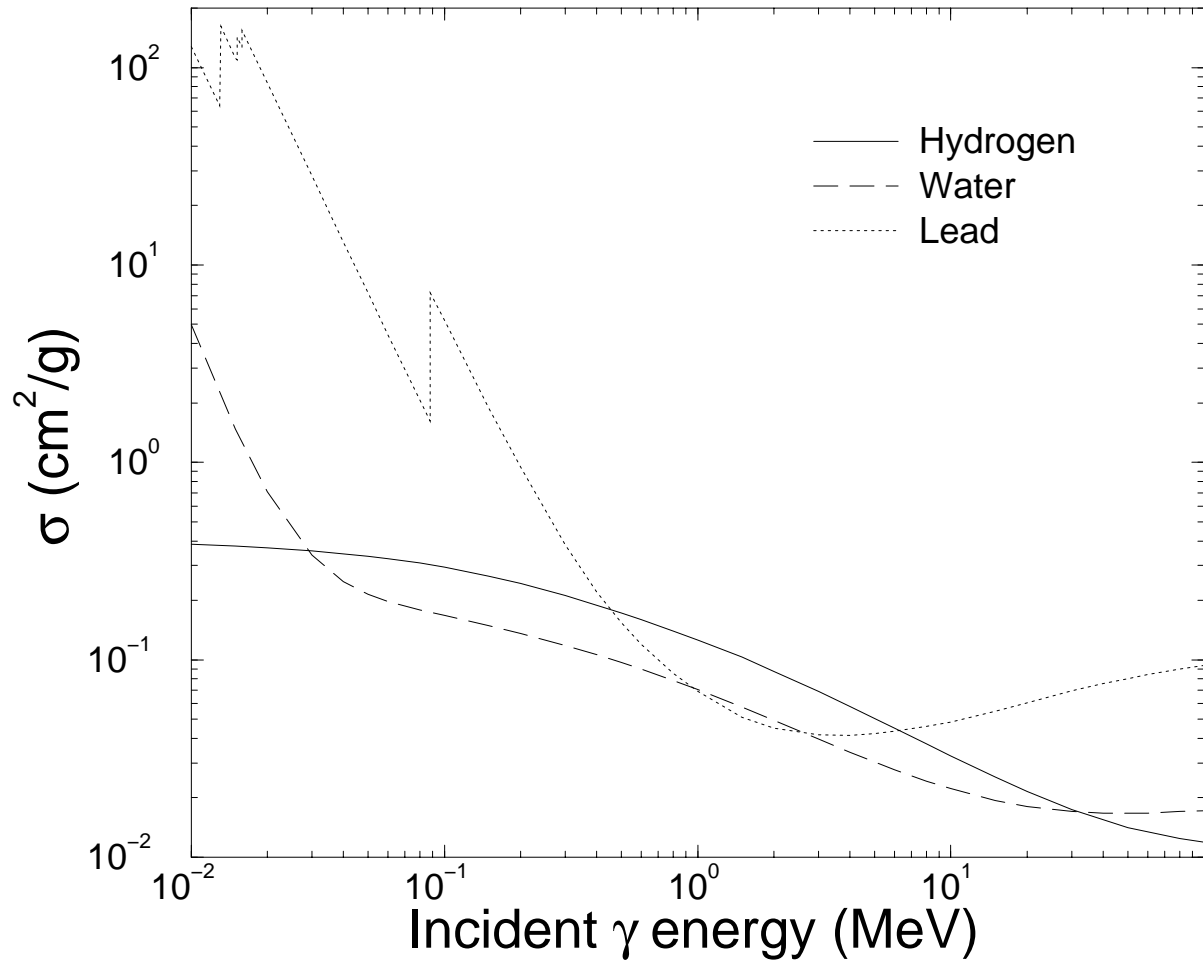


Figure 1.8: Components of the photon cross section in Lead.

Total photon σ vs γ -energyFigure 1.9: Total photon cross section *vs.* photon energy.

transport cutoff defined. Photons that fall below this cutoff are absorbed “on the spot”. We consider that they do not contribute significantly to any tallies of interest and can be ignored. Physically, this step is not really necessary—it is only a time-saving manoeuvre. In “real life” low-energy photons are absorbed by the photoelectric process and vanish. (We will see that electrons are more complicated. *Electrons are always more complicated.*)

The logic flow of photon transport proceeds as follow. The initial characteristics of a photon entering the transport routine and first tested to see if the energy is below the transport cutoff. If it is below the cutoff, the history is terminated. If the **STACK** is empty then a new particle history is started. If the energy is above the cutoff then the distance to the next interaction site is chosen, following the discussion in Chapter 3, *Transport in media, interaction models*. The photon is then transported, that is “stepped” to the point of interaction. (If the geometry is more complicated than just one region, transport through different elements of the geometry would be taken care of here.) If the photon, by virtue of its transport, has left the volume defining the problem then it is discarded. Otherwise, the branching distribution is sampled to see which interaction occurs. Having done this, the surviving particles (new ones may be created, some disappear, the characteristics of the initial one will almost certainly change) have their energies, directions and other characteristics chosen from the appropriate distributions. The surviving particles are put on the **STACK**. Lowest energy ones should be put on the top of the **STACK** to keep the size of the **STACK** as small as possible. Then the whole process takes place again until the **STACK** is empty and all the incident particles are used up.

Photon Transport

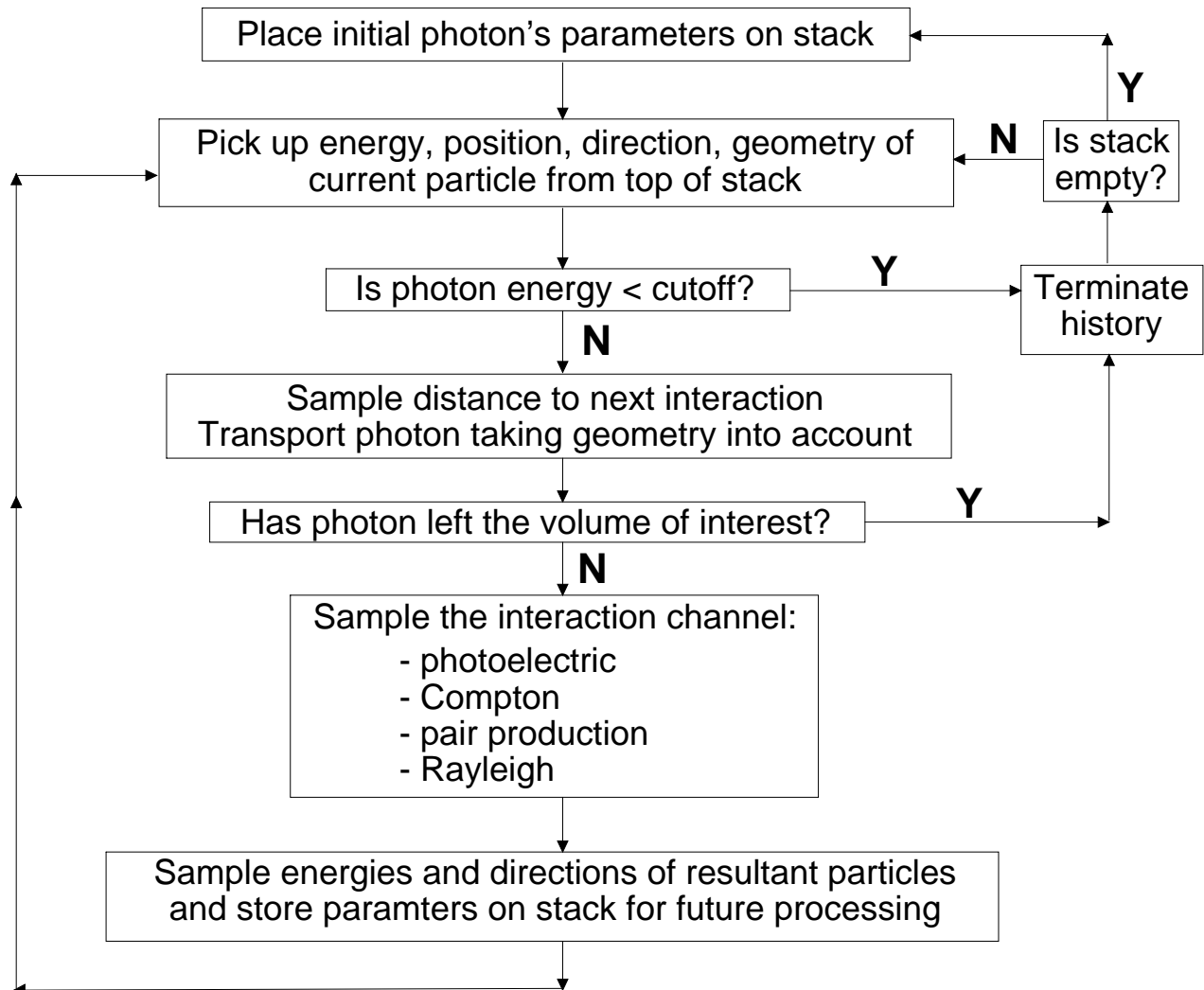


Figure 1.10: “Bare-bones” photon transport logic.

Bibliography

- [Att86] F. H. Attix. *Introduction to Radiological Physics and Radiation Dosimetry*. Wiley, New York, 1986.
- [BHNR94] A. F. Bielajew, H. Hirayama, W. R. Nelson, and D. W. O. Rogers. History, overview and recent improvements of EGS4. *National Research Council of Canada Report PIRS-0436*, 1994.
- [BW91] A. F. Bielajew and P. E. Weibe. EGS-Windows - A Graphical Interface to EGS. *NRCC Report: PIRS-0274*, 1991.
- [CA35] A. H. Compton and S. K. Allison. X-rays in theory and experiment. (*D. Van Nostrand Co. Inc, New York*), 1935.
- [DBM54] H. Davies, H. A. Bethe, and L. C. Maximon. Theory of bremsstrahlung and pair production. II. Integral cross sections for pair production. *Phys. Rev.*, 93:788, 1954.
- [Eva55] R. D. Evans. *The Atomic Nucleus*. McGraw-Hill, New York, 1955.
- [HØ79] J. H. Hubbell and I. Øverbø. Relativistic atomic form factors and photon coherent scattering cross sections. *J. Phys. Chem. Ref. Data*, 9:69, 1979.
- [JC83] H. E. Johns and J. R. Cunningham. *The Physics of Radiology, Fourth Edition*. Charles C. Thomas, Springfield, Illinois, 1983.
- [JY83] P. C. Johns and M. J. Yaffe. Coherent scatter in diagnostic radiology. *Med. Phys.*, 10:40, 1983.
- [KN29] O. Klein and Y. Nishina. . *Z. für Physik*, 52:853, 1929.
- [MOK69] J. W. Motz, H. A. Olsen, and H. W. Koch. Pair production by photons. *Rev. Mod. Phys.*, 41:581 – 639, 1969.
- [NH91] Y. Namito and H. Hirayama. Improvement of low energy photon transport calculation by EGS4 – electron bound effect in Compton scattering. *Japan Atomic Energy Society, Osaka*, page 401, 1991.

- [NHR85] W. R. Nelson, H. Hirayama, and D. W. O. Rogers. The EGS4 Code System. Report SLAC-265, Stanford Linear Accelerator Center, Stanford, Calif, 1985.
- [Sau31] F. Sauter. Über den atomaren Photoeffekt in der K-Schale nach der relativistischen Wellenmechanik Diracs. *Ann. Physik*, 11:454 – 488, 1931.
- [SF96] J. K. Shultis and R. E. Faw. *Radiation Shielding*. Prentice Hall, Upper Saddle River, 1996.
- [Tsa74] Y. S. Tsai. Pair Production and Bremsstrahlung of Charged Leptons. *Rev. Mod. Phys.*, 46:815, 1974.

Problems

1. The Klein-Nishina differential cross section is given by:

$$\frac{d\sigma_{\text{KN}}}{d\Omega_\varphi} = \frac{r_0^2}{2} \left(\frac{k'}{k}\right)^2 \left(\frac{k'}{k} + \frac{k}{k'} - \sin^2 \varphi\right)$$

where φ is the angle between the scattered photon and incoming photon directions, k is the incoming photon energy and k' is the scattered photon energy.

$$\frac{k'}{k} = \frac{1}{1 + \alpha(1 - \cos \varphi)}$$

$$\alpha = \frac{k}{m_0 c^2}$$

- (a) The kinematics of unbound electron scattering correlates absolutely any two of the four kinematic variables, k' , φ , T (the outgoing electron kinetic energy) and θ (the angle that the outgoing electron energy makes with the incoming photon direction, see Figure 7.2 in Attix [Att86]), as a function of k . Hence, there are 12 functions of the form, $k'(\varphi)$, $\varphi(k')$, $k'(\theta)$, $\theta(k')$ and so on.

Find them all and show your calculations. You must prove relation (7.10), but you may use (7.8) and (7.9) in Attix's book without proof.

- i. $k'(\varphi) =$
 - ii. $\varphi(k') =$
 - iii. $k'(\theta) =$
 - iv. $\theta(k') =$
 - v. $k'(T) =$
 - vi. $T(k') =$
 - vii. $\varphi(\theta) =$
 - viii. $\theta(\varphi) =$
 - ix. $\varphi(T) =$
 - x. $T(\varphi) =$
 - xi. $T(\theta) =$
 - xii. $\theta(T) =$
- (b) Find expressions and plot *vs.* α (low energy and high energy limits must be seen clearly)
- i. $\overline{k'/k}$

- ii. $\overline{(k'/k)^2} - \overline{k'/k}^2$
- iii. $\overline{\cos \varphi}$
- iv. $\overline{(\cos \varphi)^2} - \overline{\cos \varphi}^2$
- v. $\overline{\cos \theta}$
- vi. $\overline{(\cos \theta)^2} - \overline{\cos \theta}^2$

vii. Discuss the systematics of the above in the high and low energy limits.

Hint: If $f(x)$ is an unnormalized probability distribution defined between x_0 and x_1 , then

$$\overline{x} = \frac{\int_{x_0}^{x_1} dx \, x f(x)}{\int_{x_0}^{x_1} dx \, f(x)}$$

$$\overline{x^2} = \frac{\int_{x_0}^{x_1} dx \, x^2 f(x)}{\int_{x_0}^{x_1} dx \, f(x)}$$

Chapter 2

Electron Monte Carlo Simulation

In this chapter we discuss the electron and positron interactions and discuss the approximations made in their implementation. We give a brief outline of the electron transport logic used in Monte Carlo simulations.

The transport of electrons (and positrons) is considerably more complicated than for photons. Like photons, electrons are subject to violent interactions. The following are the “catastrophic” interactions:

- large energy-loss Møller scattering ($e^-e^- \longrightarrow e^-e^-$),
- large energy-loss Bhabha scattering ($e^+e^- \longrightarrow e^+e^-$),
- hard bremsstrahlung emission ($e^\pm N \longrightarrow e^\pm \gamma N$), and
- positron annihilation “in-flight” and at rest ($e^+e^- \longrightarrow \gamma\gamma$).

It is possible to sample the above interactions discretely in a reasonable amount of computing time for many practical problems. In addition to the catastrophic events, there are also “soft” events. Detailed modeling of the soft events can usually be approximated by summing the effects of many soft events into virtual “large-effect” events. These “soft” events are:

- low-energy Møller (Bhabha) scattering (modeled as part of the collision stopping power),
- atomic excitation ($e^\pm N \longrightarrow e^\pm N^*$) (modeled as another part of the collision stopping power),
- soft bremsstrahlung (modeled as radiative stopping power), and
- elastic electron (positron) multiple scattering from atoms, ($e^\pm N \longrightarrow e^\pm N$).

Strictly speaking, an elastic large angle scattering from a nucleus should really be considered to be a “catastrophic” interaction but this is not the usual convention. (Perhaps it should be.) For problems of the sort we consider, it is impractical to model all these interactions

discretely. Instead, well-established statistical theories are used to describe these “soft” interactions by accounting for them in a cumulative sense including the effect of many such interactions at the same time. These are the so-called “statistically grouped” interactions.

2.1 Catastrophic interactions

We have almost complete flexibility in defining the threshold between “catastrophic” and “statistically grouped” interactions. The location of this threshold should be chosen by the demands of the physics of the problem and by the accuracy required in the final result.

2.1.1 Hard bremsstrahlung production

As depicted by the Feynman diagram in fig. 2.1, bremsstrahlung production is the creation of photons by electrons (or positrons) in the field of an atom. There are actually two possibilities. The predominant mode is the interaction with the atomic nucleus. This effect dominates by a factor of about Z over the three-body case where an atomic electron recoils ($e^\pm N \rightarrow e^\pm e^- \gamma N^*$). Bremsstrahlung is the quantum analogue of synchrotron radiation, the radiation from accelerated charges predicted by Maxwell’s equations. The de-acceleration and acceleration of an electron scattering from nuclei can be quite violent, resulting in very high energy quanta, up to and including the total kinetic energy of the incoming charged particle.

The two-body effect can be taken into account through the total cross section and angular distribution kinematics. The three-body case is conventionally treated only by inclusion in the total cross section of the two body-process. The two-body process can be modeled using one of the Koch and Motz [KM59] formulae. The bremsstrahlung cross section scales with $Z(Z + \xi(Z))$, where $\xi(Z)$ is the factor accounting for three-body case where the interaction is with an atomic electron. These factors comes are taken from the work of Tsai [Tsa74]. The total cross section depends approximately like $1/E_\gamma$.

2.1.2 Møller (Bhabha) scattering

Møller and Bhabha scattering are collisions of incident electrons or positrons with atomic electrons. It is conventional to assume that these atomic electrons are “free” ignoring their atomic binding energy. At first glance the Møller and Bhabha interactions appear to be quite similar. Referring to fig. 2.2, we see very little difference between them. In reality, however, they are, owing to the identity of the participant particles. The electrons in the e^-e^+ pair can annihilate and be recreated, contributing an extra interaction channel to the cross section. The thresholds for these interactions are different as well. In the e^-e^- case,

the “primary” electron can only give at most half its energy to the target electron if we adopt the convention that the higher energy electron is always denoted “the primary”. This is because the two electrons are indistinguishable. In the e^+e^- case the positron can give up all its energy to the atomic electron.

Møller and Bhabha cross sections scale with Z for different media. The cross section scales approximately as $1/v^2$, where v is the velocity of the scattered electron. Many more low energy secondary particles are produced from the Møller interaction than from the bremsstrahlung interaction.

2.1.3 Positron annihilation

Two photon annihilation is depicted in fig. 2.3. Two-photon “in-flight” annihilation can be modeled using the cross section formulae of Heitler [Hei54]. It is conventional to consider the atomic electrons to be free, ignoring binding effects. Three and higher-photon annihilations ($e^+e^- \rightarrow n\gamma[n > 2]$) as well as one-photon annihilation which is possible in the Coulomb field of a nucleus ($e^+e^-N \rightarrow \gamma N^*$) can be ignored as well. The higher-order processes are very much suppressed relative to the two-body process (by at least a factor of 1/137) while the one-body process competes with the two-photon process only at very high energies where the cross section becomes very small. If a positron survives until it reaches the transport cut-off energy it can be converted it into two photons (annihilation at rest), with or without modeling the residual drift before annihilation.

2.2 Statistically grouped interactions

2.2.1 “Continuous” energy loss

One method to account for the energy loss to sub-threshold (soft bremsstrahlung and soft collisions) is to assume that the energy is lost continuously along its path. The formalism that may be used is the Bethe-Bloch theory of charged particle energy loss [Bet30, Bet32, Blo33] as expressed by Berger and Seltzer [BS64] and in ICRU 37 [ICR84]. This continuous energy loss scales with the Z of the medium for the collision contribution and Z^2 for the radiative part. Charged particles can also polarise the medium in which they travel. This “density effect” is important at high energies and for dense media. Default density effect parameters are available from a 1982 compilation by Sternheimer, Seltzer and Berger [SSB82] and state-of-the-art compilations (as defined by the stopping-power guru Berger who distributes a PC-based stopping power program [Ber92]).

Again, atomic binding effects are treated rather crudely by the Bethe-Bloch formalism. It assumes that each electron can be treated as if it were bound by an average binding potential. The use of more refined theories does not seem advantageous unless one wants

to study electron transport below the K-shell binding energy of the highest atomic number element in the problem.

The stopping power versus energy for different materials is shown in fig. 2.4. The difference in the collision part is due mostly to the difference in ionisation potentials of the various atoms and partly to a \bar{Z}/\bar{A} difference, because the vertical scale is plotted in $\text{MeV}/(\text{g}/\text{cm}^2)$, a normalisation by atomic weight rather than electron density. Note that at high energy the argon line rises above the carbon line. Argon, being a gas, is reduced less by the density effect at this energy. The radiative contribution reflects mostly the relative Z^2 dependence of bremsstrahlung production.

The collisional energy loss by electrons and positrons is different for the same reasons described in the “catastrophic” interaction section. Annihilation is generally not treated as part of the positron slowing down process and is treated discretely as a “catastrophic” event. The differences are reflected in fig. 2.5, the positron/electron collision stopping power. The positron radiative stopping power is reduced with respect to the electron radiative stopping power. At 1 MeV this difference is a few percent in carbon and 60% in lead. This relative difference is depicted in fig. 2.6.

2.2.2 Multiple scattering

Elastic scattering of electrons and positrons from nuclei is predominantly small angle with the occasional large-angle scattering event. If it were not for screening by the atomic electrons, the cross section would be infinite. The cross sections are, nonetheless, very large. There are several statistical theories that deal with multiple scattering. Some of these theories assume that the charged particle has interacted enough times so that these interactions may be grouped together. The most popular such theory is the Fermi-Eyges theory [Eyg48], a small angle theory. This theory neglects large angle scattering and is unsuitable for accurate electron transport unless large angle scattering is somehow included (perhaps as a catastrophic interaction). The most accurate theory is that of Goudsmit and Saunderson [GS40a, GS40b]. This theory does not require that many atoms participate in the production of a multiple scattering angle. However, calculation times required to produce few-atom distributions can get very long, can have intrinsic numerical difficulties and are not efficient computationally for Monte Carlo codes such as EGS4 [NHR85, BHNR94] where the physics and geometry adjust the electron step-length dynamically. A fixed step-size scheme permits an efficient implementation of Goudsmit-Saunderson theory and this has been done in ETRAN [Sel89, Sel91], ITS [HM84, Hal89, HKM⁺92] and MCNP [Bri86, Bri93, Bri97]. Apart from accounting for energy-loss during the course of a step, there is no intrinsic difficulty with large steps either. EGS4 uses the Molière theory [Mol47, Mol48] which produces results as good as Goudsmit-Saunderson for many applications and is much easier to implement in EGS4’s transport scheme.

The Molière theory, although originally designed as a small angle theory has been shown

with small modifications to predict large angle scattering quite successfully [Bet53, Bie94]. The Molière theory includes the contribution of single event large angle scattering, for example, an electron backscatter from a single atom. The Molière theory ignores differences in the scattering of electrons and positrons, and uses the screened Rutherford cross sections instead of the more accurate Mott cross sections. However, the differences are known to be small. Owing to analytic approximations made by Molière theory, this theory requires a minimum step-size as it breaks down numerically if less than 25 atoms or so participate in the development of the angular distribution [Bie94, AMB93]. A recent development [KB98] has surmounted this difficulty. Apart from accounting for energy loss, there is also a large step-size restriction because the Molière theory is couched in a small-angle formalism. Beyond this there are other corrections that can be applied [Bet53, Win87] related to the mathematical connection between the small-angle and any-angle theories.

2.3 Electron transport “mechanics”

2.3.1 Typical electron tracks

A typical Monte Carlo electron track simulation is shown in fig. 2.7. An electron is being transported through a medium. Along the way energy is being lost “continuously” to sub-threshold knock-on electrons and bremsstrahlung. The track is broken up into small straight-line segments called *multiple scattering substeps*. In this case the length of these substeps was chosen so that the electron lost 4% of its energy during each step. At the end of each of these steps the multiple scattering angle is selected according to some theoretical distribution. Catastrophic events, here a single knock-on electron, sets other particles in motion. These particles are followed separately in the same fashion. The original particle, if it does not fall below the transport threshold, is also transported. In general terms, this is exactly what the electron transport logic simulates.

2.3.2 Typical multiple scattering substeps

Now we demonstrate in fig. 2.8 what a multiple scattering substep *should* look like.

A single electron step is characterised by the length of total curved path-length to the end point of the step, t . (This is a reasonable parameter to use because the number of atoms encountered along the way should be proportional to t .) At the end of the step the deflection from the initial direction, Θ , is sampled. Associated with the step is the average projected distance along the original direction of motion, s . There is no satisfactory theory for the relation between s and t ! The lateral deflection, ρ , the distance transported perpendicular to the original direction of motion, is often ignored by electron Monte Carlo codes. This is *not* to say that lateral transport is not modelled! Recalling fig. 2.7, we see that such lateral

deflections do occur as a result of multiple scattering. It is only the lateral deflection during the course of a substep which is ignored. One can guess that if the multiple scattering steps are small enough, the electron track may be simulated more exactly.

2.4 Examples of electron transport

2.4.1 Effect of physical modeling on a 20 MeV e^- depth-dose curve

In this section we will study the effects on the depth-dose curve of turning on and off various physical processes. Figure 2.9 presents two CSDA calculations (*i.e.* no secondaries are created and energy-loss straggling is not taken into account). For the histogram, no multiple scattering is modeled and hence there is a large peak at the end of the range of the particles because they all reach the same depth before being terminating and depositing their residual kinetic energy (189 keV in this case). Note that the size of this peak is very much a calculational artefact which depends on how thick the layer is in which the histories terminate. The curve with the stars includes the effect of multiple scattering. This leads to a lateral spreading of the electrons which shortens the depth of penetration of most electrons and increases the dose at shallower depths because the fluence has increased. In this case, the depth-straggling is entirely caused by the lateral scattering since every electron has traveled the same distance.

Figure 2.10 presents three depth-dose curves calculated with all multiple scattering turned off - *i.e.* the electrons travel in straight lines (except for some minor deflections when secondary electrons are created). In the cases including energy-loss straggling, a depth straggling is introduced because the actual distance traveled by the electrons varies, depending on how much energy they give up to secondaries. Two features are worth noting. Firstly, the energy-loss straggling induced by the creation of bremsstrahlung photons plays a significant role despite the fact that far fewer secondary photons are produced than electrons. They do, however, have a larger mean energy. Secondly, the inclusion of secondary electron transport in the calculation leads to a dose buildup region near the surface. Figure 2.11 presents a combination of the effects in the previous two figures. The extremes of no energy-loss straggling and the full simulation are shown to bracket the results in which energy-loss straggling from either the creation of bremsstrahlung or knock-on electrons is included. The bremsstrahlung straggling has more of an effect, especially near the peak of the depth-dose curve.

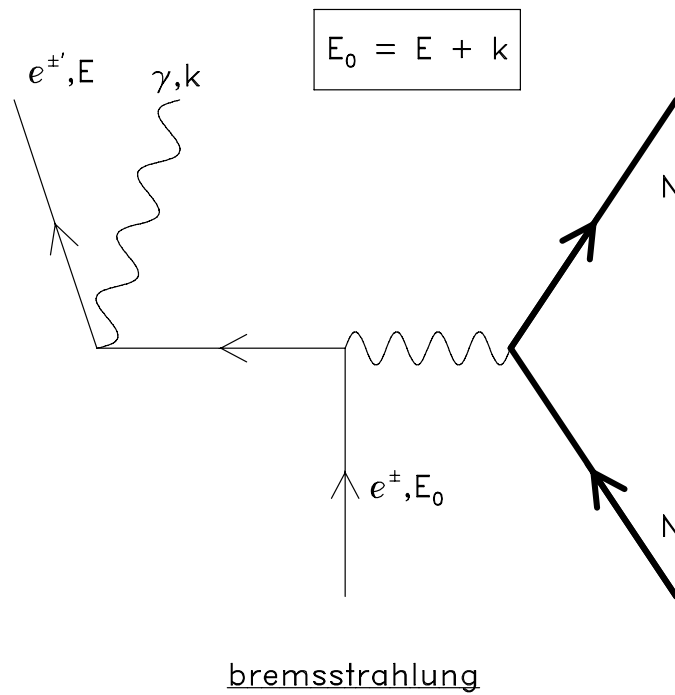


Figure 2.1: Hard bremsstrahlung production in the field of an atom as depicted by a Feynman diagram. There are two possibilities. The predominant mode (shown here) is a two-body interaction where the nucleus recoils. This effect dominates by a factor of about Z^2 over the three-body case where an atomic electron recoils (not shown).

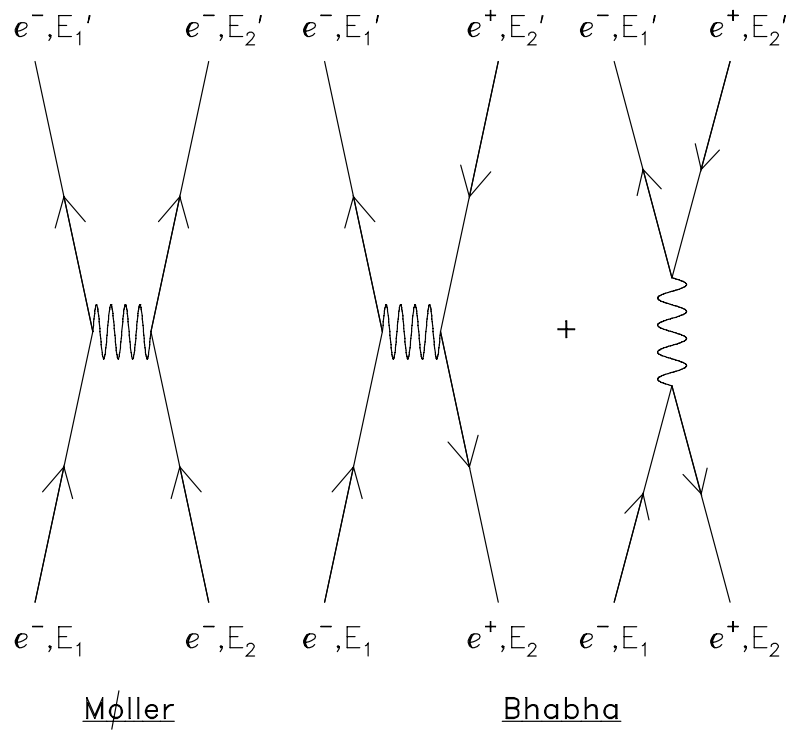


Figure 2.2: Feynman diagrams depicting the Møller and Bhabha interactions. Note the extra interaction channel in the case of the Bhabha interaction.

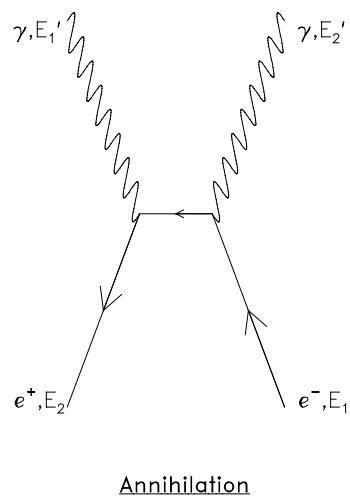
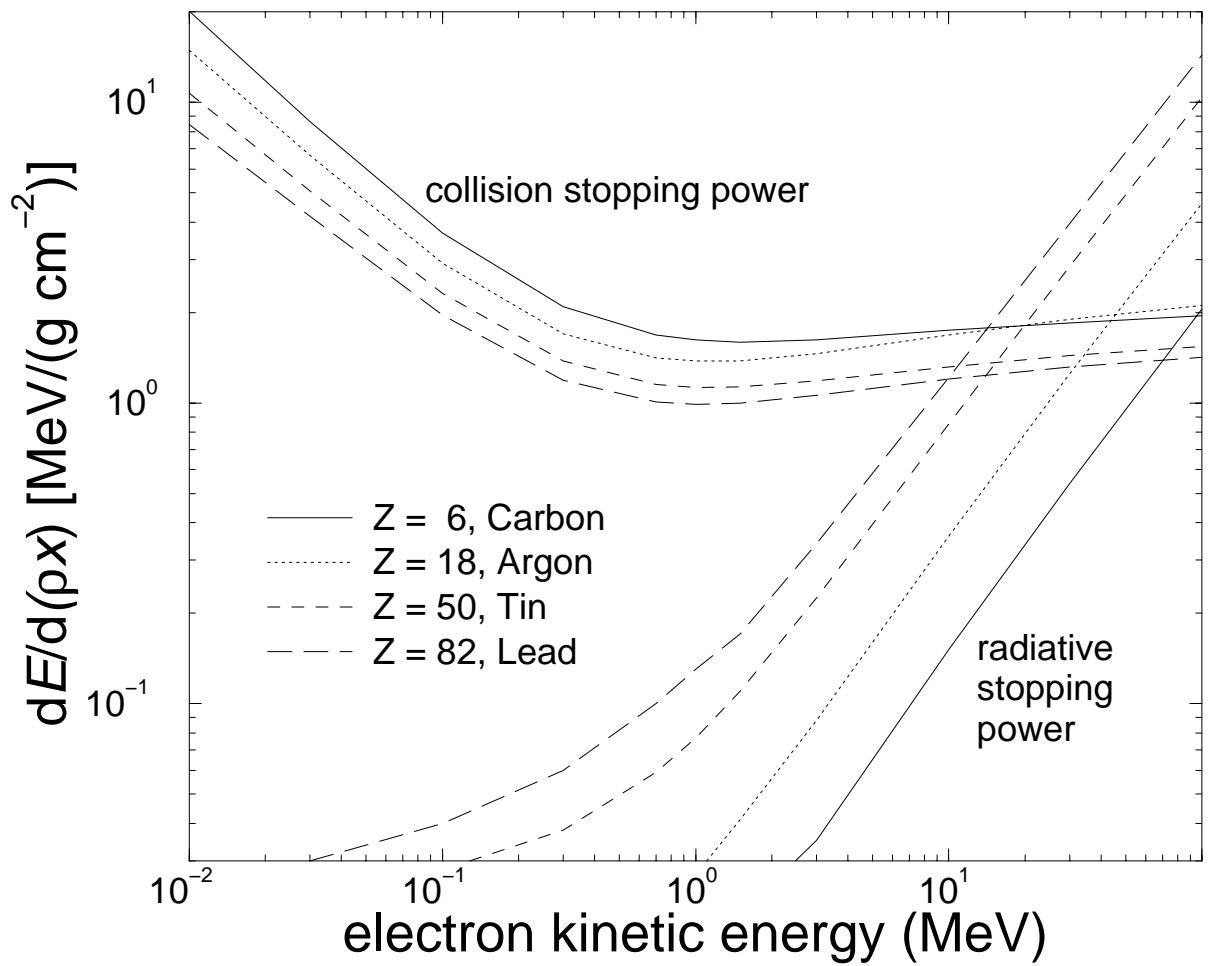


Figure 2.3: Feynman diagram depicting two-photon positron annihilation.

Figure 2.4: Stopping power *versus* energy.

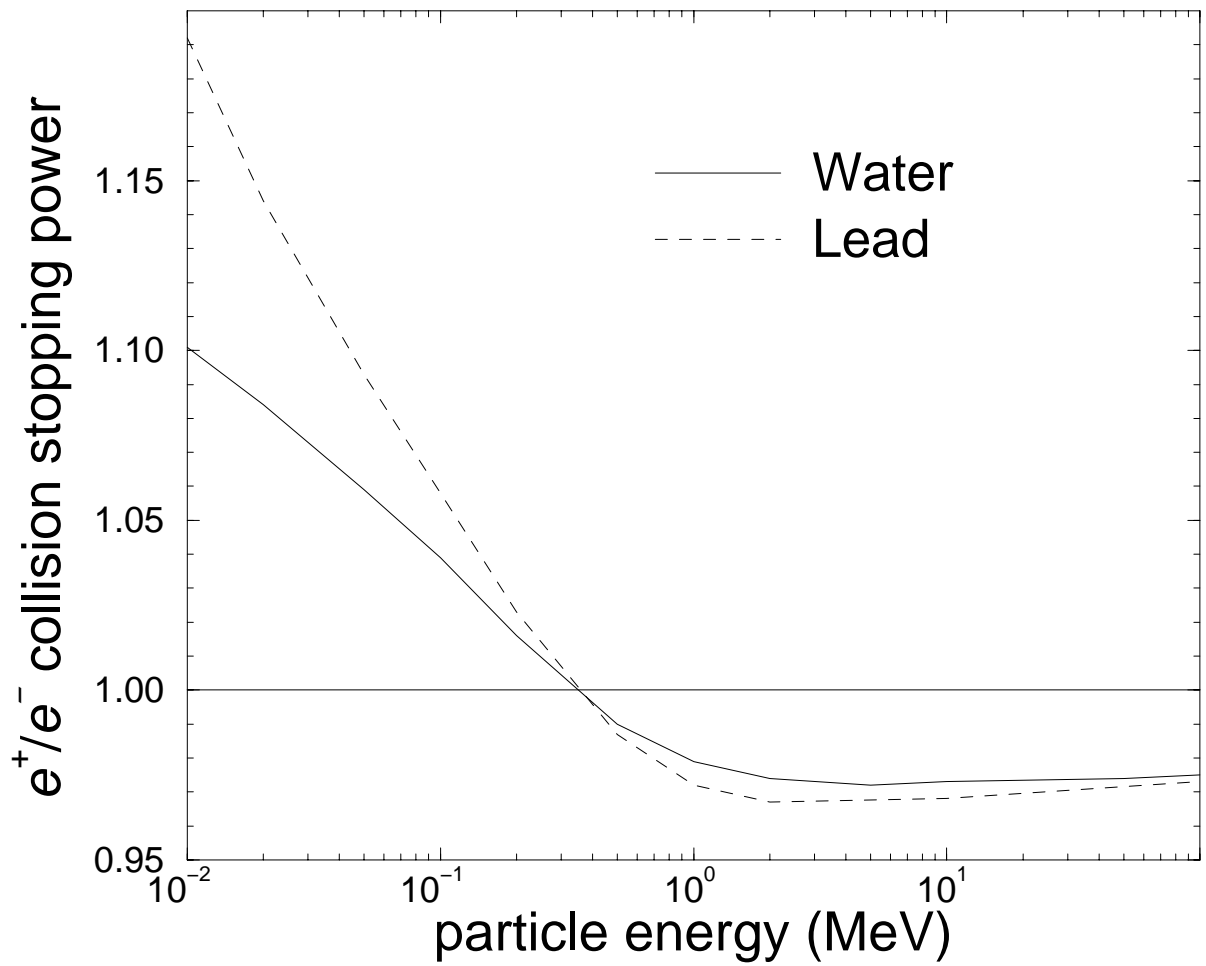


Figure 2.5: Positron/electron collision stopping power.

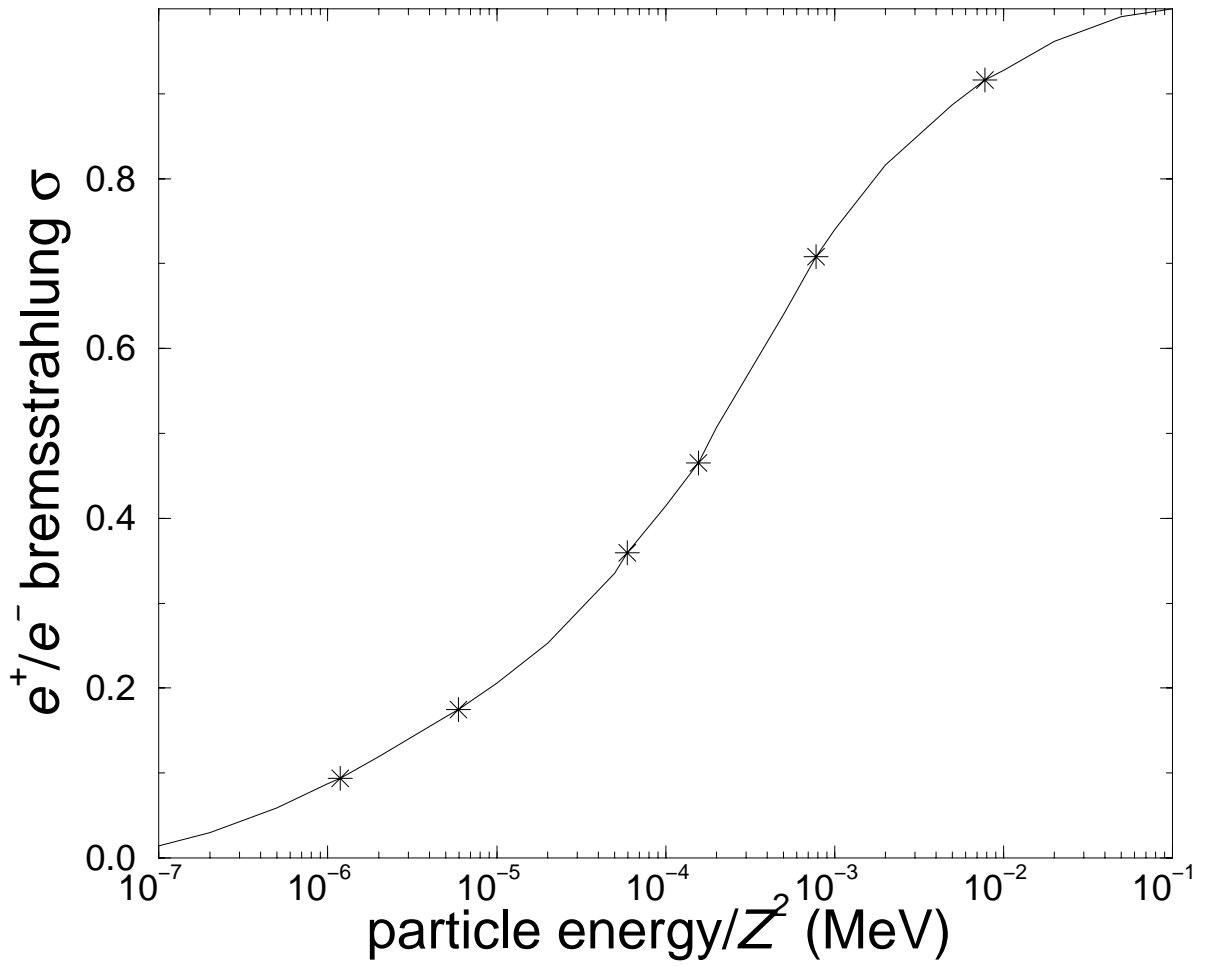


Figure 2.6: Positron/electron bremsstrahlung cross section.

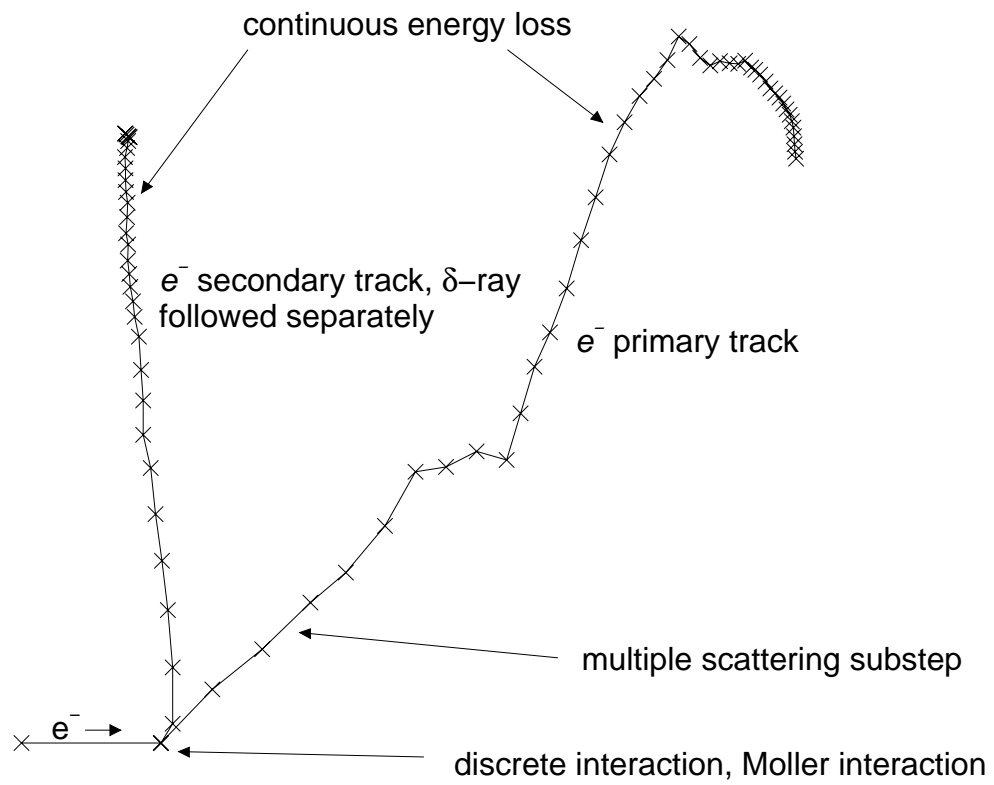


Figure 2.7: A typical electron track simulation. The vertical scale has been exaggerated somewhat.

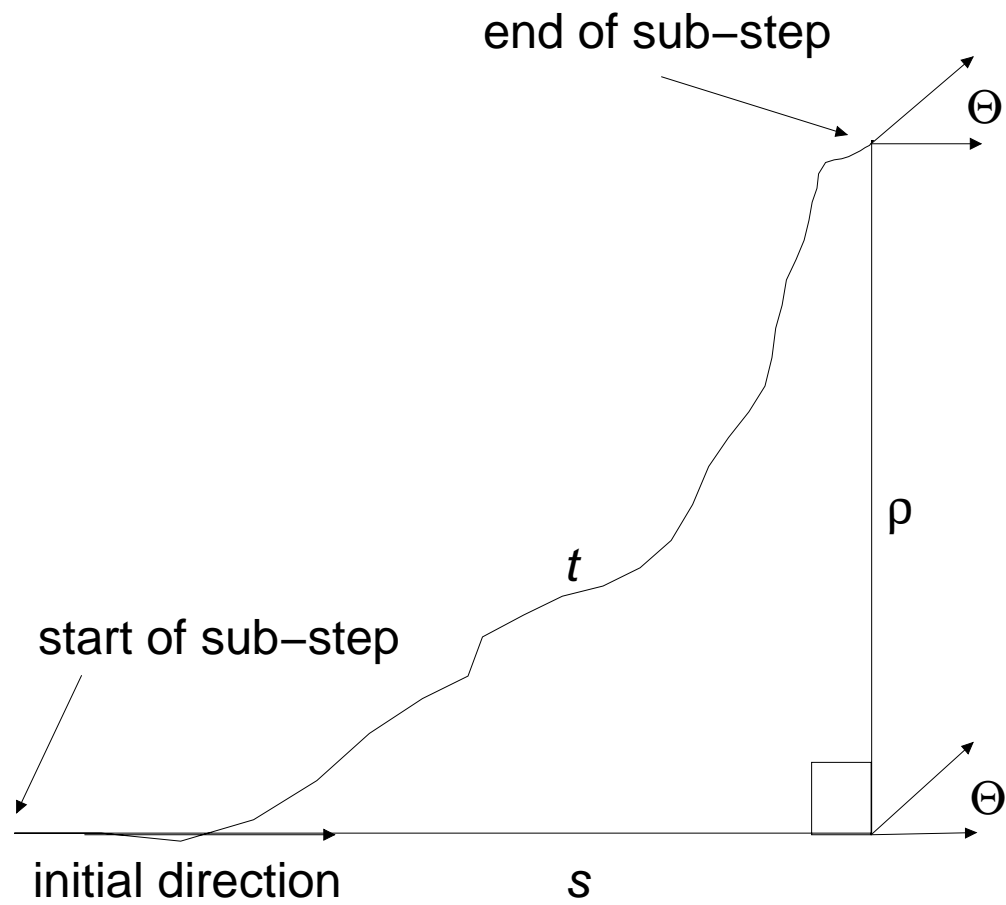


Figure 2.8: A typical multiple scattering substep.

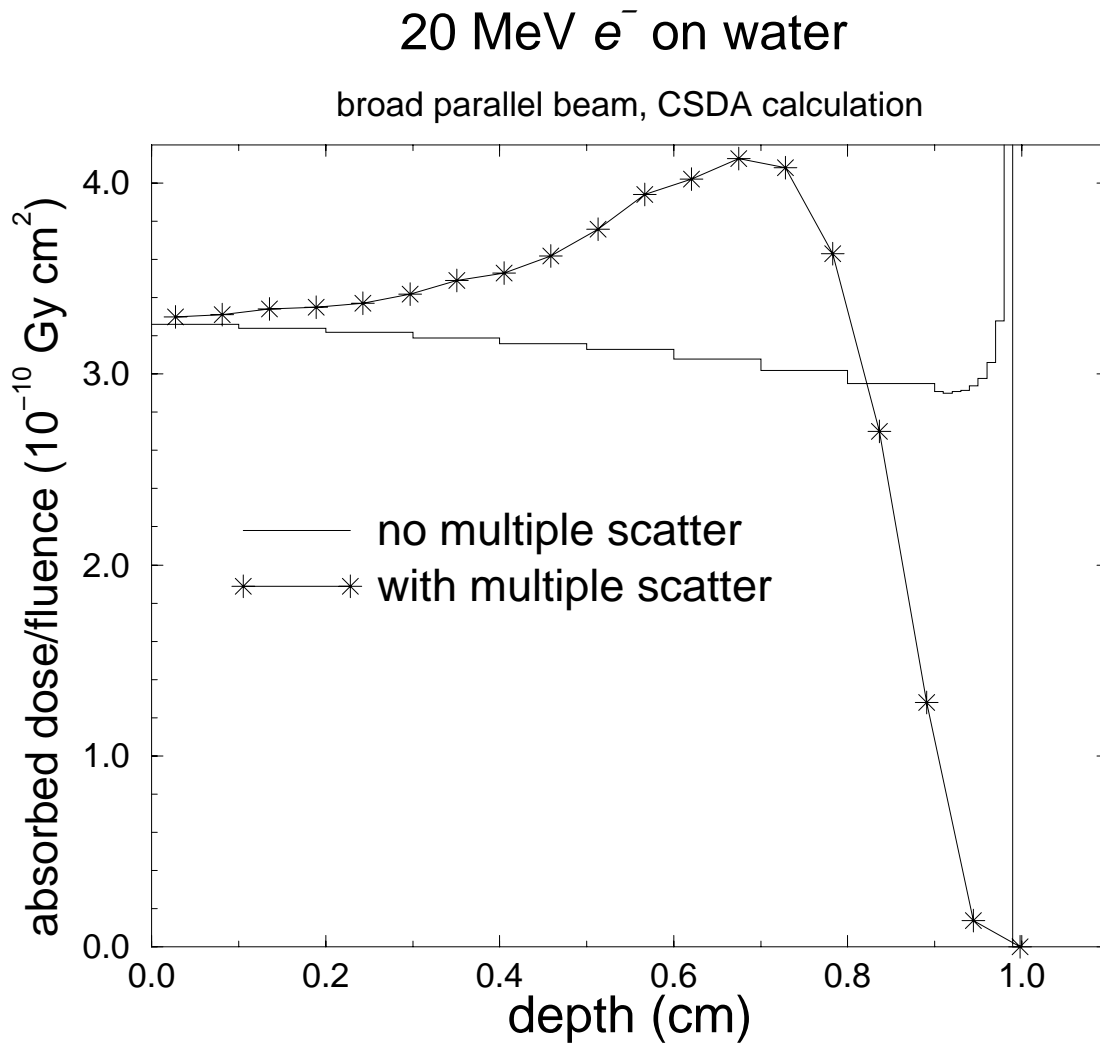


Figure 2.9: Depth-dose curve for a broad parallel beam (BPB) of 20 MeV electrons incident on a water slab. The histogram represents a CSDA calculation in which multiple scattering has been turned off, and the stars show a CSDA calculation which includes multiple scattering.

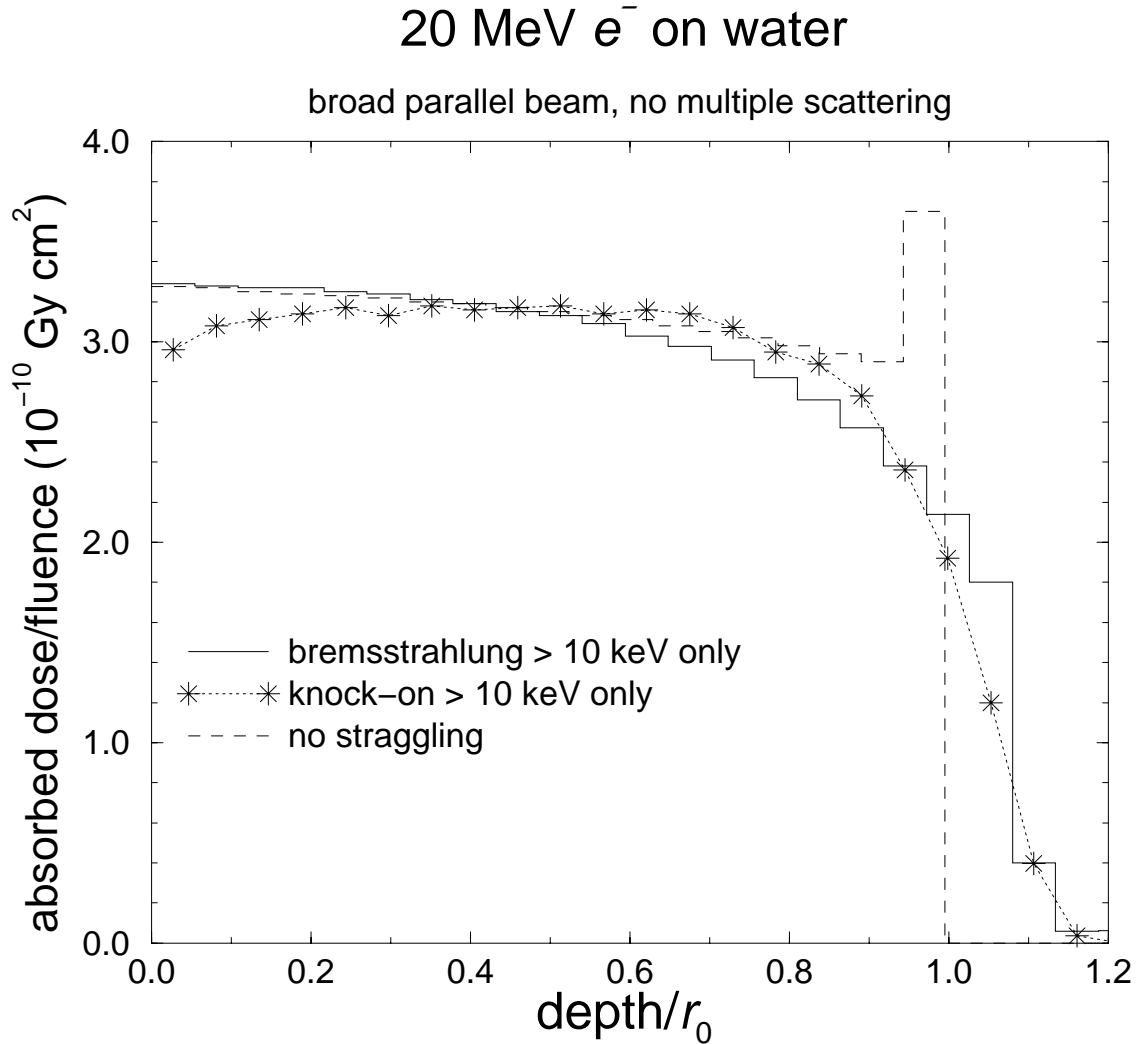


Figure 2.10: Depth-dose curves for a BPB of 20 MeV electrons incident on a water slab, but with multiple scattering turned off. The dashed histogram calculation models no straggling and is the same simulation as given by the histogram in fig. 2.9. Note the difference caused by the different bin size. The solid histogram includes energy-loss straggling due to the creation of bremsstrahlung photons with an energy above 10 keV. The curve denoted by the stars includes only that energy-loss straggling induced by the creation of knock-on electrons with an energy above 10 keV.

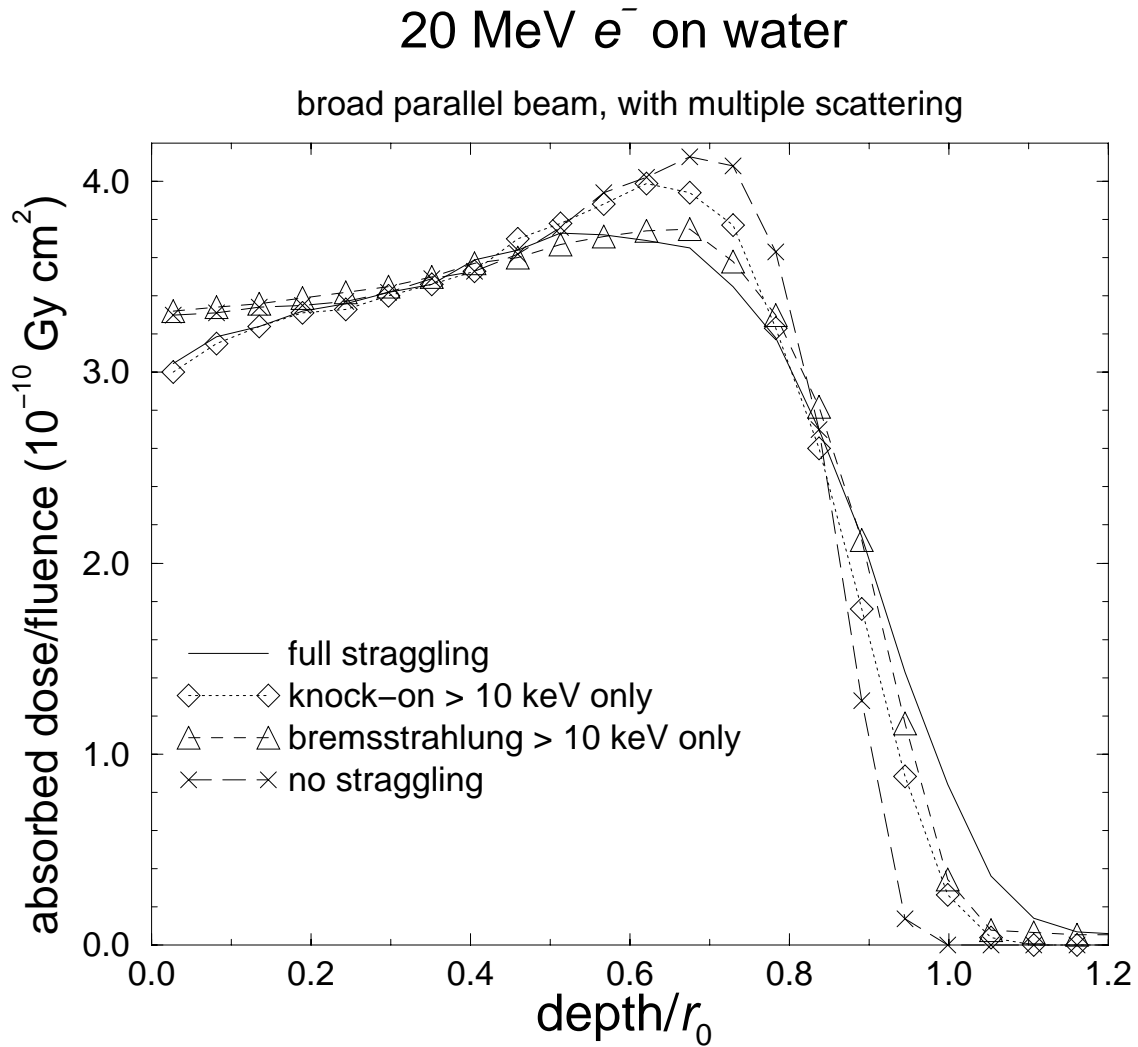


Figure 2.11: BPB of 20 MeV electrons on water with multiple scattering included in all cases and various amounts of energy-loss straggling included by turning on the creation of secondary photons and electrons above a 10 keV threshold.

2.5 Electron transport logic

Figure 2.12 is a schematic flow chart showing the essential differences between different kinds of electron transport algorithms. EGS4 is a “class II” algorithm which samples interactions discretely and correlates the energy loss to secondary particles with an equal loss in the energy of the primary electron (positron).

There is a close similarity between this flow chart and the photon transport flow chart. The essential differences are the nature of the particle interactions as well as the additional continuous energy-loss mechanism and multiple scattering. Positrons are treated by the same subroutine in EGS4 although it is not shown in fig. 2.12.

Imagine that an electron’s parameters (energy, direction, etc.) are on top of the particle stack. (STACK is an array containing the phase-space parameters of particles awaiting transport.) The electron transport routine, picks up these parameters and first asks if the energy of this particle is greater than the transport cutoff energy, called ECUT. If it is not, the electron is discarded. (This is not to that the particle is simply thrown away! “Discard” means that the scoring routines are informed that an electron is about to be taken off the transport stack.) If there is no electron on the top of the stack, control is given to the photon transport routine. Otherwise, the next electron in the stack is picked up and transported. If the original electron’s energy was great enough to be transported, the distance to the next catastrophic interaction point is determined, exactly as in the photon case. The multiple scattering step-size t is then selected and the particle transported, taking into account the constraints of the geometry. After the transport, the multiple scattering angle is selected and the electron’s direction adjusted. The continuous energy loss is then deducted. If the electron, as a result of its transport, has left the geometry defining the problem, it is discarded. Otherwise, its energy is tested to see if it has fallen below the cutoff as a result of its transport. If the electron has not yet reached the point of interaction a new multiple scattering step is effected. This innermost loop undergoes the heaviest use in most calculations because often many multiple scattering steps occur between points of interaction (see fig. 2.7). If the distance to a discrete interaction has been reached, then the type of interaction is chosen. Secondary particles resulting from the interaction are placed on the stack as dictated by the differential cross sections, lower energies on top to prevent stack overflows. The energy and direction of the original electron are adjusted and the process starts all over again.

Electron transport

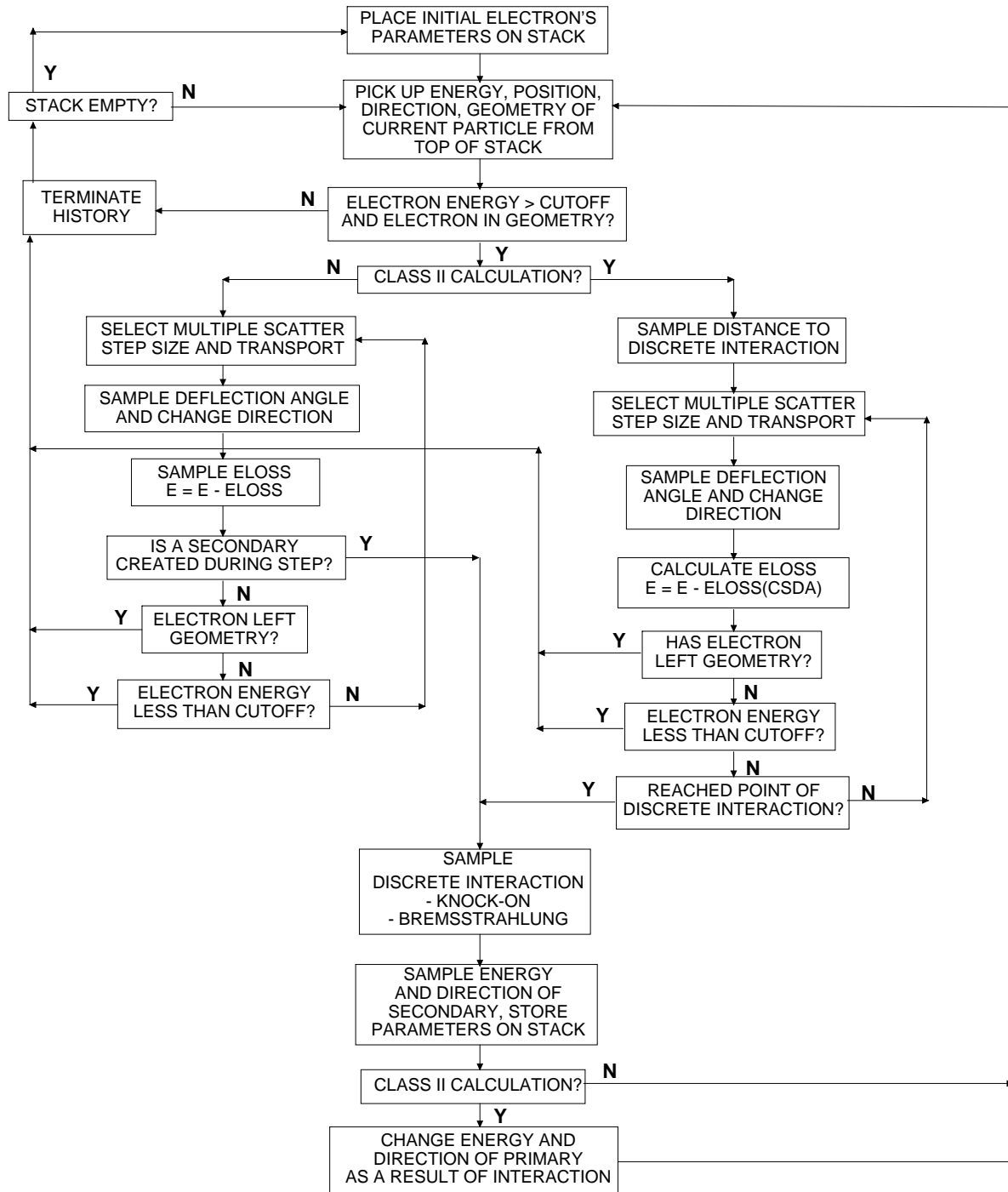


Figure 2.12: Flow chart for electron transport. Much detail is left out.

Bibliography

- [AMB93] P. Andreo, J. Medin, and A. F. Bielajew. Constraints on the multiple scattering theory of Molière in Monte Carlo simulations of the transport of charged particles. *Med. Phys.*, 20:1315 – 1325, 1993.
- [Ber92] M. J. Berger. ESTAR, PSTAR and ASTAR: Computer Programs for Calculating Stopping-Power and Ranges for Electrons, Protons, and Helium Ions. *NIST Report NISTIR-4999 (Washington DC)*, 1992.
- [Bet30] H. A. Bethe. Theory of passage of swift corpuscular rays through matter. *Ann. Physik*, 5:325, 1930.
- [Bet32] H. A. Bethe. Scattering of electrons. *Z. für Physik*, 76:293, 1932.
- [Bet53] H. A. Bethe. Molière’s theory of multiple scattering. *Phys. Rev.*, 89:1256 – 1266, 1953.
- [BHNR94] A. F. Bielajew, H. Hirayama, W. R. Nelson, and D. W. O. Rogers. History, overview and recent improvements of EGS4. *National Research Council of Canada Report PIRS-0436*, 1994.
- [Bie94] A. F. Bielajew. Plural and multiple small-angle scattering from a screened Rutherford cross section. *Nucl. Inst. and Meth.*, B86:257 – 269, 1994.
- [Blo33] F. Bloch. Stopping power of atoms with several electrons. *Z. für Physik*, 81:363, 1933.
- [Bri86] J. Briesmeister. MCNP—A general purpose Monte Carlo code for neutron and photon transport, Version 3A. *Los Alamos National Laboratory Report LA-7396-M (Los Alamos, NM)*, 1986.
- [Bri93] J. F. Briesmeister. MCNP—A general Monte Carlo N-particle transport code. *Los Alamos National Laboratory Report LA-12625-M (Los Alamos, NM)*, 1993.
- [Bri97] J. F. Briesmeister. MCNP—A general Monte Carlo N-particle transport code. *Los Alamos National Laboratory Report LA-12625-M, Version 4B (Los Alamos, NM)*, 1997.

- [BS64] M. J. Berger and S. M. Seltzer. Tables of energy losses and ranges of electrons and positrons. *NASA Report SP-3012 (Washington DC)*, 1964.
- [Eyg48] L. Eyges. Multiple scattering with energy loss. *Phys. Rev.*, 74:1534, 1948.
- [GS40a] S. A. Goudsmit and J. L. Saunderson. Multiple scattering of electrons. *Phys. Rev.*, 57:24 – 29, 1940.
- [GS40b] S. A. Goudsmit and J. L. Saunderson. Multiple scattering of electrons. II. *Phys. Rev.*, 58:36 – 42, 1940.
- [Hal89] J. Halbleib. Structure and Operation of the ITS code system. In T.M. Jenkins, W.R. Nelson, A. Rindi, A.E. Nahum, and D.W.O. Rogers, editors, *Monte Carlo Transport of Electrons and Photons*, pages 249 – 262. Plenum Press, New York, 1989.
- [Hei54] W. Heitler. The quantum theory of radiation. (*Clarendon Press, Oxford*), 1954.
- [HKM⁺92] J. A. Halbleib, R. P. Kensek, T. A. Mehlhorn, G. D. Valdez, S. M. Seltzer, and M. J. Berger. ITS Version 3.0: The Integrated TIGER Series of coupled electron/photon Monte Carlo transport codes. *Sandia report SAND91-1634*, 1992.
- [HM84] J. A. Halbleib and T. A. Mehlhorn. ITS: The integrated TIGER series of coupled electron/photon Monte Carlo transport codes. *Sandia Report SAND84-0573*, 1984.
- [ICR84] ICRU. Stopping powers for electrons and positrons. ICRU Report 37, ICRU, Washington D.C., 1984.
- [KB98] I. Kawrakow and A. F. Bielajew. On the representation of electron multiple elastic-scattering distributions for Monte Carlo calculations. *Nuclear Instruments and Methods*, B134:325 – 336, 1998.
- [KM59] H. W. Koch and J. W. Motz. Bremsstrahlung cross-section formulas and related data. *Rev. Mod. Phys.*, 31:920 – 955, 1959.
- [Mol47] G. Z. Molière. Theorie der Streuung schneller geladener Teilchen. I. Einzelstreuung am abgeschirmten Coulomb-Feld. *Z. Naturforsch.*, 2a:133 – 145, 1947.
- [Mol48] G. Z. Molière. Theorie der Streuung schneller geladener Teilchen. II. Mehrfach- und Vielfachstreuung. *Z. Naturforsch.*, 3a:78 – 97, 1948.
- [NHR85] W. R. Nelson, H. Hirayama, and D. W. O. Rogers. The EGS4 Code System. Report SLAC-265, Stanford Linear Accelerator Center, Stanford, Calif, 1985.

- [Sel89] S. M. Seltzer. An overview of ETRAN Monte Carlo methods. In T.M. Jenkins, W.R. Nelson, A. Rindi, A.E. Nahum, and D.W.O. Rogers, editors, *Monte Carlo Transport of Electrons and Photons*, pages 153 – 182. Plenum Press, New York, 1989.
- [Sel91] S. M. Seltzer. Electron-photon Monte Carlo calculations: the ETRAN code. *Int'l J of Appl. Radiation and Isotopes*, 42:917 – 941, 1991.
- [SSB82] R. M. Sternheimer, S. M. Seltzer, and M. J. Berger. Density effect for the ionization loss of charged particles in various substances. *Phys. Rev.*, B26:6067, 1982.
- [Tsa74] Y. S. Tsai. Pair Production and Bremsstrahlung of Charged Leptons. *Rev. Mod. Phys.*, 46:815, 1974.
- [Win87] K. B. Winterbon. Finite-angle multiple scattering. *Nuclear Instruments and Methods*, B21:1 – 7, 1987.

Problems

1. Basic interaction physics...

- (a) Ignoring photonuclear processes, what are the 3 most important photon interactions to the general area of medical physics? In what energy range is each dominant? What is the atomic number dependence of each?
- (b) Ignoring electronuclear processes, what are the 2 most important electron interactions to the general area of medical physics? In what energy range is each dominant? What is the atomic number dependence of each?
- (c) Ignoring electronuclear processes, what are the 3 most important positron interactions to the general area of medical physics? In what energy range is each dominant? What is the atomic number dependence of each?
- (d) A 50 MeV photon enters a thick Pb slab. Draw a representative picture of the entire life of this photon and all of its daughter particles. Make sure that you show all the interactions described above.
- (e) Repeat **(d)** with a 1 MeV photon. What processes can not occur?

Chapter 3

Transport in media, interaction models

In the previous chapter it was stated that a simulation provides us with a set of pathlengths, $(s_1, s_2, s_3 \dots)$ and an associated set of deflections, $([\Theta_1, \Phi_1], [\Theta_2, \Phi_2], [\Theta_3, \Phi_3] \dots)$ that enter into the transport and deflection machinery developed there. In this chapter we discuss how this data is produced and give some indication as to its origins. We also present some basic interaction models that are facsimiles of the real thing, just so that we can have something to model without a great deal of computational effort.

3.1 Interaction probability in an infinite medium

Imagine that a particle starts at position \vec{x}_0 in an arbitrary infinite scattering medium and that the particle is directed along an axis with unit direction vector $\vec{\mu}$. The medium can have a density or a composition that varies with position. We call the probability that a particle exists at position \vec{x} relative to \vec{x}_0 *without having collided*, $p_s(\vec{\mu} \cdot (\vec{x} - \vec{x}_0))$, the *survival probability*. The *change* in probability due to interaction is characterized by an interaction coefficient (in units L^{-1}) which we call $\mu(\vec{\mu} \cdot (\vec{x} - \vec{x}_0))$. This interaction coefficient can change along the particle flight path. The change in survival probability is expressed mathematically by the following equation:

$$dp_s(\vec{\mu} \cdot (\vec{x} - \vec{x}_0)) = -p_s(\vec{\mu} \cdot (\vec{x} - \vec{x}_0))\mu(\vec{\mu} \cdot (\vec{x} - \vec{x}_0))d(\vec{\mu} \cdot (\vec{x} - \vec{x}_0)) . \quad (3.1)$$

The minus sign on the right-hand-side indicates that the probability decreases with path-length and the proportionality with $p_s(\vec{\mu} \cdot (\vec{x} - \vec{x}_0))$ on the right-hand-side means the probability of loss is proportional to the probability of the particle *existing* at the location where the interaction takes place.

To simplify the notation we translate and rotate so that $\vec{x}_0 = (0, 0, 0)$ and $\vec{\mu} = (0, 0, 1)$. (We

can always rotate and translate back later if we want to.) However, the more complicated notation reinforces the notion that the starting position and direction can be arbitrary and that the interaction coefficient can change *along the path* of the particle's direction. In the simpler notation with a small rearrangement we have:

$$\frac{dp_s(z)}{p_s(z)} = -\mu(z)dz . \quad (3.2)$$

We can integrate this from $z = 0$ where we assume that $p(0) = 1$ to z and obtain:

$$p_s(z) = \exp\left(-\int_0^z dz' \mu(z')\right) . \quad (3.3)$$

The probability that a particle has interacted *within* a distance z is simply $1 - p_s(z)$. This is also called the *cumulative probability*:

$$c(z) = 1 - p_s(z) = 1 - \exp\left(-\int_0^z dz' \mu(z')\right) . \quad (3.4)$$

Since the medium is infinite, $c(\infty) = 1$ and $p_s(\infty) = 0$.

The differential (per unit length) probability for interaction *at* z can be obtained from the derivative of the cumulative probability $c(z)$:

$$p(z) = \frac{d}{dz} \left[1 - \exp\left(-\int_0^z dz' \mu(z')\right)\right] = \mu(z) \exp\left(-\int_0^z dz' \mu(z')\right) = \mu(z)p_s(z) . \quad (3.5)$$

There is a critical assumption in the above expression! It is assumed that the existence of a particle at z means that it has not interacted in any way. $p_s(z)$ is after all, the survival probability. Why is this important? The interaction coefficient $\mu(z)$ may represent a number of possibilities. Choosing which interaction channel the particle takes is *independent* of whatever happened along the way so long as it has survived and what happens is only dependent on the local $\mu(z)$. There will be more discussion of this subtle point later.

3.1.1 Uniform, infinite, homogeneous media

This is the usual case where it is assumed that μ is a constant, independent of position within the medium. That is, the scattering characteristic of the medium is uniform. (The interaction can depend on the energy of the incoming particle, however.) In this case we have the simplification:

$$p_s(z) = e^{-\mu z} , \quad (3.6)$$

which is the well-known exponential attenuation law for the survival probability of particles as a function of depth. The cumulative probability is:

$$c(z) = 1 - p_s(z) = 1 - e^{-\mu z} , \quad (3.7)$$

and the differential probability for interaction z is:

$$p(z) = \frac{d}{dz}[1 - e^{-\mu z}] = \mu e^{-\mu z} = \mu p_s(z) . \quad (3.8)$$

The use of random numbers to sample this probability distribution was given in Chapter ??.

3.2 Finite media

In the case where the medium is finite, our notion of probability distribution seems to break down since:

$$c(\infty) = 1 - p_s(\infty) = 1 - \exp\left(-\int_0^\infty dz' \mu(z')\right) < 1 . \quad (3.9)$$

That is, the cumulative probability at infinity is less than one because either the particle escapes a finite geometry or $\mu(z)$ is zero beyond some limit. (These are two ways of saying the same thing!)

We can recover our notion of probability theory by drawing a boundary at $z = z_b$ at the end of the geometry and rewrite the cumulative probability as:

$$c(z) = 1 - p_s(z) = 1 - \exp\left(-\int_0^z dz' \mu(z')\right) + \exp\left(-\int_0^{z_b} dz' \mu(z')\right)\theta(z - z_b) , \quad (3.10)$$

where we assume that $\mu(z) = 0$ for $z \geq z_b$. The probability distribution becomes:

$$p(z) = \mu(z) \exp\left(-\int_0^z dz' \mu(z')\right) + p_s(z_b)\delta(z - z_b) . \quad (3.11)$$

The interpretation is that once the particle reaches the boundary, it reaches it with a cumulative probability equal to one minus its survival probability. Probability **is** conserved. In fact, this is *exactly* what is done in a Monte Carlo simulation. If a particle reaches the bounding box of the simulation it is absorbed at that boundary and transport discontinues. If this were not the case, an attempt at particle transport simulation would put the logic into an infinite loop with the particle being transported elsewhere looking for more medium to interact in. In a sense, this is exactly what happens in nature! Particles escaping the earth go off into outer space until they interact with another medium or else they transport to the end of the universe. It is simply a question of conservation of probability!

3.3 Regions of different scattering characteristics

Let us imagine that our “universe” contains regions of different scattering characteristics such that it is convenient to write:

$$\mu(z) = \mu_1(z)\theta(z)\theta(b_1 - z)$$

$$\begin{aligned}
\mu(z) &= \mu_2(z)\theta(z - b_1)\theta(b_2 - z) \\
\mu(z) &= \mu_3(z)\theta(z - b_2)\theta(b_3 - z) \\
&\vdots
\end{aligned} \tag{3.12}$$

Typically, the μ 's may be constant in their own domains. However, the analysis about to be presented is much more general. Note also that there is no fundamental restriction to layered media. Since we have already introduced arbitrary translations and rotations, the notation just means that along the flight path the interaction changes in some way at certain distances that we wish to assign a particular status to.

The interaction probability for this arrangement is:

$$\begin{aligned}
p(z) &= \theta(z)\theta(b_1 - z)\mu_1(z)e^{-\int_0^z dz' \mu_1(z')} \\
&+ \theta(z - b_1)\theta(b_2 - z)\mu_2(z)e^{-\int_0^{b_1} dz' \mu_1(z')} e^{-\int_{b_1}^z dz' \mu_2(z')} \\
&+ \theta(z - b_2)\theta(b_3 - z)\mu_3(z)e^{-\int_0^{b_1} dz' \mu_1(z')} e^{-\int_{b_1}^{b_2} dz' \mu_2(z')} e^{-\int_{b_2}^z dz' \mu_3(z')} \\
&\vdots
\end{aligned} \tag{3.13}$$

Another way of writing this is:

$$\begin{aligned}
p(z) &= \theta(z)\theta(b_1 - z)\mu_1(z)e^{-\int_0^z dz' \mu_1(z')} \\
&+ p_s(b_1)\theta(z - b_1)\theta(b_2 - z)\mu_2(z)e^{-\int_{b_1}^z dz' \mu_2(z')} \\
&+ p_s(b_2)\theta(z - b_2)\theta(b_3 - z)\mu_3(z)e^{-\int_{b_2}^z dz' \mu_3(z')} \\
&\vdots
\end{aligned} \tag{3.14}$$

Now consider a change of variables $b_{i-1} \leq z_i \leq b_i$ and introduce the conditional survival probability $p_s(b_i|b_{i-1})$ which is the probability that a particle does not interact in the region $b_{i-1} \leq z_i \leq b_i$ given that it has not interacted in a previous region either. By conservation of probability:

$$p_s(b_i) = p_s(b_{i-1})p_s(b_i|b_{i-1}) . \tag{3.15}$$

Then Equation 3.14 can be rewritten:

$$p(z) = p(z_1, z_2, z_3 \dots) = p(z_1) + p_s(b_1)[p(z_2) + p_s(b_2|b_1)[p(z_3) + p_s(b_3|b_2)[\dots \tag{3.16}$$

What this means is that the variables $z_1, z_2, z_3 \dots$ can be treated as independent. If we consider the interactions over z_1 as independent, then from Equation 3.11 we have:

$$p(z_1) = \mu_1(z_1) \exp\left(-\int_0^{z_1} dz' \mu_1(z')\right) + p_s(b_1)\delta(z - b_1) . \tag{3.17}$$

If the particle makes it to $z = b_1$ we consider z_2 as an independent variable and sample from:

$$p(z_2) = \mu_2(z_2) \exp\left(-\int_0^{z_2} dz' \mu_2(z')\right) + p_s(b_2|b_1)\delta(z - b_2) . \quad (3.18)$$

If the particle makes it to $z = b_2$ we consider z_3 as an independent variable and sample from:

$$p(z_3) = \mu_3(z_3) \exp\left(-\int_0^{z_3} dz' \mu_3(z')\right) + p_s(b_3|b_2)\delta(z - b_3) , \quad (3.19)$$

and so on.

A simple example serves to illustrate the process. Consider only two regions of space on either side of $z = b$ with different interaction coefficients. That is:

$$\mu(z) = \mu_1\theta(b - z) + \mu_2\theta(z - b) . \quad (3.20)$$

The interaction probability for this example is:

$$p(z) = \theta(b - z)\mu_1 e^{-\mu_1 z} + \theta(z - b)\mu_2 e^{-\mu_1 b} e^{\mu_2(z-b)} \quad (3.21)$$

Now, treat z_1 as independent, that is

$$p(z_1) = \mu_1 e^{-\mu_1 z} + e^{-\mu_1 b} \delta(z - b) \quad (3.22)$$

If the particle makes it to $z = b$ we consider z_2 as an independent variable and sample from:

$$p(z_2) = \mu_2 e^{-\mu_2 z_2} \quad (3.23)$$

which is the identical probability distribution implied by Equation 3.21.

The importance of this proof is summarized as follows. The interaction of a particle is dependent only on the local scattering conditions. If space is divided up into regions of locally constant interaction coefficients, then we may sample the distance to an interaction by considering the space to be uniform in the local interaction coefficient. We sample the distance to an interaction and transport the particle. If a boundary demarcating a region of space with different scattering characteristics interrupts the particle transport, *we may stop at that boundary and resample using the new interaction coefficient of the region beyond the boundary.* The alternative approach would be to invert the cumulative probability distribution implied by Equation 3.4,

$$\int_0^z dz' \mu(z') = -\log(1 - r) , \quad (3.24)$$

where r is a uniform random number between 0 and 1. The interaction distance z would be determined by summing the interaction coefficient until the equality in Equation 3.24 is satisfied. In some applications it may be efficient to do the sampling directly according to the above. In other applications it may be more efficient to resample every time the interaction coefficient changes. It is simply a trade-off between the between the time taken to index the look-up table for $\mu(z)$ and recalculating the logarithm in a resampling procedure.

3.4 Obtaining μ from microscopic cross sections

A microscopic cross section is the probability per unit pathlength that a particle interacts with one scattering center per unit volume. Thus,

$$\sigma = \frac{dp}{n dz} , \quad (3.25)$$

where dp is the differential probability of “some event” happening over pathlength dz and n is the number density of scattering centers that “make the event happen”. The units of cross section are L^2 . A special quantity has been defined to measure cross sections, the *barn*. It is equal to 10^{-24} cm^2 . This definition in terms of areas is essentially a generalization of the classical concept of “billiard ball” collisions.

Consider a uniform beam of particles with cross sectional area A_b impinging on a target of thickness dz as depicted in Figure 3.1. The scattering centers all have cross sectional area σ . The density of scattering centers is n so that there are $nA_b dz$ scattering centers in the beam. Thus, the probability per unit area that there will be an interaction is:

$$dp = \frac{nA_b dz \sigma}{A_b} , \quad (3.26)$$

which is just the fractional area occupied by the scattering centers. Hence,

$$\frac{dp}{dz} = n\sigma , \quad (3.27)$$

which is the same expression given in Equation 3.25. While the classical picture is useful for visualizing the scattering process it is a little problematic in dealing with cross sections that can be dependent on the incoming particle energy or that can include the notion that the scattering center may be much larger or smaller than its physical size. The electromagnetic scattering of charged particles (*e.g.* electrons) from unshielded charged centers (*e.g.* bare nuclei) is an example where the cross section is much larger than the physical size. Much smaller cross sections occur when the scattering centers are transparent to the incoming particles. An extreme example of this would be neutrino-nucleon scattering. On the other hand, neutron-nucleus scattering can be very “billiard ball” in nature. Under some circumstances contact has to be made before a scatter takes place.

Another problem arises when one can no longer treat the scattering centers as independent. Classically this would happen if the targets were squeezed so tightly together that their cross sectional areas overlapped. Another example would be where groups of targets would act together collectively to influence the scattering. These phenomena are treated with special techniques that will not be dealt with directly in this book.

The probability per unit length, dp/dz is given a special symbol μ . That is,

$$\mu = \frac{dp}{dz} , \quad (3.28)$$

Figure to be added later

Figure 3.1: Classical “billiard ball” scattering.

which we have been discussing in the previous sections.

The cross section, σ can also depend on the energy, E , of the incoming particle. In this case we may write the cross section differential in energy as $\sigma(E)$. The symbol σ is reserved for total cross section. If there is a functional dependence it is assumed to be differential in that quantity.

Once the particle interacts, the scattered particle can have a different energy, E' and direction, Θ, Φ relative to the initial z directions. The cross section can be differential in these parameters as well. Thus,

$$\sigma(E) = \int dE' \sigma(E, E') = \int d\Omega \sigma(E, \Theta, \Phi) = \int dE' \int d\Omega \sigma(E, E', \Theta, \Phi) , \quad (3.29)$$

relates the cross section to its differential counterparts. The interaction coefficient μ can have similar differential counterparts.

Now, consider a cross section differential both in scattered energy and angle. We may write this as:

$$\mu(E, E', \Theta, \Phi) = \mu(E)p(E, E', \Theta, \Phi) , \quad (3.30)$$

where $p(E, E', \Theta, \Phi)$ is a normalized probability distribution function, which describes the scattering of particle with energy E into energy E' and angles Θ, Φ . We are now ready to specify the final ingredients in particle transport.

Given a particle with energy E and cross section $\sigma(E, E', \Theta, \Phi)$:

- Form its interaction coefficient,

$$\mu(E) = n \int dE' \int d\Omega \sigma(E, E', \Theta, \Phi) . \quad (3.31)$$

- Usually the number density n is not tabulated but it can be determined from:

$$n = \frac{\rho}{A} N_A . \quad (3.32)$$

where ρ is the mass density, A is the atomic weight (g/mol) and N_A is Avogadro's number, the number of atoms per mole ($6.0221367(36) \times 10^{23} \text{ mol}^{-1}$) [C. 98]¹.

- Assuming $\mu(E)$ does not depend on position, provide the distance to the interaction point employing (now familiar) sampling techniques:

$$s = -\frac{1}{\mu(E)} \log(1 - r) , \quad (3.33)$$

where r is a uniformly distributed random number between 0 and 1. Provide this s and execute the transport step $\vec{x} = \vec{x}_o + \vec{\mu}s$. (Do not confuse the direction cosine vector $\vec{\mu}$ with the interaction coefficient μ !)

¹The latest listing of physical constants and many more good things are available from the Particle Data Group's web page: <http://pdg.lbl.gov/pdg.html>

- Form the marginal probability distribution function in E' :

$$m(E, E') = \int d\Omega p(E, E', \Theta, \Phi) , \quad (3.34)$$

and sample E' .

- Form the conditional probability distribution function in Θ, Φ :

$$p(E, \Theta, \Phi | E') = \frac{p(E, E', \Theta, \Phi)}{m(E, E')} , \quad (3.35)$$

sample from it and provide $[\Theta, \Phi]$ to the rotation mechanism that will obtain the new direction after the scattering.

3.5 Compounds and mixtures

Often our scattering media are made up of compounds (*e.g.* water, H_2O) or homogeneous mixtures (*e.g.* air, made up of nitrogen, oxygen, water vapor and a little bit of Argon). How do we form interaction coefficients for these?

We can employ Equations 3.27 and 3.28 and extend them to include partial fractions, n_i of atoms each with its own cross section σ_i :

$$\mu(E) = \sum_i n_i \sigma_i . \quad (3.36)$$

Often, however, compounds are specified by fractional weights, w_i , the fraction of mass due to one atomic species compared to the total. From Equation 3.36 and 3.32:

$$\mu(E) = \sum_i \frac{\tilde{\rho}_i}{A_i} N_A \sigma_i . = \sum_i \tilde{\rho}_i \left(\frac{\mu_i}{\rho_i} \right) = \rho \sum_i w_i \left(\frac{\mu_i}{\rho_i} \right) , \quad (3.37)$$

or

$$\frac{\mu(E)}{\rho} = \sum_i w_i \left(\frac{\mu_i}{\rho_i} \right) . \quad (3.38)$$

where ρ_i is the “normal” density of atomic component i (very often it is μ_i/ρ_i , called the mass attenuation coefficient, that is provided in numerical tabulations), $\tilde{\rho}_i$ is the “actual” mass density of the atomic species in the compound, ρ is the mass density of the compound and the fractional weight of atomic component i in the compound is $w_i = \tilde{\rho}_i/\rho$.

3.6 Branching ratios

Sometimes the interaction coefficient represents the compound process:

$$\mu(E) = \sum_i \mu_i(E) . \quad (3.39)$$

For example, a photon may interact through the photoelectric, coherent (Rayleigh), incoherent (Compton) or pair production processes. Thus, from Equation 3.5 we have:

$$p(z) = \sum_i p_i(z) = \sum_i \mu_i(E) e^{-z\mu(E)} = \sum_i \mu_i(E) p_s(z) , \quad (3.40)$$

where we assume (a non-essential approximation) that the $\mu_i(E)$'s do not depend on position. Thus the fractional probability for interaction channel i is:

$$P_i = \frac{p_i(z)}{p(z)} = \frac{\mu_i(E)}{\mu(E)} . \quad (3.41)$$

In other words, the interaction channel is decided upon the relative attenuation coefficients at the location of the interaction, not on how the particle arrived at that point.

This is one of the few examples of discrete probability distributions and we emphasize this by writing an uppercase P for this probability. The sampling of the branching ratio takes the form of the following recipe:

1. Choose a random number r . If $r \leq \mu_1(E)/\mu(E)$, interact via interaction channel 1. Otherwise,
2. if $r \leq [\mu_1(E) + \mu_2(E)]/\mu(E)$, interact via interaction channel 2. Otherwise,
3. if $r \leq [\mu_1(E) + \mu_2(E) + \mu_3(E)]/\mu(E)$, interact via interaction channel 3. Otherwise...and so on.

The sampling must stop because $\sum_i \mu_i(E)/\mu(E)$ and a random number must always satisfy one of the conditions along the way.

Note that this technique can be applied directly to sampling from the individual atomic species in compounds and mixtures. The fractional probabilities can be calculated according to the discussion of the last section and the sampling procedure above adopted.

3.7 Other pathlength schemes

For complete generality it should be mentioned that there are other schemes for selecting pathlengths. We shall see this in the later chapter on electron transport. In many applications, electron transport steps are provided in a pre-prescribed, non-stochastic way, such as

the pathlength for which a certain average energy loss would be obtained, or a pathlength that produces a given amount of angular deflection. Deeper discussion would invoke a long discussion that we will defer until later, after we have built up all the basic of the Monte Carlo technique that we will need to solve a broad class of problems.

3.8 Model interactions

In this section we will introduce several model interactions and employ them to study some basic characteristics of Monte Carlo results.

3.8.1 Isotropic scattering

The scattering of low to medium-energy neutrons (before resonances begin to appear) is nearly isotropic in the center-of-mass. Therefore the scattering of low to medium-energy neutrons from heavy nuclei is very nearly isotropic. Isotropic scattering is sampled from the distribution function:

$$p(\Theta, \Phi) d\Theta d\Phi = \frac{1}{4\pi} \sin \Theta d\Theta d\Phi . \quad (3.42)$$

The sampling procedure is:

$$\begin{aligned} \cos \Theta &= 1 - 2r_1 \\ \Phi &= 2\pi r_2 \end{aligned} \quad (3.43)$$

where the r_i are uniform random numbers between 0 and 1.

3.8.2 Semi-isotropic or P_1 scattering

The first order correction to isotropic scattering of low to medium-energy neutrons, a correction that becomes increasingly important for scattering from lighter nuclei is the semi-isotropic cross angular distribution:

$$p(\Theta, \Phi) d\Theta d\Phi = \frac{1}{4\pi} (1 + a \cos \Theta) \sin \Theta d\Theta d\Phi \quad |a| \leq 1 . \quad (3.44)$$

The sampling procedure is:

$$\begin{aligned} \cos \Theta &= \frac{2 - a - 4r_1}{1 + \sqrt{1 - a(2 - a - 4r_1)}} \\ \Phi &= 2\pi r_2 \end{aligned} \quad (3.45)$$

where the r_i are uniform random numbers between 0 and 1.

3.8.3 Rutherfordian scattering

A reasonable approximation to the elastic scattering of charged particles is the Rutherfordian distribution:

$$p(\Theta, \Phi) d\Theta d\Phi = \frac{a(2+a)}{4\pi} \frac{\sin \Theta d\Theta d\Phi}{(1 - \cos \Theta + a)^2} \quad 0 \leq a < \infty. \quad (3.46)$$

The sampling procedure is:

$$\begin{aligned} \cos \Theta &= 1 - 2a \frac{1 - r_1}{a + 2r_1} \\ \Phi &= 2\pi r_2 \end{aligned} \quad (3.47)$$

where the r_i are uniform random numbers between 0 and 1. An interesting feature of the Rutherfordian distribution is that it becomes the isotropic distribution in the limit $a \rightarrow \infty$ and the “no-scattering” distribution $\delta(1 - \cos \Theta)$ in the limit $a \rightarrow 0$.

3.8.4 Rutherfordian scattering—small angle form

One approximation that is made to the Rutherfordian distribution in the limit of small a is to make the small-angle approximation to Θ as well. The distribution then takes the form:

$$p(\Theta, \Phi) d\Theta d\Phi = \frac{2a}{\pi} \frac{\Theta d\Theta d\Phi}{(\Theta^2 + 2a)^2} \quad 0 \leq a < \infty, 0 \leq \Theta < \infty. \quad (3.48)$$

The sampling procedure is:

$$\begin{aligned} \Theta &= \sqrt{\frac{2ar}{1-r}} \\ \Phi &= 2\pi r_2 \end{aligned} \quad (3.49)$$

If $\Theta > \pi$ is sampled in the first step, it is rejected and the distribution in Θ is resampled. One also has to take care that the denominator in the $\sqrt{\quad}$ does not become numerically zero through some quirk of the random number generator.

Bibliography

- [C. 98] C. Caso *et al.* The 1998 Review of Particle Physics. *European Physical Journal*, C3:1, 1998.

Problems

1. Give a derivation of the sampling procedure in Equation 3.45 for the semi-isotropic probability distribution given in Equation 3.44 is the isotropic distribution.
2. Prove that the $a \rightarrow \infty$ limit of the Rutherfordian distribution given in Equation 3.46 is the isotropic distribution.
3. Prove that the $a \rightarrow 0$ limit of the Rutherfordian distribution is the δ -function $\delta(1 - \cos \Theta)$.
4. Consider the small-angle form of the Rutherfordian distribution:

$$p(\Theta, \Phi) d\Theta d\Phi = N \frac{\Theta d\Theta d\Phi}{(\Theta^2 + 2a)^2} \quad 0 \leq a < \infty, 0 \leq \Theta < \pi, \quad (3.50)$$

where we now exclude the non-physical regime, $\Theta > \pi$. What is the normalization factor, N ? Develop the sampling procedure for this distribution.

Chapter 4

Macroscopic Radiation Physics

In the chapter, we define the macroscopic field quantities commonly used in radiotherapy physics and dosimetry.

4.1 Fluence

To start, we introduce the concept of radiation fluence, one of the most fundamental *radiometric*¹ quantity.

$$\varphi_i(\vec{x}, E, t) , \tag{4.1}$$

as a continuous function of 3-space, \vec{x} energy, E , and time, t . Whenever the function dependence of the fluence is necessary for clarity, we shall include it explicitly. The subscript i denotes a particular particle species, for example, we shall employ $i = e^-$ for electrons, $i = e^+$, or $i = \gamma$ for photons, but later on. Radiotherapy applications might also employ similar notation for protons, alphas, heavy ions, or even pions.

We shall more commonly consider Φ to be φ integrated over all time, namely:

$$\Phi(\vec{x}, E) = \int_{-\infty}^{+\infty} dt \varphi(\vec{x}, E, t) , \tag{4.2}$$

or, when finite time limits are required,

$$\Phi(\vec{x}, E, t_i, t_f) = \int_{t_i}^{t_f} dt \varphi(\vec{x}, E, t) . \tag{4.3}$$

One quickly notes that complete rigor causes the notation to proliferate. Henceforth, functional dependence will be tacit and assume to be clear from the context, otherwise, the functional dependence will be shown explicitly.

¹A radiometric quantity is a measurement of some aspect of the radiation field.

Fluence is a measure of the strength of the radiation field. It has two equivalent definitions. The ICRU definition [ICR80] is as follows. Imagine that a sphere of small (but non-vanishing) cross sectional area da is impinged upon by (strike the surface from outside the sphere from any angle) dN particles, of type i . Then,

$$\Phi = \lim_{da \rightarrow 0} \frac{dN}{da} . \quad (4.4)$$

An objection to the definition might be raised at this point. Since the radiation field is comprised of particles, the only mathematically sensible conclusion is that fluence is ill-defined!

The practical solution to this conundrum is realized as follows. Imagine that the sphere with cross section area is large enough so that particles do impinge upon it, and enough time is allowed so that the number of particles impinging is large, and the variance associated with that measurement is negligible. Furthermore, imagine that the radiation field has sufficient spatial uniformity so that the size of the sphere does not matter. Then, the practical realization of fluence is, dN particles, of type i . Then,

$$\Phi = \frac{\langle \Delta N \rangle}{\Delta a} . \quad (4.5)$$

There are circumstances when these conditions do not hold, for very small objects, or very weak fields, where the variances can not be ignored. This is the domain of microdosimetry, a very large topic that will not be discussed further. For this discussion, we will assume that our concept of fluence as a function that can be evaluated at a point, and can be manipulated with the mechanism of calculus, is valid. Unlike classical mechanics, however, we are far closer to the quantum limits, and we must always be aware of the limitations of the definition.

We introduced the concept of spatial uniformity of the radiation field. This will be discussed more thoroughly later in our discussion of *radiation equilibrium*. One interesting point to note, however, is that the ICRU definition, through use of a spherical detection region, works equally well in isotropic fields and directional fields, which undoubtedly was one of the motivations for that particular definition. However, it is not clear that this way of measuring fluence has anything to do with the effect of radiation on matter. How can a particle field impinging on a test sphere be related, for example, to dose? Chilton's definition below will clarify this. Note as well, that Φ has units L^{-2} .

The alternative definition of fluence is attributed to Chilton [Chi78, Chi79],

$$\Phi = \lim_{dV \rightarrow 0} \frac{\sum dl}{dV} , \quad (4.6)$$

where dV is an infinitesimal volume of *any* shape and $\sum dl$ is the sum of all the pathlengths (in some units of length measure) that traverse the interior of dV . The proof of the equivalence for spheres is left to the student. (Problems 1 and 2 at the end of this chapter). This

is a remarkable result! It also brings a closer connection to the effect of the radiation, as proportional to the track length of particles through a given volume.

The same mathematical conundrum besets us when taking the limit to small volumes. Therefore, using the same arguments as before to establish a practical value of fluence using Chilton's theorem, leads us to,

$$\Phi = \frac{\sum \Delta l}{\Delta V} , \quad (4.7)$$

where $\sum \Delta l$ involves enough trajectories to make the variance associated with it negligible, and the radiation is uniform over the volume, ΔV . It is interesting to note, that Chilton derived his expression [4.6] based on the common estimate for variance in Monte Carlo calculations, namely,

$$\tilde{\Phi} = \frac{\sum_i^{N_{\Delta V}} \Delta l_i}{\Delta V} , \quad (4.8)$$

with it's associated estimated variance,

$$\sigma_{\tilde{\Phi}}^2 = \frac{\langle (\sum_i^{N_{\Delta V}} \Delta l_i)^2 \rangle - \langle \sum_i^{N_{\Delta V}} \Delta l_i \rangle^2}{(\Delta V)^2} , \quad (4.9)$$

where $N_{\Delta V}$ is the number of particles that entered the volume ΔV .

The integral form of these Chilton's expression, extended over regions of space where the irradiation is uniform, and the surfaces may be extended to surfaces of arbitrary shape are,

$$\Phi = \frac{\int dn}{S_e} = \frac{\int dl}{V} , \quad (4.10)$$

where $\int dn$ is the number of particles impinging on the outer surface of the volume, S_e is the cross section of the surface exposed to the source, V is the volume of the source, and $\int dl$ is the sum of tracklengths through the source.

In general, tracklength summations in some volume, V , may be calculated analytically using,

$$\int dl_V = \frac{1}{4\pi} \int d\Omega \int_S d\vec{S} \cdot \vec{\Omega} \Theta(\vec{S} \cdot \vec{\Omega}) n(\vec{x}_S, \vec{\Omega}) l(\vec{\Omega}, \vec{\Omega}_S) , \quad (4.11)$$

where $n(\vec{x}_S, \vec{\Omega})$ is the number of particles per unit area with direction $\vec{\Omega}$ striking the surface element, $d\vec{S}$ (that has its normal pointed toward the interior of the volume), $\Theta()$ is unity when its argument is positive and zero otherwise, and $l(\vec{\Omega}, \vec{\Omega}_S)$ is the distance from the entrance point on the volume to first exit from the volume.

The total number of particle impinging a surface maybe calculated from,

$$\int dn = \frac{1}{4\pi} \int d\Omega \int_S d\vec{S} \cdot \vec{\Omega} \Theta(\vec{S} \cdot \vec{\Omega}) n(\vec{x}_S, \vec{\Omega}) , \quad (4.12)$$

and the cross section of the surface visible to the source, S_e , from,

$$S_e(\vec{\Omega}) = \frac{1}{4\pi} \int d\Omega \int_S d\vec{S} \cdot \vec{\Omega} \Theta(\vec{S} \cdot \vec{\Omega}) , \quad (4.13)$$

where Ω relates to the angular distribution of the source, as emphasized above.

4.2 Radiation equilibrium

All radiometric quantities measure particle fluence in some fashion, as fluence is the most fundamental quantity describing a radiation field, from which all others may be derived. The statement of radiation equilibrium is as follows, assuming we have a fluence measuring device that may or may not have a directional dependence in a monodirectional field, is sensitive to only one of the particle species in the radiation field, and is sensitive to only one energy component, E , of the radiation field. We shall call this detector $D_i(E, \vec{\Omega}_D)$. We may also consider that there may be an externally defined constant vector (gravity, magnetic field, electric field, some aspect of the source) that provides a coordinate system orientation for the detector's $\vec{\Omega}_D$.

A region of space, V , is considered to be in a state of radiation equilibrium with respect to particle species i , if that radiation field is constant in time, and any measurement of $\Phi(\vec{x}, E)$ is invariant with respect to translations of the detector from \vec{x} to \vec{x}' within V . In this case we conclude that $\Phi(\vec{x}, E) = \Phi(E)$ within V .

A second statement is required for isotropic radiation.

A region of space, V , is considered to be in a state of isotropic radiation equilibrium with respect to particle species i , if that radiation field is constant in time, and any measurement of $\Phi(\vec{x}, E)$ is invariant with respect to translations of the detector from \vec{x} to \vec{x}' within V and invariant with respect to rotations of the detector, $\vec{\Omega}_D \rightarrow \vec{\Omega}'_D$ in V , providing that the detector response is uniform with respect to externally defined directions (gravity, electric and magnetic fields). In this case we conclude that $\Phi(\vec{x}, E) = \Phi(E)$ within V , and that the source is isotropic.

The consequences of radiation equilibrium are central to radiation dosimetry. Consider the first case, where the radiation field has a direction associated with it, but the detector is insensitive to it's orientation within this fields. This idealization is closely approximated by good radiation detectors. Let us imagine that we have such an ideal detector, and it is spherical in shape, clearly insensitive to direction. Moreover, the size of this detector, so long that it fits in V always measures the same fluence. Now, take an arbitrarily-shaped detector, still that fits in V . Form this arbitrary shape from spherical detectors of smaller and smaller size, so that in the limit, the volume of this aggregation of spheres equals the volume of the arbitrarily-shaped detector and the shape is the same in the limit of small

spheres. (See Figure 4.1.) Each one of these spheres measures the same fluence, and hence, so the the arbitrarily shaped one. The conclusion is that an ideal detector is independent of its shape and orientation in a radiation field that is in equilibrium.

Remarkably, conditions of near particle equilibrium and near ideal detectors do exist in radiation physics and enable accurate dosimetry to be done without excessive concern about exact detector positioning and orientation. (They still are, however, important.) Real detectors are prone to positioning and orientation differences. Thankfully, they are minimized so long as the radiation fields are near equilibrium.

Finally, sources that produce uniform fields maybe be realized by several means, first as mathematical ideals, and nearly, as physical constructs. An isotropic source may be produced at the center of a very large sphere with a uniform surface source, or uniform volume source ($R \gg \Delta a$). A monodirectional source may be produced by a point source moved a very long distance away from the detector ($D \gg \Delta a$). A uniform source with angular dependence may be produced by a very large plane source ($D \gg \Delta a$), of some uniform thickness with a source distributed through its volume. Self-shielding will cause an angular dependence in this case.

4.2.1 Planar fluence

Planar fluence is often confused with fluence. Therefore it is important to clarify that point now. Planar fluence is the number of particles that strike a surface irrespective of direction. It may be calculated using the fluence from the relation,

$$\varphi_i(\vec{x}, E, t) = \frac{1}{4\pi} \int d\Omega \left(\frac{dn_i(\vec{x}, \vec{\Omega}, E, t)}{|\vec{\Omega} \cdot \vec{n}_S|} \right), \quad (4.14)$$

where \vec{n}_S is the inward normal to the surface. Often, one is interested in separating the planar fluence based on its orientation with respect to the surface. In this case, we write,

$$dn_i(\vec{x}, \vec{\Omega}, E, t) = dn_i^+(\vec{x}, \vec{\Omega}, E, t) + dn_i^-(\vec{x}, \vec{\Omega}, E, t), \quad (4.15)$$

for the ingoing and outgoing parts.

This planar fluence is also sometimes called the *total scalar flux*. It is also possible to define the *net scalar flux* as,

$$dn_i(\vec{x}, \vec{\Omega}, E, t) = dn_i^+(\vec{x}, \vec{\Omega}, E, t) - dn_i^-(\vec{x}, \vec{\Omega}, E, t). \quad (4.16)$$

It is important to note that planar fluence and fluence are fundamentally different. Fluence is a point function defined as a volumetric quantity, even in the limit that this volume is made vanishingly small. The ICRU definition obscures this fact, which is probably the source of

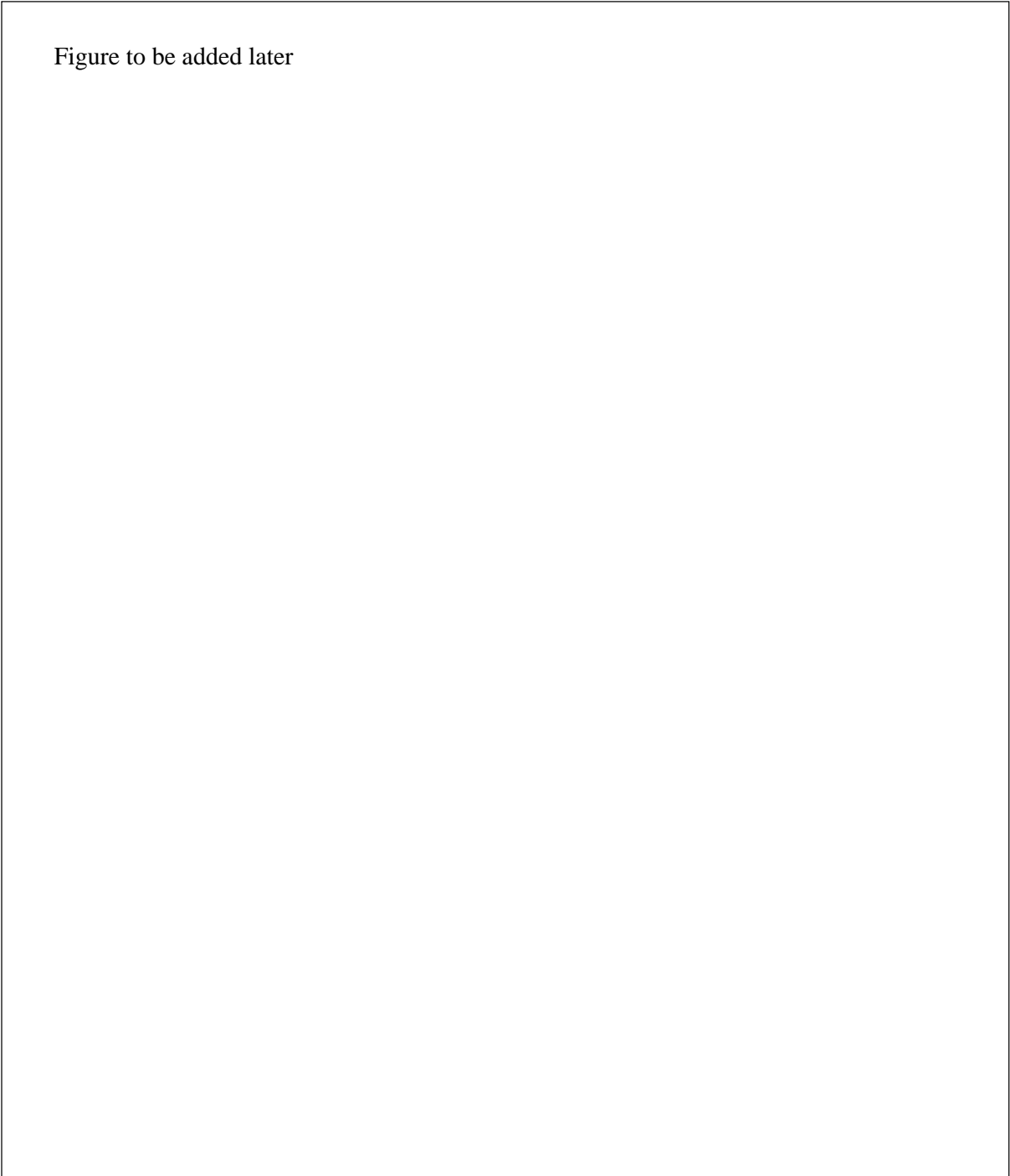


Figure to be added later

Figure 4.1: An ideal detector of arbitrary shape may be made of up small spherical ideal detectors.

confusion, but Chilton's definition makes it clear. Planar fluence is a surface-related quantity, and embeds within it, information about the source. This is best illustrated by an example.

Consider a uniform, monodirectional fluence, Φ and a right cylindrical detector with radius a and depth d . The integrated inward flux of the detector and the fluence are related by,

$$\Phi = \frac{n(\theta)}{\pi a(a \cos \theta + d|\sin \theta|)} , \quad (4.17)$$

where $n(\theta)$ is the number of particles measured with orientation θ , θ is the angle the normal the flat face of the detector with respect to the incident fluence direction. Thus, a measurement of planar fluence can yield the value of the fluence. Equation (4.17) appears to be singular in the limit $d \rightarrow 0, \theta \rightarrow \pi/2$. However, in this limit, $n \rightarrow 0$ as well. Φ really is a well-defined number in this context, and it is a constant in this example, independent of orientation.

4.3 Fluence-related radiometric quantities

4.3.1 Energy fluence

Just as fluence provides a sensible measure of the intensity of a radiation field, the energy fluence provides a way of measuring the ability of the radiation field to effect change, assuming that that change is proportional to the energy in the radiation field. The energy fluence is defined as,

$$\psi_i(\vec{x}, E, t) = E\varphi_i(\vec{x}, E, t) . \quad (4.18)$$

Generally, we will be investigating time and energy integrated energy fluences, such as,

$$\Psi(E, t_i, t_f) = \int_{t_i}^{t_f} dt E\varphi(E, t) , \quad (4.19)$$

$$\Psi(E) = \int_{-\infty}^{\infty} dt E\varphi(E, t) , \quad (4.20)$$

$$\Psi(E_i, E_f) = \int_{E_i}^{E_f} dE \varphi(E) , \quad (4.21)$$

$$\Psi = \int_{-\infty}^{\infty} dE \varphi(E) . \quad (4.22)$$

Note that only for the case where the field is monochromatic, may we write an expression like

$$\Psi = E_0\Phi(E_0) . \quad (4.23)$$

4.4 Attenuation, radiological pathlength

We start by considering the classical derivation of the attenuation law.

Imagine a monoenergetic, monodirectional beam of particles aligned with the \hat{z} -axis, with energy E , with infinitesimal cross sectional area dB impinging normally on a semi-infinite plane of matter. The matter is composed homogeneously of identical “scattering centers” with cross sectional area $\sigma(E)$. At some depth x , the probability of a single particle in the beam interacting with one of the scattering centers is:

$$dp = n_s(\vec{x})(dBdz) \left(\frac{\sigma}{dB} \right) , \quad (4.24)$$

where $n_s(x)$ is the density of scatterers (units: L^{-3}), $n_s(x)dBdx$ is the number of scatterers in $dBdx$, and σ/B is the fractional area covered by the scatterers. Assuming, for the time being, that the scatterers are atomic centers, we may write,

$$dp = \rho(\vec{x}) \frac{N_A}{A} \sigma dz , \quad (4.25)$$

where $\rho(\vec{x})$ is the mass density (units: ML^{-3}), N_A is Avogadro’s number ($6.023 \times 10^{23} \text{ (mole}^{-1})$) and A is the atomic mass (units: $M\text{-mole}^{-1}$). Therefore, the change in primary fluence is described by,

$$d\Phi_0(\vec{x}) = -\Phi_0(\vec{x})\mu\rho(\vec{x})dz , \quad (4.26)$$

where

$$\mu = \frac{N_A}{A} \sigma , \quad (4.27)$$

μ is the *mass linear attenuation coefficient* (units: L^2/M). It is a function of the particle energy. It is usually a constant in space unless the atomic composition of the medium changes. The *mass linear attenuation coefficient* or *macroscopic cross section* is

$$\Sigma(\vec{x}) = \rho(\vec{x})\mu , \quad (4.28)$$

is sometimes used, but is proportional to the density. We mention it here for convenience, but shall rarely use it.

The integral in expression 4.27 is elementary, yielding,

$$\Phi_0(\vec{x}, E) = \Phi_0(\vec{x}; z = 0, E) \exp \left(- \int_0^z dz \mu(E)\rho(x, y, z') \right) . \quad (4.29)$$

The factor,

$$\int_0^z dz \mu(E) \rho(x, y, z') , \quad (4.30)$$

is called the *radiological path*.

We often consider the case where the density of the material is a constant. In this case, the above simplifies to:

$$\Phi_0(\vec{x}, E) = \Phi_0(\vec{x}; z = 0, E) e^{-\mu(E)\rho z} , \quad (4.31)$$

the most familiar form of the exponential attenuation “law”.

4.4.1 Solid angle subtended by a surface

We shall have need for this type of calculation shortly, and establish the notation now.

Consider a surface S , a surface element dS at \vec{x}_S , and its unit normal $\hat{n}(\vec{x}_S)$. The solid angle element of that surface element

$$d\Omega = dS \frac{|\hat{n}(\vec{x}_S) \cdot (\vec{x} - \vec{x}_S)|}{|\vec{x} - \vec{x}_S|^3} , \quad (4.32)$$

which is just the surface element, divided by the r^{-2} term, times the magnitude of the cosine of the angle between \hat{n} and the vector $\vec{x} - \vec{x}_S$.

The total solid angle of the surface with respect to the point \vec{x} is:

$$\Omega_S = \int_{S_v} dS \frac{|\hat{n}(\vec{x}_S) \cdot (\vec{x} - \vec{x}_S)|}{|\vec{x} - \vec{x}_S|^3} , \quad (4.33)$$

where the integral only includes surface elements that are visible to point \vec{x} .

Clearly, the solid angle of any closed surface enclosing \vec{x} is 4π . Also, for closed surfaces, whether or not \vec{x} is located inside the surface, we can relax the visibility criterion, and integrate over the entire surface, as follows.

$$\Omega_S = \left| \int_S dS \frac{\hat{n}(\vec{x}_S) \cdot (\vec{x} - \vec{x}_S)}{|\vec{x} - \vec{x}_S|^3} \right| . \quad (4.34)$$

The absolute value is required because the direction of \hat{n} is arbitrary.

4.4.2 Primary fluence determinations

Distributed volumetric source

Consider an elemental volumetric source, in vacuum, of radiation emitting particles with energy E at a rate $\dot{n}(\vec{x}', \vec{\Omega}, E, t)d\vec{x}'$. A measurement of fluence at \vec{x} is,

$$d\varphi_i(\vec{x}, E, t) = \frac{1}{4\pi} \frac{\dot{n}(\vec{x}', \vec{\Omega}_{\vec{x}-\vec{x}'}, E, t)d\vec{x}'}{(\vec{x} - \vec{x}')^2} \exp\left(-\int_{\vec{x}'}^{\vec{x}} dl \mu(E, l)\rho(l)\right), \quad (4.35)$$

where the integral over l is the straight-line path from the source element to the point of fluence measurement, and accounts for attenuation. Note that both the material composition and the density of the medium can vary along this path.

Integrating over the source gives

$$\varphi_i(\vec{x}, E, t) = \frac{1}{4\pi} \int_V \frac{\dot{n}(\vec{x}', \vec{\Omega}_{\vec{x}-\vec{x}'}, E, t)d\vec{x}'}{(\vec{x} - \vec{x}')^2} \exp\left(-\int_{\vec{x}'}^{\vec{x}} dl \mu(E, l)\rho(l)\right). \quad (4.36)$$

A common example is for a fluence measurement at $\vec{x} = 0$, due to a point, isotropic, monoenergetic source, constant in time, with uniform intervening medium, for which the result is:

$$\Phi(E) = n_0 \frac{e^{-\mu(E)\rho r}}{4\pi r^2}. \quad (4.37)$$

4.4.3 Volumetric symmetry

The result of the previous section may be used to illustrate an interesting symmetry. Imagine that a measurement, M , involves an integral over the volume of a detector, and the response function of the detector $R(E)$. The measurement is expressed as follows,

$$M_{D \leftarrow S}(E) = \int_D d\vec{x} \Phi_i(\vec{x}, E) R(E) = \frac{1}{4\pi} \int_D d\vec{x} \int_S \frac{n(\vec{\Omega}_{|\vec{x}-\vec{x}'|}, E)d\vec{x}'}{(\vec{x} - \vec{x}')^2} \exp\left(-\int_{\vec{x}'}^{\vec{x}} dl \mu(E, l)\rho(l)\right), \quad (4.38)$$

where the subscripts D and S refer to the detector and source regions respectfully, and the source is homogeneous and has the symmetry, $n(\vec{\Omega}_{\vec{x}-\vec{x}'}, E) = n(\vec{\Omega}_{|\vec{x}-\vec{x}'|}, E)$. This is the case for isotropic sources, and can be arranged for directional sources.

Note that

$$M_{D \leftarrow S}(E) = M_{S \leftarrow D}(E), \quad (4.39)$$

under conditions where the material making up the detector is the same as the source, and the source has the above reflection symmetry.

Therefore, under these conditions, the response of the detector to primary fluence in volume D due to source at S is the same as if the source occupied region D and the detector occupied region S .

Simpler “geometry symmetry” relations may be derived from equation 4.38 directly.

4.5 Fano's theorem

Consider the time-independent transport equation in a uniform medium,

$$\vec{\Omega} \cdot \vec{\nabla} n(\vec{x}, \vec{\Omega}, E) + \Sigma(\vec{x}, E) n(\vec{x}, \vec{\Omega}, E) = S(\vec{x}, \vec{\Omega}, E) + \int_0^\infty dE' \int_{4\pi} d\Omega' \Sigma_s(\vec{x}, E' \rightarrow E, \vec{\Omega} \cdot \vec{\Omega}') n(\vec{x}, \vec{\Omega}', E'), \quad (4.40)$$

where $n(\vec{x}, \vec{\Omega}, E)$ is the total scalar flux, $\Sigma(\vec{x}, E)$ is the “out-scattering” macroscopic cross section (“out in the sense of out from $(E, \vec{\Omega})$ to a different energy and/or direction, $\Sigma_s(\vec{x}, E' \rightarrow E, \vec{\Omega} \cdot \vec{\Omega}')$ is the “in-scattering” macroscopic cross section (“in” in the sense of from $(E', \vec{\Omega}')$ to $(E, \vec{\Omega})$, and $S(\vec{x}, \vec{\Omega}, E)$ is the source. Assume that the local density, $\rho(\vec{x})$ is everywhere non-zero, and that Σ , Σ_s , and S are proportional to the local ρ . That is,

$$\begin{aligned} \Sigma(\vec{x}, \vec{\Omega}, E) &= \rho(\vec{x}) \mu(\vec{\Omega}, E) \\ \Sigma_s(\vec{x}, E' \rightarrow E, \vec{\Omega} \cdot \vec{\Omega}') &= \rho(\vec{x}) \mu_s(E' \rightarrow E, \vec{\Omega} \cdot \vec{\Omega}') \\ S(\vec{x}, \vec{\Omega}, E) &= \rho(\vec{x}) s(\vec{\Omega}, E) \end{aligned} \quad (4.41)$$

(The macroscopic usually are unless the atomic composition changes. We are making an assumption about the source, in this case.) Divide by the local density to give,

$$\frac{\vec{\Omega} \cdot \vec{\nabla} n(\vec{x}, \vec{\Omega}, E)}{\rho(\vec{x})} + \mu(E) n(\vec{x}, \vec{\Omega}, E) = s(\vec{\Omega}, E) + \int_0^\infty dE' \int_{4\pi} d\Omega' \mu_s(E' \rightarrow E, \vec{\Omega} \cdot \vec{\Omega}') n(\vec{x}, \vec{\Omega}', E'). \quad (4.42)$$

Now consider the tentative solution for the total scalar flux,

$$\mu(E) n_0(\vec{\Omega}, E) = s(\vec{\Omega}, E) + \int_0^\infty dE' \int_{4\pi} d\Omega' \mu_s(E' \rightarrow E, \vec{\Omega} \cdot \vec{\Omega}') n_0(\vec{\Omega}', E'), \quad (4.43)$$

with the same $\mu(E)$, $\mu_s(E' \rightarrow E, \vec{\Omega} \cdot \vec{\Omega}')$, and $s(\vec{\Omega}, E)$.

Since there should be a unique solution to the transport equation, this solution, independent of \vec{x} is also a solution to the space-dependent equation 4.42. Therefore, invoking this property of uniqueness, we may identify $n(\vec{x}, \vec{\Omega}, E)$ in equation 4.42 with $n_0(\vec{\Omega}, E)$ in equation 4.43.

Therefore, under the conditions specified by expressions 4.41,

$$\vec{\nabla} n(\vec{x}, \vec{\Omega}, E) = 0 . \quad (4.44)$$

In other words, if the macroscopic cross sections and the source are proportional to density, the total scalar flux is independent of \vec{x} , irrespective of how the density changes. In addition, since fluence may be derived from total scalar flux via equation 4.14.

This is a powerful result and, along with the concept of radiation equilibrium has far-reaching consequences for radiation dosimetry. It has already been argued that if radiation equilibrium exists in some volume of space, measurements become insensitive to position of the detector. Now, we find that under these conditions, the density of the medium may change arbitrarily, so long as the source and scattering physics are proportional to density. Again, we shall find that conditions of radiation equilibrium are not uncommon in our applications. Therefore, as we shall see shortly, we wish to determine the dose to water (for example) in a region of near equilibrium, we may use a detector of any density, so long as the atomic composition is the same. Air-filled ionization chambers are such a device. It is truly remarkable that we may take an ionization chamber measurement in water and measure the dose to within an accuracy of a few percent. The few-percent departures account for departures from equilibrium and atomic composition, and may be calculated or measured to within an accuracy of a percent or so with good confidence. (We shall discuss this topic in detail later.) Were this not the case, the entire field of radiation dosimetry, that requires accuracy to within a percent or so for medical physics purposes, would be on very shaky ground. Fortunately, dosimetry methods are very robust, and obtaining sufficient accuracy is always possible in the field with enough care and practice.

Bibliography

- [Chi78] A. B. Chilton. A note on the fluence concept. *Health Physics*, 34:715 – 716, 1978.
- [Chi79] A. B. Chilton. Further Comments on an Alternative Definition of Fluence. *Health Phys.*, 35:637 – 638, 1979.
- [ICR80] ICRU. Radiation Quantities and Units. ICRU Report 33, ICRU, Bethesda, MD, 1980.

Problems

1. (a) What is the definition of fluence?
 (b) What is the definition of planar fluence?
 (c) What does Chilton's theorem on fluence state?
 (d) A monodirectional photon beam characterized by N photons/cm² is incident normally on a cylindrical disk with radius a and depth L . Ignoring interactions in this disk, what is the photon fluence within it? If the disk were rotated Θ degrees with respect to the beam, what would the photon fluence within it be?
 (e) If only the primary photons were allowed to interact in the disk above, qualitatively explain what would the primary photon fluence as a function of Θ would be.

2. A fluence, differential in energy E has the form

$$\varphi(E) = \frac{A}{E} \quad E_{\min} \leq E \leq E_{\max}$$

and zero everywhere else.

- (a) What is the total fluence? Hint: $\Phi = \int dE \varphi(E)$ over the appropriate limits.
 - (b) What is the energy fluence, differential in energy?
 - (c) What is the total energy fluence?
3. A fluence, differential in energy E has the form

$$\varphi(E) = \frac{A}{E^2} \quad E_{\min} \leq E \leq E_{\max}$$

and zero everywhere else. A is a constant.

- (a) What is the total fluence? Hint: $\Phi = \int dE \varphi(E)$ over the appropriate limits.
 - (b) What is the energy fluence, differential in energy?
 - (c) What is the total energy fluence?
4. Assume that a fluence, Φ , is uniform in space and that the radiation is monodirectional. A perfect fluence detector (one that responds equally to all fluence at any energy with the same reading), comprised of a right circular cylinder, is employed to take measurements.
 - (a) If the detector is placed such that its axis is in the same direction as the beam, what track length per unit volume does it measure?

- (b) If the detector is placed such that its axis is perpendicular to the direction of the beam, what track length per unit volume does it measure?
 - (c) If the detector is placed such that its axis is 45° to the direction of the beam, what track length per unit volume does it measure?
5. A perfect planar fluence detector, in the shape of a right circular cylinder, is employed to take measurements in the same radiation field as the above. A perfect planar fluence detector counts the number of particles that strike its surface.
- (a) If the detector is placed such that its axis is in the same direction of the beam, how many particles does it detect?
 - (b) If the detector is placed such that its axis is perpendicular to the direction of the beam, how many particles does it detect?
 - (c) If the detector is placed such that its axis is 45° to the direction of the beam, how many particles does it detect?
6. A small isotropically radiating source is situated at point **A** in vacuum. The rate of particles emanating from the source is constant per unit time. The center of a detector with the shape of a thin disk (diameter \gg length) is situated at point **B**, a flat side facing the source. The detector is so thin that it perturbs negligibly the radiation field.
- (a) As a function of distance, what is the relative number of source particles per unit time that strike the disk's surface?
 - (b) As a function of distance, what is the relative fluence rate of source particles within the detector? A practical realization of fluence is "track length per unit volume".
 - (c) At large distances, what is the ratio fluence rate to the number of particles per unit time that impinge the surface of the detector.
 - (d) Sketch the ratio of the fluence rate to the number that strike the detector surface per unit time normalized to unity at large distances.
7. Consider a spherical volume in vacuum with radius R impinged upon by a monodirectional field of particles with incident fluence Φ_0 . Starting with expression [4.11] calculate explicitly $\int dl$. Draw a conclusion regarding the consistency of Chilton's definition of fluence yields and the ICRU definition for finite volumes.
8. Consider a spherical volume in vacuum with radius R impinged upon by an isotropic field of particles with incident fluence Φ_0 . Calculate Starting with expression [4.11] calculate explicitly $\int dl$. Draw a conclusion regarding the consistency of Chilton's definition of fluence yields and the ICRU definition for finite volumes.

9. (a) As a function of z , what is the fluence inside and outside an infinite plane (in the lateral sense) at $z = Z$, of thickness t with a uniform volume source that has a constant attenuation factor Σ ? What happens when $z \rightarrow Z$ and $t \rightarrow 0$?
- (b) An infinitely thin uniform line source of radiation is situated at $\vec{x} = ([-L \rightarrow L], 0, D)$. What is the primary fluence in vacuum at $\vec{x} = (0, 0, 0)$, with and without attenuation?
- (c) An infinitely thin uniform disk source of radiation is situated at $\vec{x} = (|\vec{\rho}| \leq a, D)$. What is the primary fluence in vacuum at $\vec{x} = (0, 0, 0)$, with and without attenuation?
10. A radioactive monoenergetic source of photons is sprayed uniformly on a thin spherical shell, with an areal decay rate \dot{n}_0 [$1/(L^2T)$]. In the following, derive all your results, show your work and discuss the results.

- (a) Assume the shell is infinitely thin, and is filled inside and outside with vacuum. The shell has radius R . As a function of r , the distance from the center, what is the fluence rate $\dot{\varphi}(r)$ for $0 \leq r < \infty$?
- (b) Under the assumptions stated in (a), what is $\dot{\varphi}(0)$?
- (c) Under the assumptions stated in (a), what is the leading order asymptotic behavior of $\dot{\varphi}(r)$ in the limit $r \gg R$? From your expression, what can you conclude?
- (d) Now assume that the sphere is filled with material of uniform density, ρ , and atomic composition, characterized by a mass linear attenuation coefficient, μ , which attenuates the photons and does not cause any scattered radiation of any kind. Show that the fluence rate inside the sphere is given by:

$$\dot{\varphi}(r) = \frac{\dot{n}_0}{2x} \int_{1-x}^{1+x} d\nu \frac{e^{-\epsilon\nu}}{\nu},$$

where $x = r/R$, and $\epsilon = \mu\rho R$.

- (e) Under conditions (d), show that the fluence rate outside the sphere may be expressed as:

$$\dot{\varphi}(r) = \frac{\dot{n}_0}{2x} \left[\frac{1}{2} \log \left(\frac{x+1}{x-1} \right) + \int_{\sqrt{x^2-1}}^{x+1} d\nu \frac{e^{-\epsilon l(x,\nu)}}{\nu} \right],$$

where $l(x, \nu) = (1 + \nu^2 - x^2)/\nu$.

- (f) Take the limit $\epsilon \rightarrow \infty$ in (e) and discuss your result.
- (g) Obtain the leading order behavior in x for (f). Interpret your result.
11. Consider an isotropically radiating source of radiation at point **A**. An observer is at point **B**, some distance away from **A**. The observer wants to make it to location **C** with as little exposure as possible to the radiation.

- Points **A**, **B**, **C** form an equilateral triangle.
- The observer can only move at constant velocity.
- The dimensions of the observer and the source are very small compared to the distance between **A** and **B**.

The observer considers two possible paths:

Path 1 A straight-line path between **B** and **C**.

Path 2 A circular path between **B** and **C** with the center of the circle situated at point **A**.

Ignoring air scatter or scatter from the ground,

- (a) Which is the better path to take?
 - (b) What is the ratio of the exposure of Path 1 to Path 2?
 - (c) It turns out that neither of the above paths is the optimum solution to this problem. What is the best path to take? Hint: A technique called “Calculus of Variations” may be used to solve this problem efficiently.
12. A dirty bomb is a conventional explosive packed with radioactive material. Dirty bombs are nasty, anti-social things.

(a) **The full calculation**

Compute the fluence at point $(x, y) = (L, 0)$ from a dirty bomb (you may consider it to be a point source) launched with velocity v at angle θ_0 with respect to the ground. v is large so that we may approximate the trajectory of the projectile as $y = x \tan \theta_0$, $0 \leq x \leq \infty$. The motion takes place entirely in the $x - y$ plane. The activity (photons/second) of the source is N_0 and is made up entirely of monoenergetic photons. Account for attenuation through the attenuation constant μ and scatter using a build-up factor. The buildup factor is discussed starting on page 53 of Attix.

The resulting integral can not be performed analytically. Leave your calculation in integral form.

(b) **An approximate calculation**

Now, ignore attenuation and scatter. Perform the integral. You might find the following expression useful:

$$\int_{z_0}^{z_1} dz \frac{1}{z^2 + 1} = \arctan z_1 - \arctan z_0$$

Discuss the following:

- i. $v \rightarrow 0, v \rightarrow \infty$
- ii. $L \rightarrow 0, L \rightarrow \infty$
- iii. $\theta_0 \rightarrow 0, \theta_0 = \pi/2$

Chapter 5

Photon dose calculation models

5.1 Kerma, collision kerma, and dose for photo irradiation

5.1.1 Kerma

Now we specialize to the case where the incident particle field is comprised of photons, and consider energy deposition in a medium.

Consider a volume, V , in space comprised of some medium, where a photon with energy E_γ , interacts, and transfers energy to charged particles. The interactions that cause charged particles to be set into motion occur via three mechanisms: 1) the Compton or incoherent interaction, 2) pair (including triplet and higher order) production, and 3) the photoelectric effect. Figure 5.1 illustrates this. Each of these interactions is governed by its own microscopic cross section, and the individual mass attenuation coefficients are called $\mu_{\text{inc}}(E_\gamma)$, $\mu_{\text{pp}}(E_\gamma)$, and $\mu_{\text{ph}}(E_\gamma)$, respectfully. Since Rayleigh (coherent) scattering does not set charged particles into motion, we ignore it in this discussion. In this figure we ignore all secondary interactions, except for the annihilation of the positron in the case of pair production and the corresponding annihilation quanta. The relative proportions of the primary photon interacting via one of these interaction channels (branching ratios) are given by $\mu_{\text{inc}}(E_\gamma)/\mu(E_\gamma)$ for the incoherent interaction, $\mu_{\text{pp}}(E_\gamma)/\mu(E_\gamma)$ for pair production, and $\mu_{\text{ph}}(E_\gamma)/\mu(E_\gamma)$ for the photoelectric interaction, where $\mu(E_\gamma) = \mu_{\text{inc}}(E_\gamma) + \mu_{\text{pp}}(E_\gamma) + \mu_{\text{ph}}(E_\gamma)$.

In the kerma approximation, we imagine that the volume shrinks to a point, but on its way to collapse at this point, the primary charged particle tracks, and all their daughter particles (δ -rays, and bremsstrahlung γ 's), except for the annihilation quanta and Compton scattered photon from the primary interaction, are trapped within V , as depicted in Figure 5.2. These charged particles have some kinetic energy associated with them, and that energy

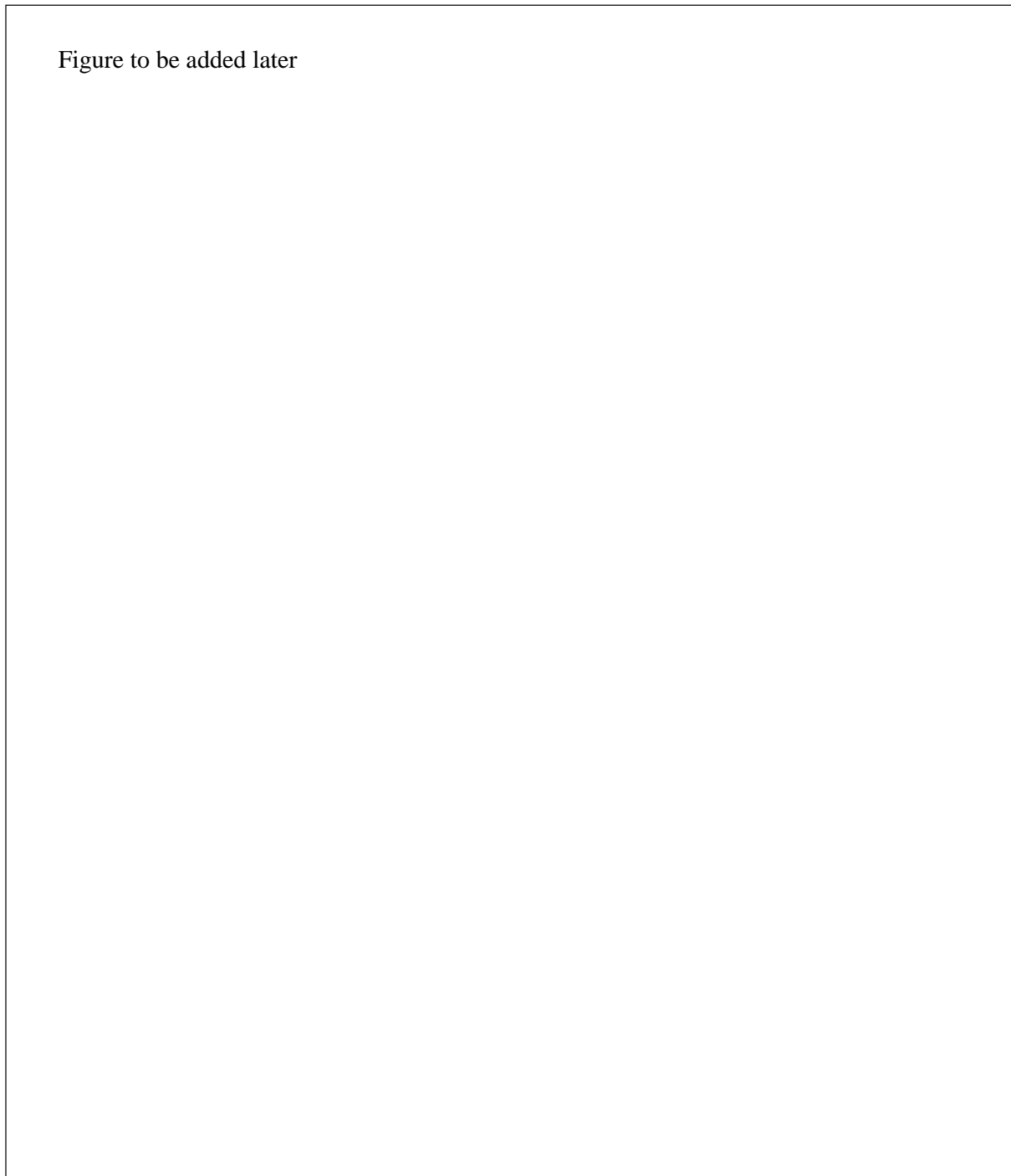


Figure 5.1: Idealizations of photons interacting in matter, employed to construct the Kerma.

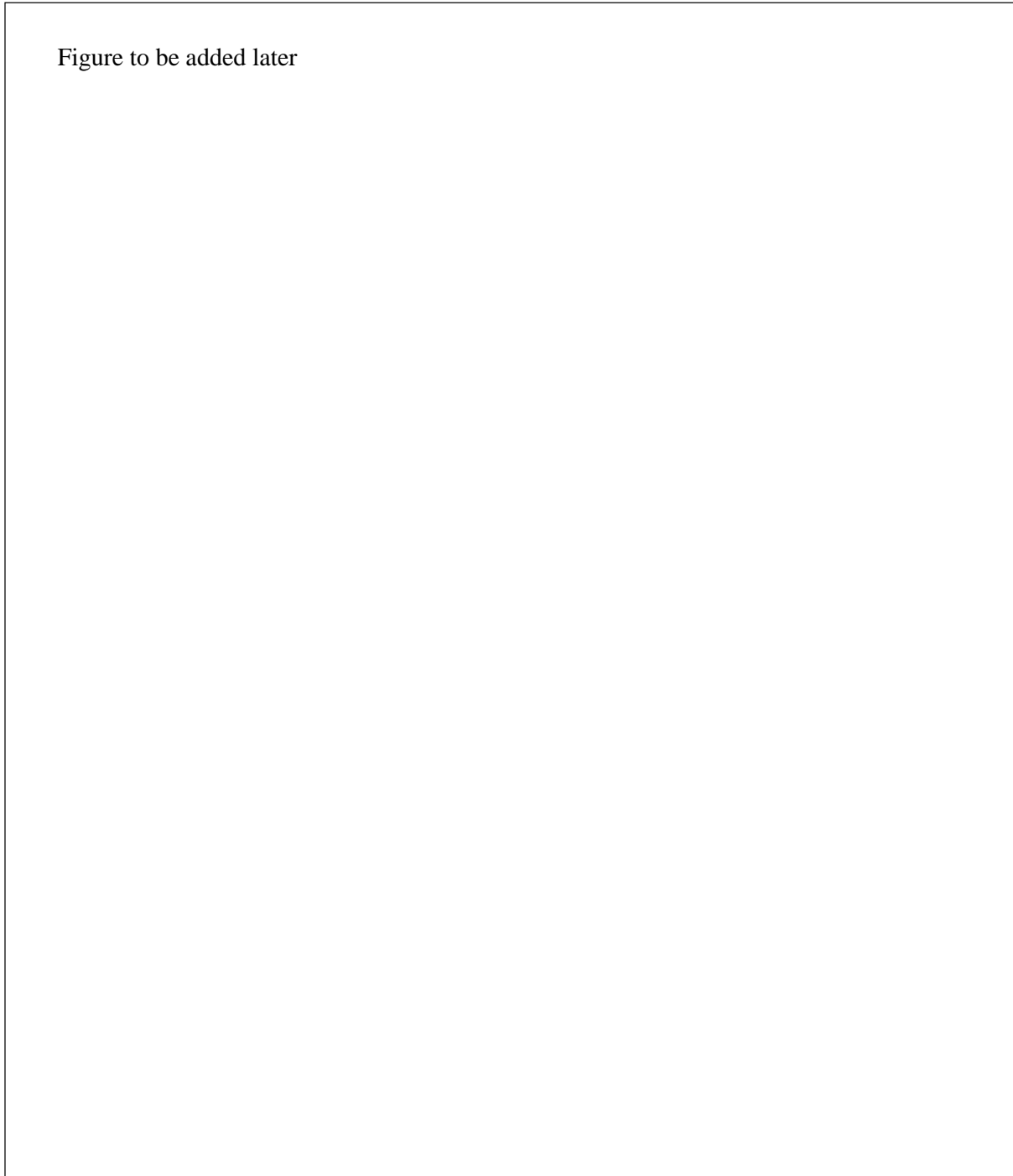


Figure 5.2: Trapping the primary charged particles within a small volume to illustrate Kerma.

is “trapped” inside V . The Kerma is defined as the ratio of the kinetic energy of the primary electrons trapped in this way, less the energy of the annihilation quanta that arise from the annihilation of the positrons within V , with one of the electrons in an atomic shell of one of the constituent atoms in V .

The *mass energy transfer coefficient* for each interaction channel is calculated according to,

$$\mu_{\text{tr}}(E_\gamma) = \frac{\mu(E_\gamma)}{E_\gamma} \int_0^\infty dE_{e^\pm}^{\text{kin}} E_{e^\pm}^{\text{kin}} \tilde{\sigma}(E_\gamma, E_{e^\pm}^{\text{kin}}), \quad (5.1)$$

where $\tilde{\sigma}()$ is the microscopic cross section that is normalized according to,

$$\tilde{\sigma}(E_\gamma, E_{e^\pm}^{\text{kin}}) = \sigma(E_\gamma, E_{e^\pm}^{\text{kin}}) / \left(\int_0^\infty dE_{e^\pm}^{\text{kin}} \sigma(E_\gamma, E_{e^\pm}^{\text{kin}}) \right). \quad (5.2)$$

Expression 5.1 is somewhat symbolic. However, it is meant to define the ratio of kinetic energy that goes into the primary charged particle(s) to the kinetic energy of the primary photon. Tables of $\mu_{\text{tr}}(E_\gamma)$ may be found in standard reference texts, for example, Attix’s book [[Att86]].

Finally, we may state the definition of Kerma,

$$K(\vec{x}) = \int_0^{E_\gamma^{\text{max}}} dE_\gamma \Phi(\vec{x}, E_\gamma) E_\gamma \mu_{\text{tr}}(E_\gamma), \quad (5.3)$$

An alternative microscopic form for K is,

$$K(\vec{x}) = \lim_{\Delta V \rightarrow 0} \frac{\langle \Delta \varepsilon_{\text{kin}}^0 \rangle}{\rho(\vec{x}) \Delta V}, \quad (5.4)$$

where $\langle \Delta \varepsilon_{\text{kin}}^0 \rangle$ is the expectation value of the kinetic energy of primary charged particles set in motion in ΔV . Note that K has units $E \cdot M^{-1}$.

5.1.2 Collision Kerma

If one were more faithful to the physics, and allowed the primary electron to generate δ -rays, and also allowed all charged particles to create bremsstrahlung, we could imagine this process to look somewhat like the idealized version shown in Figure 5.3. This time, allow V to shrink. However, the shrinking traps all charged particles, and allows all photons to escape, as seen in Figure 5.4. This concept is intended to separate local deposition of energy, ionizations and excitations by charged particles, from non-local energy transport, carried away by photons.

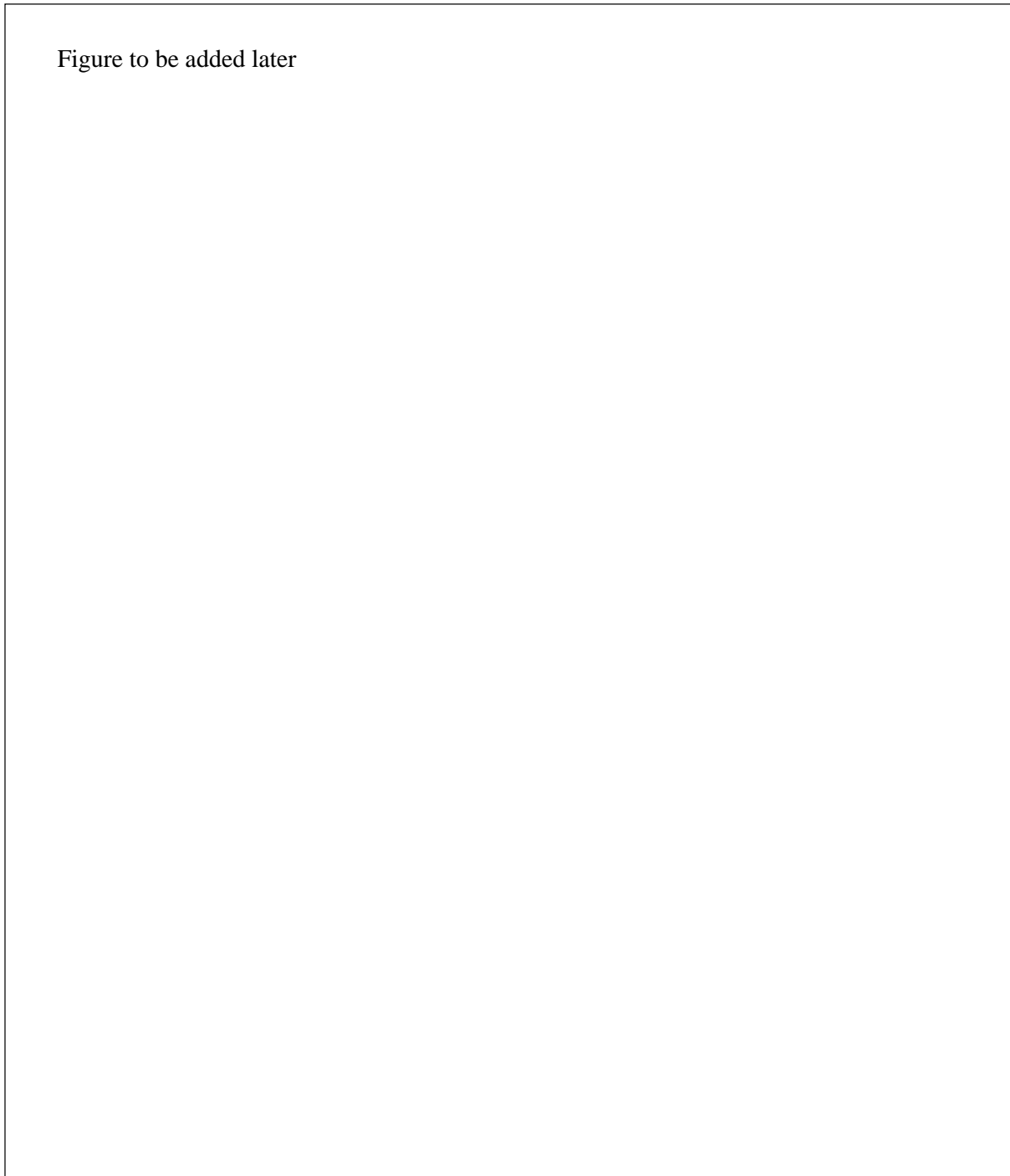


Figure 5.3: Idealizations of photons interacting in matter, employed to construct the collision Kerma.

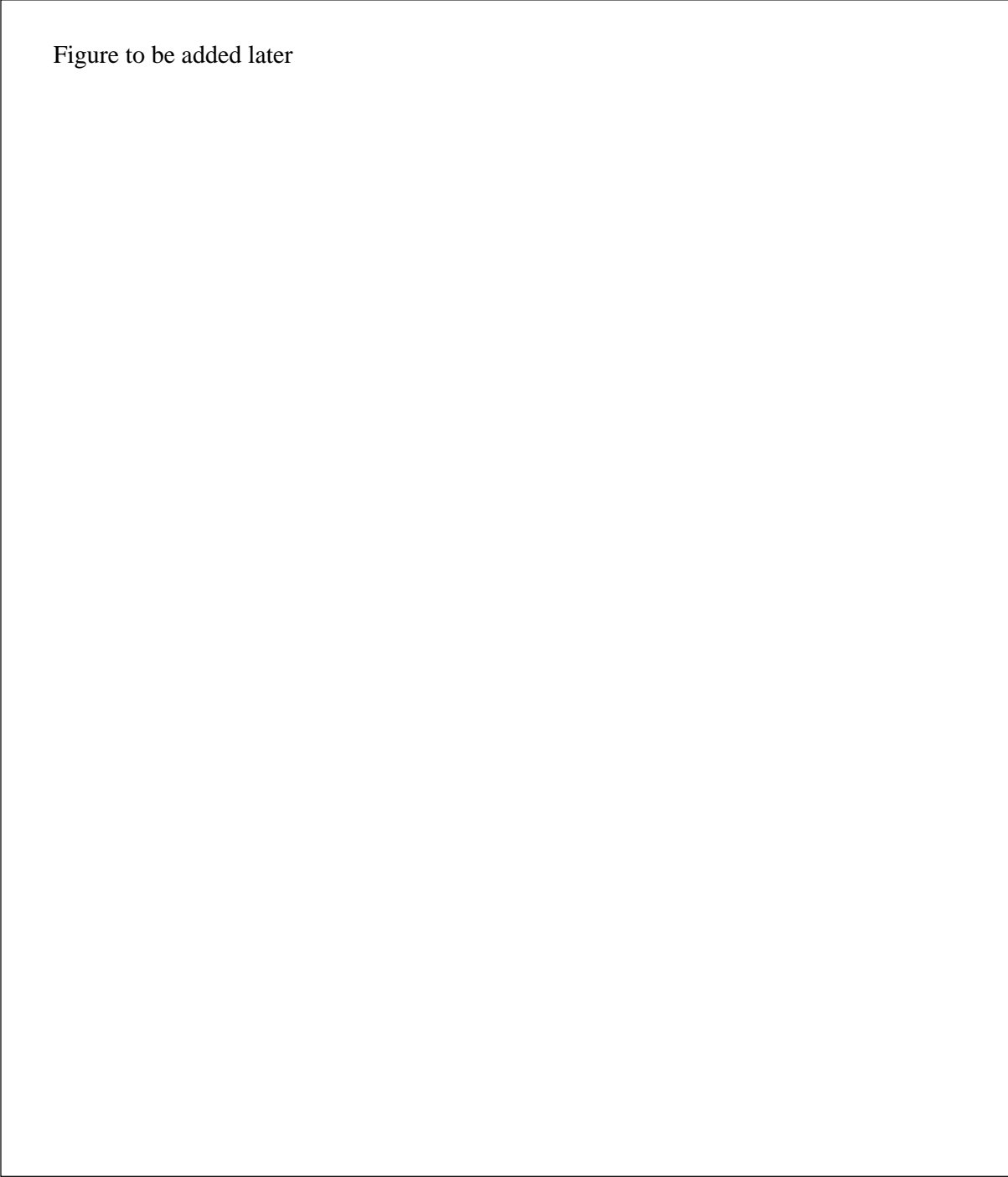


Figure to be added later

Figure 5.4: Trapping all the charged particles within a small volume to illustrate collision Kerma.

This fraction of energy carried away by secondary photons is characterized by the *mass energy absorption coefficient* $\mu_{\text{en}}(E_\gamma)$ and allows us to define the collision Kerma,

$$K_c(\vec{x}) = \int_0^{E_\gamma^{\text{max}}} dE_\gamma \Phi(\vec{x}, E_\gamma) \mu_{\text{en}}(E_\gamma) , \quad (5.5)$$

An alternative microscopic form for K is,

$$K_c(\vec{x}) = \lim_{\Delta V \rightarrow 0} \frac{\langle \Delta \varepsilon_{\text{kin}} \rangle}{\rho(\vec{x}) \Delta V} , \quad (5.6)$$

where $\langle \Delta \varepsilon_{\text{kin}} \rangle$ is the expectation value of the energy of ionizations and excitations caused by charged particles set in motion in ΔV . Note that $\mu_{\text{en}}(E_\gamma) < \mu_{\text{tr}}(E_\gamma)$, hence, $K_c(\vec{x}) < K(\vec{x})$. Tables of $\mu_{\text{en}}(E_\gamma)$ may be found in standard reference texts, for example, Attix's book [Att86]. It should be mentioned that $\mu_{\text{en}}(E_\gamma)$ can be estimated analytically by integrating the bremsstrahlung and annihilation cross sections as a function of electron or positron energy. However, this neglects the small component of bremsstrahlung that arises from δ -rays. One can appeal to Monte Carlo calculations to provide the small corrections necessary.

5.1.3 Dose

Finally, we get to *dose*. Consider Figure 5.5, that illustrates the definition of dose. Dose is only defined as follows,

$$D(\vec{x}) = \lim_{\Delta V \rightarrow 0} \frac{\langle \Delta \varepsilon_{\text{in}}^r - \Delta \varepsilon_{\text{out}}^r \rangle}{\rho(\vec{x}) \Delta V} , \quad (5.7)$$

where $\Delta \varepsilon_{\text{in}}^r$ is the total kinetic energy of all particles entering ΔV and $\Delta \varepsilon_{\text{out}}^r$ is the total kinetic energy of all particles leaving ΔV . Thus, although the charged particles are generated within ΔV , and may be transported in the vicinity of ΔV , they are allowed to leave. The energy left behind goes into ionizations and excitations, and these effect radiological change. Moreover, the effects of electron transport are incorporated. These are important, particularly at higher energies where the electrons may transport a large distance (in terms of the underlying structures) away from their point of generation.

Thus we see how collision Kerma and Kerma are approximations to dose, the first ignoring electron transport, and the second ignoring non-local deposition do to radiant photons. Under certain situations, collision Kerma may be a good approximation if there exists a state of charged particle equilibrium. This sometimes occurs, but never in cases where there is a strong charged particle disequilibrium. Without getting into details of electron transport, we may illustrated some of these concepts using idealized thought experiments.

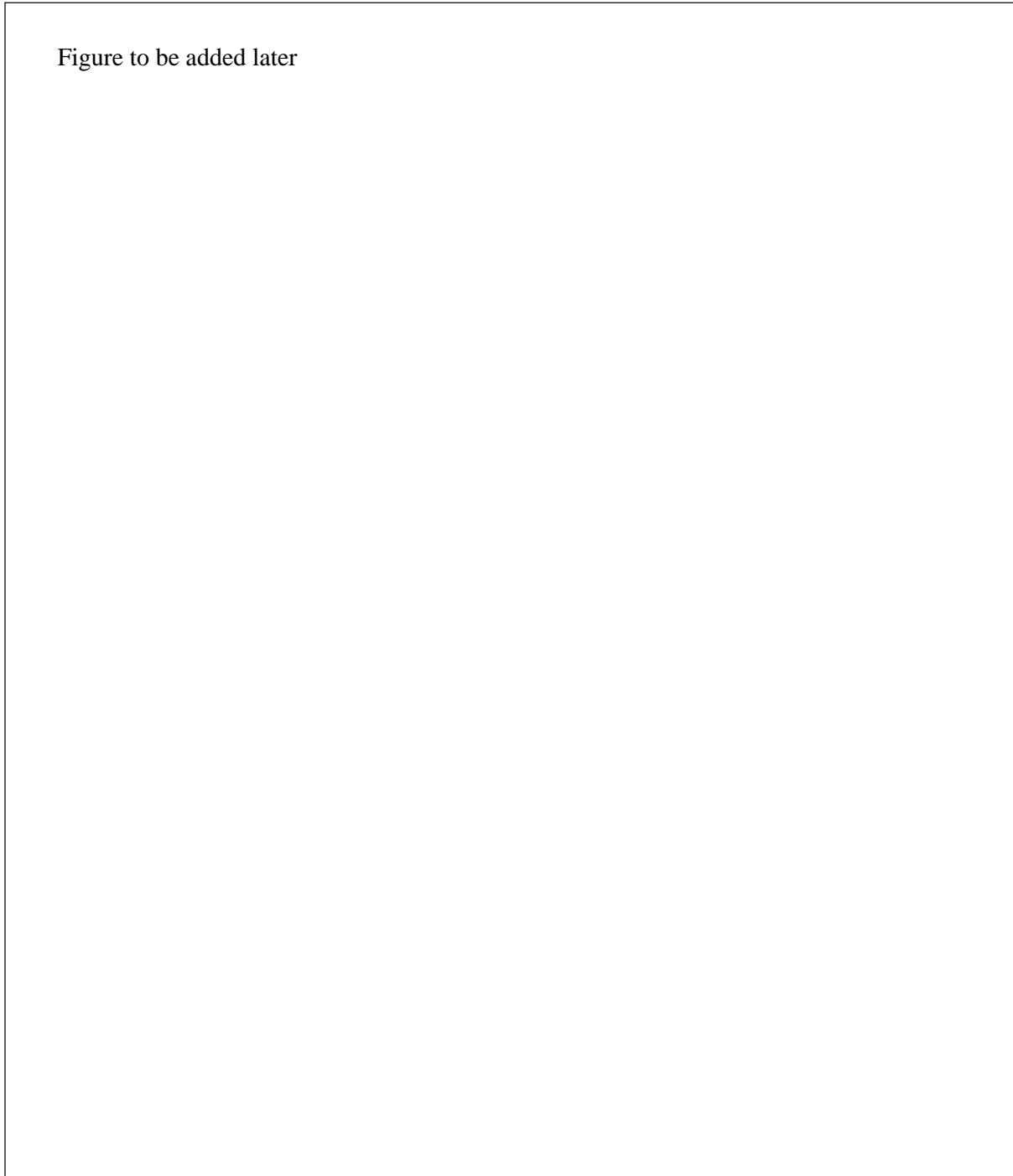


Figure 5.5: Idealizations of photons interacting in matter, employed to construct the dose.

5.1.4 Comparison of dose deposition models

Let us construct a fictitious medium that allows primary photons to interact with it, but then by some mysterious process, regenerates the primary photon at the point of interaction with the original energy and direction¹. Given this artifice, we may sketch the behavior with depth, of $K^0(\vec{\rho}, z)$, $K_c^0(\vec{\rho}, z)$ and $D^0(\vec{\rho}, z)$, due to a beam of monoenergetic (E_0) photons, with intensity Φ_0 incident normally at the surface ($0 \leq \vec{\rho} \leq R_B$), and monodirectionally ($\vec{\Omega} = \hat{z}$) on a semi-infinite plane ($0 \leq \vec{\rho} < \infty, z > 0$) of this fictitious material. Everywhere else, there is vacuum. (We are only considering dose due to primary photons.)

By construction, K^0 and K_c^0 are constants inside the “tube” defined by the beam. So, in this example,

$$K^0(\vec{\rho}, z) = \Theta(R_B - |\vec{\rho}|)\Psi_0\mu_{\text{tr}}(E_0)$$

,

and

$$K_c^0(\vec{\rho}, z) = \Theta(R_B - |\vec{\rho}|)\Psi_0\mu_{\text{en}}(E_0).$$

To sketch $D^0(\vec{\rho}, z)$ we need only introduce the barest of details of electron transport, namely, 1) electrons have a finite range, that we’ll call R_e , 2) because of multiple scattering, electron transport is ergodic within a sphere of radius R_e *i.e.* will visit the entire sphere given enough electrons starting at its center), and 3) the electron transport is somewhat forward directed within this sphere. Given this knowledge we may sketch qualitatively the 3 quantities in question. This is done in Figure 5.6. In this example, we have considered that $R_e < R_B$, and shown the central axis dose, and two lateral profiles, one where $z < R_e$ and one where $z > R_e$.

We note the following features. K^0 and K_c^0 are constants within the tube of the beam and zero everywhere else. $K^0 > K_c^0$ within the tube of the beam. $D(|\vec{\rho}|, 0)$ is non-zero at the surface of the material, because electrons can transport backwards (via multiple scattering) from their point of generation.

- $D(|\vec{\rho}| < R_B - R_e, z \geq R_e) = K_c^0(|\vec{\rho}| < R_B - R_e, z \geq R_e)$.
- $D(|\vec{\rho}| < R_B + R_e, z > 0)$ is non-zero, and zero elsewhere.
- $D(R_B - R_e \leq |\vec{\rho}| \leq R_B + R_e, z \geq R_e)$ falls monotonically to zero at $|\vec{\rho}| = R_B + R_e$ and equals K_c^0 at $|\vec{\rho}| = R_B - R_e$.

¹A purist might object to our violation of physical laws to illustrate a pedagogical point at the juncture. Certainly such a material does not exist in reality. However, it is very easy to do so in a Monte Carlo calculation, or in theory. Moreover, we shall use exactly such a construct later on in our development of ionization chamber theory.

Figure to be added later

Figure 5.6: $K^0(\vec{\rho}, z)$, $K_c^0(\vec{\rho}, z)$ and $D^0(\vec{\rho}, z)$ for our model problem.

- $D(|\vec{\rho}| < R_B - R_e, z < R_e) < K_c^0$ there.
- $D(R_B - R_e \leq |\vec{\rho}| \leq R_B + R_e, z < R_e)$ falls monotonically zero at $|\vec{\rho}| = R_B + R_e$.

Thus, we see by construct, we have formed a zone of radiation equilibrium within the coordinates ($|\vec{\rho}| < R_B - R_e, z \geq R_e$) for which we may easily predict the dose from the collision kerma. In this zone, we may also vary the density of the medium arbitrarily and still calculate the same dose! Such is the power of the results of Fano's theorem combined with the concept of radiation equilibrium!

The zone ($R_B - R_e \leq |\vec{\rho}| < R_B - R_e, z \geq 0$) is the region of strong electron disequilibrium. Without further insight we can only be qualitative. The zone ($|\vec{\rho}| < R_B - R_e, z \geq 0$) has no dose because electrons can not reach there. The zone ($z < 0$) has no dose because there is no material there to deposit in.

5.1.5 Transient charged particle equilibrium

The previous section bent the laws of physics to illustrate the power of radiation equilibrium. Even when we allow for primary beam attenuation, however, we are close to this idealization. Consider the same beam, but now, allow the medium to attenuate the primary photons. Now, K^0 and K_c^0 are no longer constants inside the "tube" defined by the beam. However, we may still calculate them easily. In this example,

$$K^0(\vec{\rho}, z) = \Theta(R_B - |\vec{\rho}|) \Psi_0 \mu_{\text{tr}}(E_0) \exp[-\mu(E_0) \rho(\vec{x}) z] ,$$

and

$$K_c^0(\vec{\rho}, z) = \Theta(R_B - |\vec{\rho}|) \Psi_0 \mu_{\text{en}}(E_0) \exp[-\mu(E_0) \rho(\vec{x}) z] .$$

The same considerations with respect to electron transport apply, and we may draw the following conclusions:

- $D(|\vec{\rho}| < R_B - R_e, z \geq R_e) > K_c^0(|\vec{\rho}| < R_B - R_e, z \geq R_e)$, but only slightly.
- $D(|\vec{\rho}| < R_B + R_e, z > 0)$ is non-zero, and zero elsewhere.
- $D(R_B - R_e \leq |\vec{\rho}| \leq R_B + R_e, z \geq R_e)$ falls monotonically to zero at $|\vec{\rho}| = R_B + R_e$ and equals it's equilibrium value, slightly greater than K_c^0 at $|\vec{\rho}| = R_B - R_e$.
- $D(|\vec{\rho}| < R_B - R_e, z < R_e) < K_c^0$ there. (It can be slightly greater at $z = R_e$, depending on the model of electron transport.)

Figure to be added later

Figure 5.7: $K^0(\vec{\rho}, z)$, $K_c^0(\vec{\rho}, z)$ and $D^0(\vec{\rho}, z)$ for our more realistic model.

- $D(R_B - R_e \leq |\vec{\rho}| \leq R_B + R_e, z < R_e)$ falls monotonically zero at $|\vec{\rho}| = R_B + R_e$.

These results are illustrated in Figure 5.7.

The region forms a zone of *transient charged particle equilibrium* (TCPE) within the coordinates ($|\vec{\rho}| < R_B - R_e, z \geq R_e$) for which we may easily predict the dose from the collision kerma, plus a small correction. In this zone, we may also vary the density of the medium arbitrarily and still calculate nearly the same dose! Generally the perturbations by the density variations is quite small owing to the fact that $R_e \ll \mu^{-1}$. Hence, the intensity of the primary photon fluence varies very little over distances characteristic of electron transport.

The small correction factor arises because the electrons are produced (on average) upstream from where they deposit dose. The attenuation is less then, hence the correction factor is greater than unity, but only slightly. This correction factor is often quoted as $\exp(\mu(E_0)\langle z_{\text{drift}} \rangle)$, for monoenergetic beams. This is really an approximation and depends on the electron transport model. We shall have more to say on this topic after we cover the basics of electron transport.

5.1.6 Dose due to scattered photons

We return to our general expression for dose in the collision Kerma approximation, expressed by Equation 5.5, however, we now split off the primary photon fluence from all other photon fluences, that arise from scattering process. That is,

$$K_c(\vec{x}) = K_c^0(\vec{x}) + K_c^s(\vec{x}) = K_c^0(\vec{x}) + \int_0^{E_s^{\max}} dE_s \Phi_s(\vec{x}, E_s) \mu_{\text{en}}(E_s) . \quad (5.8)$$

In order to calculate $\Phi_s(\vec{x}, E_s)$, we start with a fluence of primary photons on a surface S , $\Phi_0(\vec{x}_S, E_\gamma)$. We assume that the photon fluence arising from an interaction of the primary photon at \vec{x}' is given generically by a function of the form,

$$\Phi_s(\vec{x}, E_s; \vec{x}', E_\gamma) = \frac{f(E_\gamma, E_s, \cos \theta_{\vec{x}', \vec{x} - \vec{x}'})}{4\pi |\vec{x} - \vec{x}'|^2} \exp \left(- \int_0^{|\vec{x} - \vec{x}'|} dl \rho(\vec{l}) \mu(\vec{l}, E_s) \right) , \quad (5.9)$$

in other words, a function of the distance from the interaction, the energy of the photon that set the scattered photon into motion, and the angle between the initiating photon direction and vector from that point to \vec{x} ,

$$\cos \theta_{\vec{x}', \vec{x} - \vec{x}'} = \frac{\vec{x}' \cdot (\vec{x} - \vec{x}')}{|\vec{x}'| |\vec{x} - \vec{x}'|} .$$

and the radiological path and attenuation from the interaction point.

The number of a primary photons with energy E_γ starting at \vec{x}_S and interacting at \vec{x}' is,

$$n(\vec{x}', E_\gamma) d\vec{x}' dE_\gamma = \Phi_0(\vec{x}_S, E_\gamma) \rho(\vec{x}') \mu(E_\gamma) d\vec{x}' dE_\gamma \exp\left(-\int_0^{|\vec{x}'-\vec{x}_S|} dl \rho(\vec{l}) \mu(\vec{l}, E_\gamma)\right), \quad (5.10)$$

accounting for the attenuation via the radiological path, and an incident photon fluence that is differential in energy.

Therefore,

$$K_s(\vec{x}) = \int d\vec{x}' \int_0^\infty dE_\gamma n(\vec{x}', E_\gamma) \int_0^\infty dE_s \Phi_e(\vec{x}, E_s; \vec{x}', E_\gamma) E_s \mu_{\text{en}}(E_s), \quad (5.11)$$

which also may be written,

$$K_s(\vec{x}) = \int d\vec{x}' \rho(\vec{x}') \int_0^\infty dE_\gamma K_c(\vec{x}', E_\gamma) \frac{1}{\langle E_e(E_\gamma) \rangle} \int_0^\infty dE_s \Phi_s(\vec{x}, E_s; \vec{x}', E_\gamma) E_s \mu_{\text{en}}(E_s), \quad (5.12)$$

where $\langle E_e(E_\gamma) \rangle$ is the mean energy deposited by an electron and its δ -rays set in motion by a photon with energy E_γ .

Bibliography

- [Att86] F. H. Attix. *Introduction to Radiological Physics and Radiation Dosimetry*. Wiley, New York, 1986.

Problems

There are no problems made up for this chapter yet.

Chapter 6

Electron dose calculation models

6.1 The microscopic picture of dose deposition

All energy deposition occurs due to electron transport, irrespective of the quality of the initiating interaction, be it high-energy photons or electrons. The high-energy photons set primary electrons into motion and these lose energy through creating δ -rays, which make more δ -rays, and so on. The only real difference between high-energy photons or electrons as sources is that high-energy electrons are a “surface” dose for subsequent electron sub-tracks, while high-energy photons are a volume dose for these subsequent electron sub-tracks.

Eventually, the bulk of the damage is done by electrons in the 10 eV range, that cause ionizations directly on the DNA itself (*direct effect*), or by ionizing water in the surrounding sheath of the DNA molecule. These radicals may then diffuse, before de-excitation, may diffuse to the DNA molecule, and cause further damage (*indirect effect*). Currently it is thought that the direct and indirect effects are about equal in their abilities to cause lesions on the DNA, and two and especially more lesions within two base pairs on the DNA chain, are thought to be lethal to the cell, in the sense that its reproduction can not continue.

So, a complete picture of dosimetry and radiotherapy calculation might include a precise calculation of the electron fluences down to energies less than 10 eV and coupling those with response functions that measure damage. In this realm, we are still in the early stages of predicting damage at this level of resolution. For now, for most calculations, we are limited to transport down to 1 keV or so, even by the best Monte Carlo codes, and rely upon “dose” as a surrogate for our lack of fine detail. Keep in mind, however, that dose, as defined previously, is only an approximate picture of the truth.

These approximations are buried deeply into our concept of “stopping” power, which we now discuss in detail.

6.2 Stopping power

Consider the picture of electron slowing down in condensed matter, as depicted in Figure 6.1. The macroscopic picture shows an entire electron track. For typical radiotherapy energy electrons, in the 1 - 20 MeV range, this track, in water can be about 5mm to 10cm in total length. These electron tracks twist and turn as they encounter nuclei that change their direction, usually smoothly, but occasionally by large discrete angular jumps. They also ionize and excite atoms along the way, and lose energy in those processes. There can also be bremsstrahlung that removes energy from the electron and transports it out of the vicinity. It appears that at this level of resolution, the electron tracks can be described by continuous functions in space, and the loss of energy along the way described similarly.

The mesoscopic picture shows that all tracks have subtracks of δ -rays, with their own subtracks and so on. This level of resolution is sub-millimeter. We have turned off angular scattering to simplify the representation. The tracks look similar to a “fractal tree” although the bifurcation into separate tracks can not continue forever. It also appears as if the “continuous” functional distributions persist at this level.

Finally, we arrive at the microscopic level. (Perhaps nanoscopic would have been more apropos.) Here, we see the individual atoms, and see that the “continuous” model of energy deposition breaks down. This is the realm of microdosimetry where our definition of dose, as defined earlier in Equation 5.7 becomes problematic. Recall that definition,

$$D(\vec{x}) = \lim_{\Delta V \rightarrow 0} \frac{\langle \Delta \varepsilon_{\text{in}}^r - \Delta \varepsilon_{\text{out}}^r \rangle}{\rho(\vec{x}) \Delta V}, \quad (6.1)$$

we note that our continuous model no longer applies. Energy is transferred via discrete ionisation and excitation events, and the fluctuations in $\langle \Delta \varepsilon_{\text{in}}^r - \Delta \varepsilon_{\text{out}}^r \rangle$ are large. Moreover, since the events are discrete, the spatial and temporal correlations of the individual events will play a critical role in our understanding of the radiological effect of electron “dose”. Aside from recognizing its importance, and noting that this is the launchpad of a microdosimetric discussion, an interesting and rich science unto itself. For now, we step back and draw the line at the mesoscopic level, and pretend that the electron energy losses are described by continuous functions, and that “dose”, as defined above is well-defined.

This continuous slowing down description has several realizations.

6.2.1 Total mass stopping power

The *total mass stopping power* of electrons and photons is calculated from the first energy moment of the macroscopic cross section (Møller, Bhabha, and bremsstrahlung) in the following way.

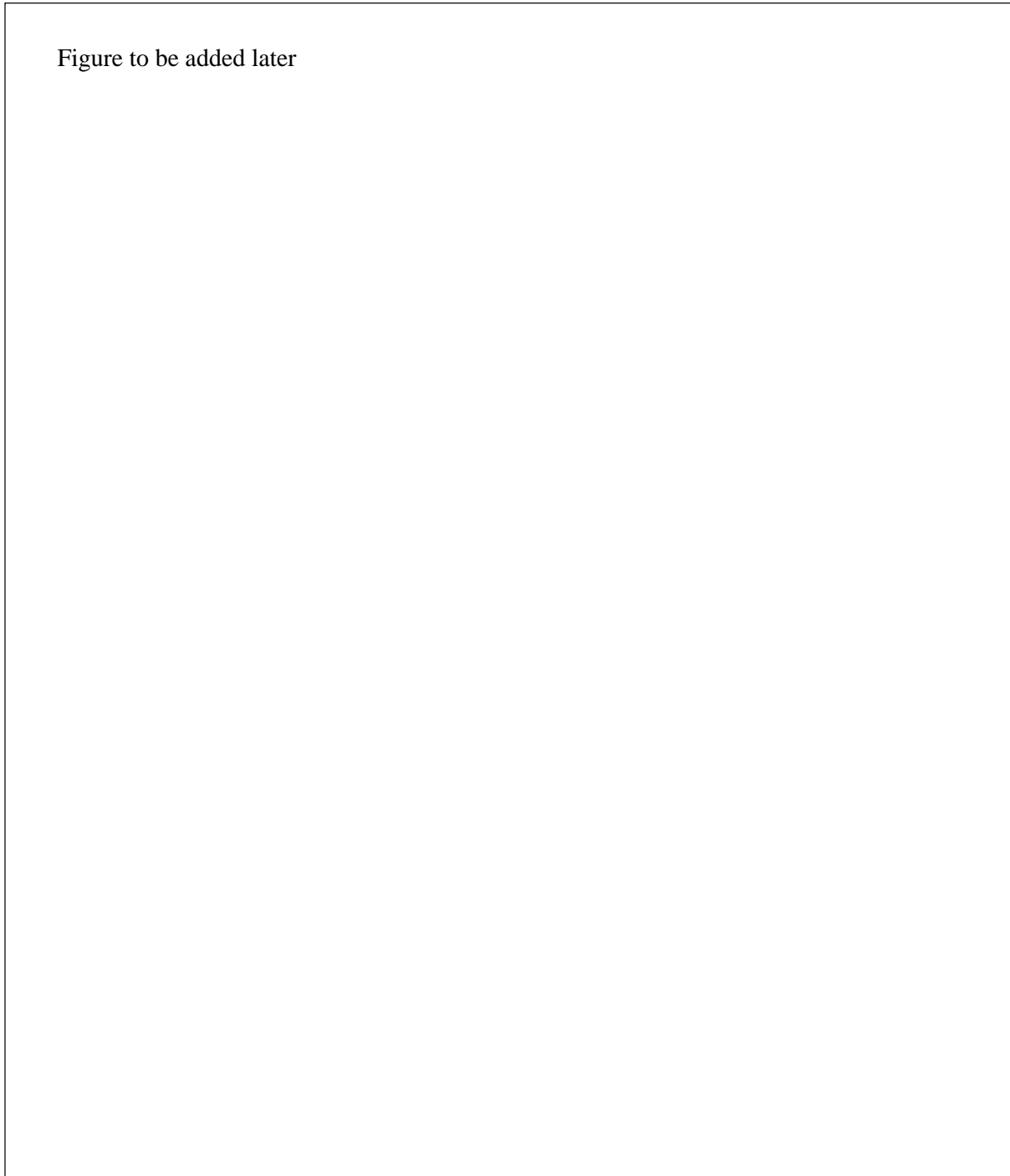


Figure 6.1: Electron trajectories in condensed matter at 3 levels of resolution, macroscopic, mesoscopic, and microscopic.

For electrons,

$$s^{e^-}(E) = s_c^{e^-}(E) + s_r^{e^-}(E) , \quad (6.2)$$

splitting the stopping power into a collisional part, due to Møller interactions,

$$s_c^{e^-}(E) = \int_0^{E/2} dE_\delta E_\delta \mu_\delta^{e^-}(E, E_\delta) , \quad (6.3)$$

and a radiative part, due to bremsstrahlung emission,

$$s_r^{e^-}(E) = \int_0^E dE_\gamma E_\gamma \mu_\gamma^{e^-}(E, E_\gamma) . \quad (6.4)$$

Note that the upper limit integral in Equation 6.3 stops at $E/2$. This is because the Møller interaction has two electrons in the final phase space. The δ -ray is defined as that having the lower energy.

Similarly, for positrons,

$$s_c^{e^+}(E) = \int_0^E dE_\delta E_\delta \mu_\delta^{e^+}(E, E_\delta) , \quad (6.5)$$

and a radiative part, due to bremsstrahlung emission,

$$s_r^{e^+}(E) = \int_0^E dE_\gamma E_\gamma \mu_\gamma^{e^+}(E, E_\gamma) . \quad (6.6)$$

Note that the total mass stopping power is in units E - L^2 - M^{-1} .

The idea of exploiting the total stopping power is as follows. Consider a small volume ΔV with an electron that enters, produces a δ -ray and a bremsstrahlung photon. Both these daughter particles escape ΔV in this example. (See Figure 6.2.) Now, consider a model that estimates the dose to ΔV by assuming that the daughter particles all “curl up” and deposit all their energy in ΔV . If the tracklength of the primary electron in ΔV is Δt , then, the energy deposited in this example is,

$$\Delta E = \int_0^{\Delta t} dt' \rho(\vec{x}, t') s(E(t')) ,$$

where we have explicitly accounted for the possibility that the stopping-power may change over the track of the particle, and the density of the material might have a spatial variation in ΔV . Also, this integral is a path integral over the path of the electron, which accounts for the possibility that electron paths are curved due to the underlying scattering processes.

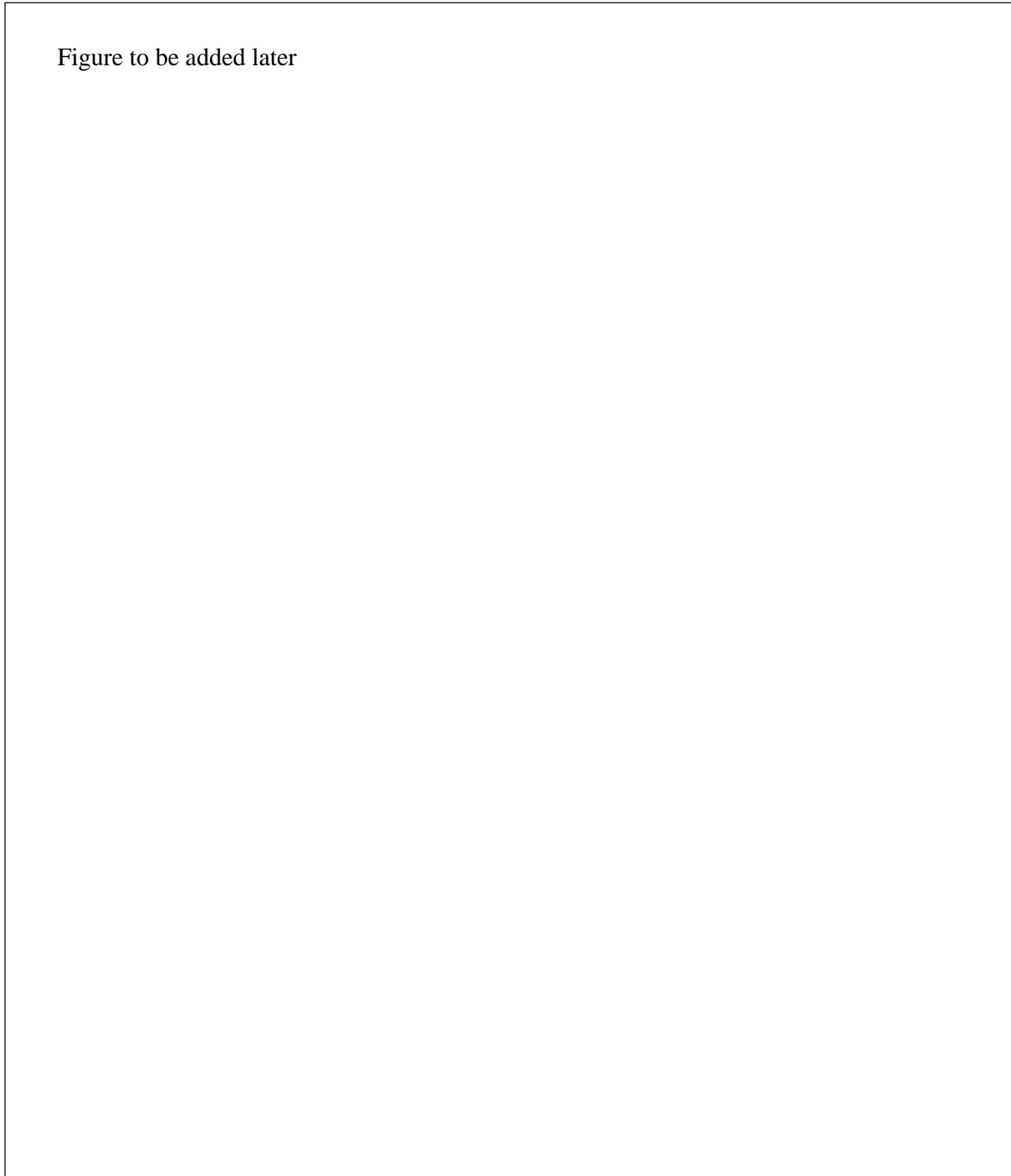


Figure 6.2: Various ways of computing the dose using total stopping power.

Therefore, the above equation is really a formal equation unless we provide some information about the underlying scattering processes.

However, in the limit as $\Delta V \rightarrow 0$, we note that,

$$\Delta E = \lim_{\Delta V \rightarrow 0} \int_0^{\Delta t} dt' \rho(\vec{x}, t') s(E(t')) = \Delta t \rho(\vec{x}) s(E) .$$

This permits us to write the dose, in this model, for a fluence, $\Phi_{e^-}^0(\vec{x}, E)$ of primary electrons,

$$D(\vec{x}) = \int_0^\infty dE \Phi_{e^-}^0(\vec{x}, E) s(E) . \quad (6.7)$$

The model expressed by Equation 6.7 tacitly assumes that all daughter particles “curl up” and deposit all their energy at the point \vec{x} . If there is a substantial radiative component, and that radiation component is not in equilibrium, we may wish to consider only the dose due to collisional processes,

$$D(\vec{x}) = \int_0^\infty dE \Phi_{e^-}^0(\vec{x}, E) s_c(E) . \quad (6.8)$$

Nonetheless, these are dose deposition models, with varying degrees of approximation.

There are similar models for positrons that extend the above in the obvious ways. Tables of electron and photon total mass collision stopping powers are available [ICR84], and employed for calculations.

6.2.2 Restricted mass stopping power

Appealing again to Figure 6.2, and considering the aforementioned models, we see that even high-energy δ -rays may escape the volume, ΔV . We may undo that approximation, but first we have to define the *restricted mass stopping power*, $l_{ell}(E, \Delta E_{e^-}, \Delta E_\gamma)$, both the collisional and radiative components, as follows.

For electrons,

$$l_{e^-}(E, \Delta E_{e^-}, \Delta E_\gamma) = l_c^{e^-}(E, \Delta E_{e^-}) + l_r^{e^-}(E, \Delta E_\gamma) , \quad (6.9)$$

splitting the restricted stopping power into a collisional part, due to Møller interactions,

$$l_c^{e^-}(E, \Delta E_{e^-}) = \int_0^{\min[E/2, \Delta E_{e^-}]} dE_\delta E_\delta \mu_\delta^{e^-}(E, E_\delta) , \quad (6.10)$$

and a radiative part, due to bremsstrahlung emission,

$$\ell_r^{e^-}(E, \Delta E_\gamma) = \int_0^{\Delta E_\gamma} dE_\gamma E_\gamma \mu_\gamma^{e^-}(E, E_\gamma) . \quad (6.11)$$

Note that the upper limit integral in Equation 6.3 stops at $E/2$. This is because the Møller interaction has two electrons in the final phase space. The δ -ray is defined as that having the lower energy.

Similarly, for positrons,

$$\ell_c^{e^+}(E, \Delta E_{e^-}) = \int_0^{\min[E/2, \Delta E_{e^-}]} dE_\delta E_\delta \mu_\delta^{e^+}(E, E_\delta) , \quad (6.12)$$

and a radiative part, due to bremsstrahlung emission,

$$\ell_r^{e^+}(E, \Delta E_\gamma) = \int_0^{\Delta E_\gamma} dE_\gamma E_\gamma \mu_\gamma^{e^+}(E, E_\gamma) . \quad (6.13)$$

Now, we have a more accurate model that estimates the dose to ΔV by assuming that only those daughter particles below the ΔE_{e^-} , ΔE_γ energy thresholds, “curl up” and deposit all their energy in ΔV . Those above the threshold are allowed to transport out of the volume, ΔV . If the tracklength of an electron in ΔV is Δt , then, the energy deposited in this example is,

$$\Delta E = \int_0^{\Delta t} dt' \rho(\vec{x}, t') \ell(E(t'), \Delta E_{e^-}, \Delta E_\gamma) ,$$

As before, we now shrink ΔV , permitting us to provide the dose at a point, in this model, to a fluence of electrons.

$$D(\vec{x}) = \int_0^\infty dE \Phi_{e^-}(\vec{x}, E) \ell(E, \Delta E_{e^-}, \Delta E_\gamma) . \quad (6.14)$$

Note that if an electron in the fluence spectrum has an energy below the cutoff values, total stopping powers should replace the restricted stopping powers in the above expression. Also, all electrons, not just primaries, are represented in the electron fluence.

The data required to tabulate $\ell(E, \Delta E_{e^-}, \Delta E_\gamma)$ is voluminous. Fortunately, there are computer programs available for this purpose [Ber92].

6.3 Electron angular scattering

As mentioned previously, electrons scatter into different directions predominantly from elastic Coulomb interactions with nuclei (Rutherford scattering), and, to a lesser extent, from

inelastic interactions with atomic electrons. The Coulomb interaction is long range, the cross sections are very large, and the deflection from each interaction is very small, except occasionally, an electron makes a close approach to a nucleus and the deflection can be very large. A relativistic electron can undergo as many as 10^5 elastic electron-nuclear interactions and 10^6 inelastic electron-electron interactions in the course of its entire trajectory.

Adding to this complication is the non-linear and coupled aspect of the electron-photon of the transport process. Electrons can set other electrons into motion, electrons can emit bremsstrahlung photons, and photons can set electrons into motion in a variety of ways.

Even if we ignored the non-linearity of the transport and transport the primary electron by modelling energy losses in using the total stopping power (this is called the CSDA, continuous slowing down approximation), a complete mathematical prescription, one with sufficient accuracy for radiotherapy and dosimetry, has not been found.

Therefore, in the following development, we describe, however briefly, Monte Carlo calculations. Only Monte Carlo calculations can provide the required accuracy, but do little to build our intuition on the behavior of particle fields, except by the laborious process of virtual experimentation. We do, however, introduce a simple analytic model that is too approximate for quantitative results, yet has enough physical content to permit semi-quantitative understanding, and intuitive fortification.

6.4 Dose due to electrons from primary photon interaction

Equation 6.14 provides a general form for energy deposition due to electrons. We now restrict the discussion to those electrons that arise from primary photon interactions.

We start with a fluence of primary photons on a surface S , $\Phi_0(\vec{x}_S, E_\gamma)$. We assume that the electron fluence arising from an interaction of the primary photon at \vec{x}' is given generically by a function of the form,

$$\Phi_e(\vec{x}, E_e; \vec{x}', E_\gamma) = f(E_\gamma, E_e, |\vec{x} - \vec{x}'|, \cos \theta_{\vec{x}', \vec{x} - \vec{x}'}), \quad (6.15)$$

in other words, a function of the distance from the interaction, the energy of the photon that set the electron into motion, and the angle between the initiating photon direction and vector from that point to \vec{x} ,

$$\cos \theta_{\vec{x}', \vec{x} - \vec{x}'} = \frac{\vec{x}' \cdot (\vec{x} - \vec{x}')}{|\vec{x}'| |\vec{x} - \vec{x}'|}$$

The number of a primary photons with energy E_γ starting at \vec{x}_S and interacting at \vec{x}' is,

$$n(\vec{x}', E_\gamma) d\vec{x}' dE_\gamma = \Phi_0(\vec{x}_S, E_\gamma) \rho(\vec{x}') \mu(E_\gamma) d\vec{x}' dE_\gamma \exp\left(-\int_0^{|\vec{x}'-\vec{x}_S|} dl \rho(\vec{l}) \mu(\vec{l}, E_\gamma)\right), \quad (6.16)$$

accounting for the attenuation via the radiological path, and an incident photon fluence that is differential in energy. Therefore,

$$D(\vec{x}) = \int d\vec{x}' \int_0^\infty dE_\gamma n(\vec{x}', E_\gamma) \int_0^\infty dE_e \Phi_e(\vec{x}, E_e; \vec{x}', E_\gamma) \ell(E, \Delta E_e, \Delta E_\gamma), \quad (6.17)$$

which also may be written,

$$D(\vec{x}) = \int d\vec{x}' \rho(\vec{x}') \int_0^\infty dE_\gamma K_c^0(\vec{x}', E_\gamma) \frac{1}{\langle E_e(E_\gamma) \rangle} \int_0^\infty dE_e \Phi_e(\vec{x}, E_e; \vec{x}', E_\gamma) \ell(E, \Delta E_e, \Delta E_\gamma), \quad (6.18)$$

where $\langle E_e(E_\gamma) \rangle$ is the mean energy deposited by an electron and its δ -rays set in motion by a photon with energy E_γ .

Energy conservation is thus implied, for in infinite media,

$$\frac{1}{\langle E_e(E_\gamma) \rangle} \int d\vec{x} \int_0^\infty dE_e \Phi_e(\vec{x}, E_e; \vec{x}', E_\gamma) \ell(E, \Delta E_e, \Delta E_\gamma) = 1. \quad (6.19)$$

We can also note, if we “curl up” the electrons by letting,

$$\Phi_e(\vec{x}, E_e; \vec{x}', E_\gamma) = \delta(\vec{x} - \vec{x}') \Phi_e(E_e; , E_\gamma),$$

we recover charged particle equilibrium, and Equation 6.18 collapses to,

$$D_{\text{CPE}}(\vec{x}) = \int_0^\infty dE_\gamma K_c^0(\vec{x}', E_\gamma) = K_c^0(\vec{x}). \quad (6.20)$$

6.4.1 A practical semi-analytic dose deposition model

The following model for electron transport is remarkable effective for describing electron transport, at least in a semi-quantitative way, when those electrons are set in motion by external photon fields.

- Energy loss is constant. The energy of an electron at any point in its trajectory is

$$E(t) = E_0 \left(1 - \frac{t}{R_e}\right), \quad (6.21)$$

where E_0 is the initial energy, R_e is its range, and t is the straight line distance from the point in space where the electron was set in motion.

- The angular distribution of is given either by the forward approximation,

$$\Phi_e(\vec{x}, E_e; \vec{x}', E_\gamma) = \frac{1}{4\pi} \Theta(z - z') \Theta(z - z' - R_e) \delta(E_e - \langle E_e(E_\gamma) \rangle) \delta(1 - \cos \theta'), \quad (6.22)$$

where θ is the polar angle with respect to the photon that set the electron in motion. Another more realistic approximation is the semi-isotropic approximation,

$$\Phi_e(\vec{x}, E_e; \vec{x}', E_\gamma) = \frac{1}{4\pi} \delta(E_e - \langle E_e(E_\gamma) \rangle) \Theta(|\vec{x} - \vec{x}'| \leq R_e) (1 + \omega \cos \theta'), \quad (6.23)$$

where ω is an anisotropy factor. When $\omega = 0$, the distribution is isotropic. As ω increases, the distribution gets more forward directed. The logical upper limit is $\omega = 1$, to prevent the angular distribution from becoming negative. The lower limit is $\omega = -1$, which describes a distribution that is directed backwards, a theoretical curiosity, but admitted by the mathematics.

Dose due to primary photons in the straight ahead approximation

Imagine a uniform broad beam source of monoenergetic photons, $E = E_\gamma$ impinging normally on a semi-infinite volume of water.

The dose in this model is obtained by substituting Equation 6.22 into eqnref6.4.0.5, to give,

$$D(z) = K_c^0(0) \left(\Theta(1 - x) \int_0^x + \Theta(x - 1) \int_{x-1}^x \right) dx' \exp(-\epsilon x'), \quad (6.24)$$

where $x = z/R_e$ and $\epsilon = \mu(E_0^\gamma) \rho R_e$.

The integrals are elementary, and results in,

$$\frac{D(z)}{K_c^0(z)} = \left(\Theta(1 - x) \frac{e^{\epsilon x} - 1}{\epsilon} + \Theta(x - 1) \frac{e^\epsilon - 1}{\epsilon} \right). \quad (6.25)$$

Note that the dose goes to zero at the surface in the build-up region, $\Theta(1 - x)$, and the ratio of dose to collision Kerma is a constant in the exponential tail region $\Theta(x - 1)$. In the limit $\epsilon = \mu(E_0^\gamma) \rho R_e \ll 1$, the usual physical situation, we may write.

$$\frac{D(z)}{K_c^0(z)} = \Theta(1-x)x \left(1 + \frac{\epsilon x}{2}\right) + \Theta(x-1) \left(1 + \frac{\epsilon}{2}\right), \quad (6.26)$$

The constant offset in the exponential tail is often interpreted (perhaps mistakenly) as an average drift factor, for, in the same spirit of approximation, we may write,

$$\left(1 + \frac{\epsilon}{2}\right) = \exp(\mu(E_0^\gamma)\rho\langle z_d \rangle), \quad (6.27)$$

identifying the drift as,

$$\langle z_d \rangle = \frac{R_e}{2},$$

in this model, as expected.

At least this model captures the concept of electron drift from an upstream interaction. However, the model is unrealistic, as a plot of the predicted curve would reveal. The build-up portion goes to zero at the surface and has a discontinuous slope at $z = R_e$, counter to the real situation. We shall try a more realistic model in the next section.

Dose due to primary photons in the semi-isotropic approximation

The dose in this model is obtained by substituting Equation 6.23 into Equation 6.18, to give,

$$\frac{D(z)}{K_c^0(z)} = \Theta(1-x)I_{<}(x) + \Theta(x-1)I_{>}, \quad (6.28)$$

where, after some analysis it can be shown for the exponential tail, that,

$$I_{>} = \frac{1}{2} \int_{-1}^1 dy (1 - \omega y) \left(\frac{1 - e^{-\epsilon y}}{\epsilon y} \right), \quad (6.29)$$

and, for the build-up region,

$$I_{<}(x) = I_{>} - \frac{1}{2} \int_x^1 dy (1 + \omega y) \left(\frac{e^{\epsilon y} - e^{\epsilon x}}{\epsilon y} \right), \quad (6.30)$$

expressed as integrals.

At the time of this writing, I have not found a non-integral form for $I_{<}(x)$, but I have for $I_{>}(x)$ ¹ Now, the results are more realistic. The surface dose is non-zero, and the slope continuous at $x = 1$, and the shape is more realistic.

However, the physics is further revealed by an expansion in small- ϵ expansion, which yields,

-

$$\frac{D(0)}{K(0)} = \frac{1}{2} \left[1 - \frac{\omega}{2} - \frac{\epsilon}{4} \left(1 - \frac{2}{3}\omega \right) \right] ,$$

In the case the $\omega = 1$, the dose at the surface is about half the Kerma, less a small portion for attenuation.

- The peak occurs slightly to the left of $x = 1$, at

$$x_{\max} = 1 - \frac{2\epsilon}{1 + \omega} ,$$

and the dose there is,

$$D(x_{\max}) = D(1) \left(1 + \frac{\epsilon^2}{1 + \omega} \right) .$$

- The longitudinal shift, owing to lesser attenuation upstream, in the fall-off region is,

$$\Delta x = \frac{w}{6} + \frac{\epsilon}{18} \left(1 - \frac{\omega^2}{4} \right) .$$

This identifies the average drift as

$$\langle z_d \rangle = \frac{\omega R_e}{6} .$$

¹

$$I_{>} = \frac{1}{\epsilon^2} \{ \epsilon Si(\epsilon) + \omega [sinh(\epsilon) - \epsilon] \} ,$$

where

$$Si(\epsilon) = \int_0^\epsilon du \frac{sinh(u)}{u} .$$

6.5 The convolution method

The convolution method derives its formal basis from Equation 6.18. The basic idea is to take the conditional electron kernel, $\Phi_e(\vec{x}, E_e; \vec{x}', E_\gamma)$, and rewrite it as follows,

$$\Phi_e(\vec{x}, E_e; \vec{x}', E_\gamma) = \Phi_e^0(\vec{x}, E_e; \vec{x}', E_\gamma) + \Phi_e^1(\vec{x}, E_e; \vec{x}', E_\gamma) , \quad (6.31)$$

where $\Phi_e^0()$ contains all the electrons and their δ -rays from the primary photon interaction, and $\Phi_e^1()$ that contains all other electrons, irrespective of origin, higher Compton scatter, and those set in motion by all generations of bremsstrahlung photons. The motivation for doing so is that these two fluences are very different. The first is tightly centered within an electron range of the primary interaction point. The second is highly diffuse, governed by the interaction length of the primary photons. These kernels can be calculated analytically or computed via Monte Carlo calculations.

Although the convolution method is approximately 20 years old, there is not much more sophistication to the method than looking up pre-computed tables of data. To my knowledge, there has been no practical exploitation of the very different natures of these kernels.

6.6 Monte Carlo methods

To be added later

Bibliography

- [Ber92] M. J. Berger. ESTAR, PSTAR and ASTAR: Computer Programs for Calculating Stopping-Power and Ranges for Electrons, Protons, and Helium Ions. *NIST Report NISTIR-4999 (Washington DC)*, 1992.
- [ICR84] ICRU. Stopping powers for electrons and positrons. ICRU Report 37, ICRU, Washington D.C., 1984.

Problems

1. A 50 MeV beam of photons with fluence rate $\dot{\Phi}_\gamma$ is incident normally on a thin slab of lead of thickness d . A 50 MeV beam of electrons with fluence rate $\dot{\Phi}_{e^-}$ is incident normally on the same slab. The incident photon fluence is 100 times that of the incident electron fluence. Assume that the slab is thin in the sense that any electrons that are generated in the slab have ranges that greatly exceed the slab thickness.
 - (a) Using reasonable approximations that you must justify, at least in words, estimate the dose rate in the slab due to the incident photons.
 - (b) Using reasonable approximations that you must justify, at least in words, estimate the dose rate in the slab due to the incident electrons.
 - (c) Using the results of the above, what thickness would the plate have to be so that the dose due to the incident electrons and photons is the same. Provide a numerical result. Was the thin slab approximation a good one?

Hints: The photon data can be found on page 553 of Attix. The electron data can be found on page 573 of Attix. (Use the CSDA range.) The density of lead is 11.33 gm/cm³.

2. A beam of monoenergetic electrons with an energy of 30 MeV and a fluence of 10000 electrons/cm²/s is normally incident on a lead foil of thickness 0.1 gm/cm². (See the tables in Attix for physical data. You are expected to provide numerical answers. The density of lead is 11.35 g/cm³.)
 - (a) What is the dose deposited in the foil in 1 minute?
 - (b) The foil is now 10 cm thick. What is the dose deposited in the foil in 1 minute?
 - (c) The foil is now 1 cm thick. What is the dose deposited in the foil in 1 minute? You must make some assumptions to calculate a numerical answer in this case. Assume that all the bremsstrahlung photons that are generated are generated at the front face of the foil, are forward directed and have energy 10 MeV.
 - (d) Without resorting to any approximations, qualitatively sketch the dose in the foil for thicknesses 0 to 100 cm.
3. Consider a beam of photons collimated to radius R , that is, $\sqrt{x^2 + y^2} \leq R$, impinging on a semi-infinite medium ($-\infty < x, y < \infty$, $0 \leq z < \infty$) characterized by $\frac{\mu}{\rho}(E)$ the mass attenuation constant for photons of energy E , $\frac{\mu_{en}}{\rho}(E)$ and $\rho(\vec{x})$.

In all the cases below, you will derive expressions for $D(\vec{x})$ where you must specify the full functional relationships on \vec{x} and E . In all cases, you must sketch the dose on the central axis $D_{\text{CAX}}(x, y, z) = D(0, 0, z)$ and two radial profiles $D(x, y, 0)$ and $D(x, y, z_1)$ where $z_1 \gg R_{e,\text{max}}$ and $R_{e,\text{max}}$ is the range of the maximum energy electron that can

exist in the problem. You may assume, in all cases, that cylindrical symmetry holds, that is, $D(\vec{x}) = D(\sqrt{x^2 + y^2}, z)$.

Approximation I

- The beam is monoenergetic at energy E_0
- The beam is normal to the surface
- The beam at the surface is in radiation equilibrium (RE) for $\sqrt{x^2 + y^2} \leq R$
- Use the K_c approximation for dose
- Include beam attenuation
- Ignore the dose deposited by scattered photons
- The medium is homogeneous

Justifying every part of your derivation, show that the solution in this case is...

$$D_{\text{I}}(\vec{x}) = E_0 \Phi_0 \exp \left[-\frac{\mu}{\rho}(E_0) \rho z \right] \left(\frac{\mu_{\text{en}}}{\rho}(E_0) \right) \Theta(R - \sqrt{x^2 + y^2}) \Theta(z)$$

where Φ_0 is the fluence of the beam at the surface. Note that the theta function $\Theta(u)$ is shorthand for $\Theta(u) = 1 \forall u \geq 0 \cap \Theta(u) = 0 \forall u < 0$, in other words, the step function.

(Don't forget to do the sketches!)

Approximation II

Case I, except that the medium is no longer uniform in space. Justifying every part of your derivation, show that the solution in this case is...

$$D_{\text{II}}(\vec{x}) = E_0 \Phi_0 \exp \left[-\int_0^z dz' \left(\frac{\mu}{\rho}(E_0) \right) \rho(x, y, z') \right] \left(\frac{\mu_{\text{en}}}{\rho}(E_0) \right) \Theta(R - \sqrt{x^2 + y^2}) \Theta(z)$$

In your plots, assume that there is a slab of different material centered at z_1 . Compare with the plots of Approximation I.

Approximation III

Case I, except that the fluence has an energy distribution. $\varphi(E)$, between 0 and E_0 . Justifying every part of your derivation, show that the solution in this case is...

$$D_{\text{III}}(\vec{x}) = \int_0^{E_0} dE E \varphi(E) \exp \left[-\frac{\mu}{\rho}(E) \rho z \right] \left(\frac{\mu_{\text{en}}}{\rho}(E) \right) \Theta(R - \sqrt{x^2 + y^2}) \Theta(z)$$

Compare your plots with those of Approximation I.

Approximation IV

Case I, except that the photons arise from an isotropically radiating point source located at $(0, 0, -L)$. Although the RE is now violated, the K_c approximation for

dose still makes sense if L is large enough. Answer the question, “Large enough compared to what?”

Compare your plots with those of Approximation I.

Approximation V

Case I, except you must now account for the dose that arises from the first scattered photon. Only the Compton interaction is to be considered.

Approximation VI

Case I, except now we relax the K_c approximation for dose. Assume that electrons with energy $\frac{1}{2}E_0$ are transported in the forward direction away from the interaction point. Assume that the stopping power is a constant.

Approximation VII

Case VI, except assume that the electrons are emitted isotropically.

Bonus!

This is optional and worth bonus points, although the extra marks will be very tough to get! Turn off as many approximations as you can. If you wish to consider electron transport in detail, you may assume that the electron fluence arising from an interaction at the origin directed along the z -axis has a form $f(\sqrt{x^2 + y^2}, z, E_\gamma, E)$, where E_γ is the energy of the photon that set it in motion and E is the electron’s energy at \vec{x} . Typically, $f()$ is calculated by detailed Monte Carlo calculations or measured. This technique forms the basis for the convolution/superposition dose calculation model that is the state-of-the art dose calculation technique presently. However, in a few years, this model will be replaced completely by *ab initio* Monte Carlo calculations.

4. A circular beam of monoenergetic photons is incident normally on a semi-infinite phantom of water, $z \geq 0$, $0 \leq \rho < \infty$. (Here, ρ is the radius in cylindrical coordinates.) The incident fluence is Φ_0 for $\rho \leq a$, $z < 0$, $\Phi_0 \exp(-\mu z)$ for $\rho \leq a$, $z \geq 0$, and zero elsewhere. Ignoring photon scattering but accounting for primary photon attenuation and electron scattering via the $1 + \omega \cos \Theta$ transport model, provide an analytic expression for $D(z, \rho, \phi)$ for $z \geq R_e$. In addition, sketch $K_c(z, \rho)/K_c(0, 0)$ and $D(z, \rho)/K_c(0, 0)$ at some depth $z > R_e$, for $a - R_e \leq \rho \leq a + R_e$.

Chapter 7

Ionization chamber-based air kerma standards

7.1 Bragg-Gray cavity theory

Imagine an interface formed by two materials, the one on the left $z < 0$ we will call (suggestively) material “w” and the one on the right $z > 0$, material “g”. We consider an electron transport model in the vicinity of the interface where energy losses are computed using total mass collision stopping powers. That is, δ -rays are not transported explicitly, but their energies are “rolled up” in the stopping powers. Now, imagine an electron beam that crosses the interface. Since electron fluence is conserved across the interface, we can say that,

$$\Phi_e^0(E_e, x, y, 0-) = \Phi_e^0(E_e, x, y, 0+) = \Phi_e^0(E_e, x, y, 0) , \quad (7.1)$$

$$D_w(x, y, 0-) = \int_0^\infty dE_e \Phi_e^0(x, y, 0) s_w(E_e) , \quad (7.2)$$

and,

$$D_g(x, y, 0+) = \int_0^\infty dE_e \Phi_e^0(x, y, 0) s_g(E_e) , \quad (7.3)$$

from which we can infer that,

$$\frac{D_g(x, y, 0+)}{D_w(x, y, 0-)} = (\bar{s})_w^g \quad (7.4)$$

where,

$$(\bar{s})_w^g \equiv \frac{\int_0^\infty dE_e \Phi_e^0(x, y, 0) s_g(E_e)}{\int_0^\infty dE_e \Phi_e^0(x, y, 0) s_w(E_e)} . \quad (7.5)$$

Now consider a volume of material “w” (wall material). We wish to measure the dose at some point \vec{x} in “w” by placing within it, a gas cavity “g” that has \vec{x} within its domain. Thus, under the following assumptions:

BG-1 the size of the gas layer is so small that in any dimension it is smaller than R_e^w , the electron range in the “w” material,

BG-2 the dose in the cavity is assumed to be deposited entirely by electrons crossing it, photon interactions in the cavity may be ignored,

then,

$$D_w(\vec{x}) = D_g(\vec{x})(\bar{s})_g^w . \quad (7.6)$$

That is, we can determine the dose to the wall material from a measurement of the dose to the gas.

Note that under conditions of charged particle equilibrium, but with the proviso that the atomic composition of the gas and wall material are the same, **BG-1** may be relaxed, and the cavity allowed to assume any shape and size.

Under these conditions, we may also write,

$$K_c^w(\vec{x}) = K_c^g(\vec{x})(\bar{s})_g^w . \quad (7.7)$$

7.1.1 Exposure measurements

Often, ionization chamber measurements are made in terms of exposure. Dose and “exposure” are related by the following relation,

$$D_g = \left(\frac{\Delta Q}{\Delta m} \right) \left(\frac{\overline{W}}{e} \right)_g , \quad (7.8)$$

where, ΔQ is the charge of the ions of one sign collected (assuming complete collection) from the “active volume” of the gas during irradiation, Δm is the mass of the “active volume” of the gas, and $\left(\frac{\overline{W}}{e} \right)_g$ is the average energy deposited in the gas divided by the charge of one of

the ion pairs, per ion pair created. The concept of “active volume” just means that volume of the gas for which electric field lines can sweep ions toward the electrodes. There may be “guard” volumes or inactive volumes that still logically comprise the cavity volume, but do not participate in sweeping the ions toward the electrodes.

Therefore, assuming an exposure measurement has been made, we may write,

$$D_w = \left(\frac{\Delta Q}{\Delta m} \right) \left(\frac{\overline{W}}{e} \right)_g (\overline{s})_g^w . \quad (7.9)$$

Corollary 1: Same wall, different gases

Consider two exposure measurements involving the same instrument involving the same source of radiation, but one in which the gas may be substituted. It can be shown, from Equation 7.9, that,

$$\frac{\Delta Q_2}{\Delta Q_1} = \left(\frac{\rho_2}{\rho_1} \right) \frac{(\overline{W}/e)_1}{(\overline{W}/e)_2} (\overline{s})_{g_1}^{g_2} . \quad (7.10)$$

It appears that the wall material has vanished from the above equation! However, it is still there, represented by the electron fluence within it, in the stopping power ratio. That the fluence is not perturbed by the gas cavity bears some emphasis here.

Corollary 2: Different walls, same gases

Consider two exposure measurements involving the similar instruments involving the same source of radiation, but one in which the wall material may be substituted, and the gas, while remaining the same, may occupy a different volume. To start, imagine that the cavity region is filled with wall material. Under conditions of charged particle equilibrium, we note that the dose to any point in this location is,

$$D_w^{\text{CPE}} = K_c = \int_0^\infty dE_\gamma \Psi(E_\gamma) \mu_{\text{en}}(E_\gamma) , \quad (7.11)$$

or,

$$D_w^{\text{CPE}} = \Psi \overline{\mu}_{\text{en}} , \quad (7.12)$$

where,

$$\Psi = \int_0^\infty dE_\gamma \Psi(E_\gamma) , \quad (7.13)$$

and,

$$\bar{\mu}_{\text{en}} = \frac{1}{\Psi} \int_0^\infty dE_\gamma \Psi(E_\gamma) \mu_{\text{en}}(E_\gamma) . , \quad (7.14)$$

Therefore,

$$\frac{D_{w_2}}{D_{w_1}} = (\bar{\mu}_{\text{en}})_{w_1}^{w_2} , \quad (7.15)$$

where,

$$(\bar{\mu}_{\text{en}})_{w_1}^{w_2} = \frac{\int_0^\infty dE_\gamma \Psi(E_\gamma) \mu_{\text{en}}^{w_2}(E_\gamma)}{\int_0^\infty dE_\gamma \Psi(E_\gamma) \mu_{\text{en}}^{w_1}(E_\gamma)} , \quad (7.16)$$

from which it can be shown, from Equation 7.9, that,

$$\frac{\Delta Q_2}{\Delta Q_1} = \left(\frac{\Delta V_2}{\Delta V_1} \right) (\bar{\mu}_{\text{en}})_{w_1}^{w_2} (\bar{s})_{w_2}^{w_1} . \quad (7.17)$$

It appears that the gas material has vanished from the above equation, except for the volume they occupy. This is an interesting consequence of radiation equilibrium.

7.2 Spencer-Attix cavity theory

The substantial improvement Spencer and Attix made to Bragg-Gray cavity theory was to employ restricted stopping powers, assuming that the high-energy δ -ray fluence spectrum might be sensitive to atomic differences at the interface. Therefore, the foregoing discussion may be modified straightforwardly by employing restricted stopping powers.

Ignoring the contribution of bremsstrahlung to the stopping power, the dose may be calculated from

$$D = \int_0^\infty dE \Phi_e(E) \ell_c(E, \Delta) , \quad (7.18)$$

where Δ is the energy above which electrons can be set in motion and contribute to the electron fluence spectrum, $\Phi_{e^-}(E)$. The choice of Δ is an interesting one. General practice is to set Δ to an energy that corresponds to an electron range, $R_e(\Delta)$, in the gas material that is characteristic of the size of the cavity. To my knowledge, this parameter has not been effectively tested over a range of materials and parameter-size selections.

Direct analytic calculations of Equation 7.18 are problematic, as there is no sufficiently accurate theory to predict $\Phi_e(E)$. However, as we shall soon see in “Modern Cavity Theory” that analytic calculations still have an important role to play.

7.3 Modern cavity theory

Radiation equilibrium is a mathematical fiction, yet, it is closely approximated by thick-walled ionization chambers. In this section we develop modern cavity theory and demonstrate the important role of radiation equilibrium conditions and the role of Fano’s theorem.

Consider a volume of gas material in which there exists an electron fluence of any character. The dose to that gas, obtained by integrating over the energy deposited in the gas, and dividing by it’s mass, may be written as

$$D_g = \frac{1}{V_g} \int dE_e \int d\vec{x} \varphi_g(E_e, \vec{x}) R_g(E_e, \vec{x}) , \quad (7.19)$$

where V_g is the volume of the gas, $\varphi_g(E_e, \vec{x})$ is the electron fluence arising from all sources, and $R_g(E_e, \vec{x})$ is a response function of the gas, that has units $EL2/M$. We keep the discussion general for now, but have in mind to use restricted stopping powers later on. Henceforth, we will employ a compact notation for the above,

$$D_g = \int \varphi_g R_g . \quad (7.20)$$

We would like to transform Equation 7.19 into a form that exhibits radiation equilibrium explicitly. It will take many steps to get there.

First, split the electron fluence into that which arises from the primary interaction of a photon, including all δ -rays. Bremsstrahlung and annihilation photons are considered, but if they produce an electron fluence in the cavity, that fluence goes into the “scattered” part. Therefore, we write, $\varphi_g = \varphi_g^0 + \varphi_g^s$, and we rewrite the dose as,

$$D_g = \left(\int \varphi_g^0 R_g \right) A_{\text{scat}} , \quad (7.21)$$

where

$$A_{\text{scat}} = \frac{1 + \left(\int \varphi_g^s R_g \right)}{\int \varphi_g^0 R_g} . \quad (7.22)$$

A_{scat} is usually close to unity, for most ionization chambers, since the scattered radiation that results in ionization in the chamber is usually overwhelmed by the primary ionization.

Now the strategy is revealed. We will keep simplifying the electron fluence until we get it into equilibrium, and produce correction factors that are close to unity (we hope) and amenable to analytic or Monte Carlo calculations.

The primary photon fluence is not yet in equilibrium, since it is attenuating across the chamber. Therefore, assume that we can undo this contribution to disequilibrium, thereby producing a primary electron fluence that arises from unattenuated primary photons. We call this fluence, $\tilde{\varphi}_g^0$ and rewrite Equation 7.21 as,

$$D_g = \left(\int \tilde{\varphi}_g^0 R_g \right) A_{\text{scat}} A_{\text{att}} , \quad (7.23)$$

where

$$A_{\text{att}} = \frac{\int \varphi_g^0 R_g}{\int \tilde{\varphi}_g^0 R_g} . \quad (7.24)$$

As, A_{scat} is close to, but greater than unity, A_{att} is close to, but less than unity. To some extent they undo each other, as the action of attenuation usually leads to scattered radiation.

We still have not completely undone primary photon equilibrium, because the photon fluence arises from a geometric source, usually a near-point source, distance from the chamber. Nonetheless, $1/r^2$ -effects and other geometric effects must be undone. We determine the photon fluence at the center of the chamber (one may use the center-of-mass to define this) and call this the *point of measurement*. The source can then be converted into a broad parallel beam with the same energy spectrum. Now we rename the electron fluence obtained in this way, $\tilde{\varphi}_g^{0,\parallel}$, and rewrite as,

$$D_g = \left(\int \tilde{\varphi}_g^{0,\parallel} R_g \right) A_{\text{scat}} A_{\text{att}} A_{\text{pn}} , \quad (7.25)$$

where

$$A_{\text{pn}} = \frac{\int \varphi_g^0 R_g}{\int \tilde{\varphi}_g^{0,\parallel} R_g} . \quad (7.26)$$

A typical source configuration for a standards measurement is a small radioactive source about 1 cm across at a distance of 100 cm. So, this correction is near unity as well.

Now, the primary photon fluence that set the electrons in motion is in, however, the electron fluence is not. Imagine that we have wall material in the place of the cavity, and we employ that fluence, but with the gas response function. That permits a rewrite of Equation 7.25 as,

$$D_g = \left(\int \tilde{\varphi}_w^{0,\parallel} R_g \right) A_{\text{scat}} A_{\text{att}} A_{\text{pn}} A_{\text{fl}} , \quad (7.27)$$

where

$$A_{\text{fl}} = \frac{\int \tilde{\varphi}_{\text{g}}^0 R_{\text{g}}}{\int \tilde{\varphi}_{\text{w}}^{0,\parallel} R_{\text{g}}} . \quad (7.28)$$

A_{fl} is a correction that accounts for the perturbation of the electron fluence by the gas cavity. If the atomic composition of the gas and the wall is not too dissimilar, this is expected to be a small effect.

We may also rewrite Equation 7.27 to be,

$$D_{\text{g}} = \left(\int \tilde{\varphi}_{\text{w}}^{0,\parallel} R_{\text{w}} \right) A_{\text{scat}} A_{\text{att}} A_{\text{pn}} A_{\text{fl}} (\bar{s})_{\text{w}}^{\text{g}} , \quad (7.29)$$

where

$$(\bar{s})_{\text{w}}^{\text{g}} = \frac{\int \tilde{\varphi}_{\text{g}}^0 R_{\text{g}}}{\int \tilde{\varphi}_{\text{w}}^{0,\parallel} R_{\text{w}}} . \quad (7.30)$$

Here we identify $(\bar{s})_{\text{w}}^{\text{g}}$ as a generalized “stopping power” ratio. We can also identify the first term in Equation 7.29 as the dose to the wall material due to primary photons in a state of complete radiation equilibrium. Thus, Equation 7.29 can also be expressed as,

$$D_{\text{g}} = \Psi^{0,\parallel} (\bar{\mu}_{\text{en}})_{\text{w}} (\bar{s})_{\text{w}}^{\text{g}} A_{\text{scat}} A_{\text{att}} A_{\text{pn}} A_{\text{fl}} , \quad (7.31)$$

where,

$$(\bar{\mu}_{\text{en}})_{\text{w}} = \frac{1}{\Psi^{0,\parallel}} \int_0^{\infty} dE_{\gamma} \Psi^{0,\parallel}(E_{\gamma}) \mu_{\text{en}}(E_{\gamma}) . \quad (7.32)$$

Finally, we may rewrite Equation 7.32 as, or equivalently,

$$D_{\text{g}} = K_{\text{c}}^{0,\parallel} (\bar{\mu}_{\text{en}})_{\text{q}}^{\text{w}} (\bar{s})_{\text{w}}^{\text{g}} A_{\text{scat}} A_{\text{att}} A_{\text{pn}} A_{\text{fl}} , \quad (7.33)$$

which related a real measurement of dose to the gas to it’s collision Kerma under conditions of radiation equilibrium. The connection between the two is really a ratio of factors quite close to unity.

7.4 Interface effects

To be written later

7.5 Saturation corrections

To be written later

7.6 Burlin cavity theory

To be written later

7.7 The dosimetry chain

We start with Equation 7.33, but expressed as a charge measurement of the primary standard instrument in a Standards Laboratory. That is,

$$\left(\frac{\Delta Q}{\Delta m}\right) \left(\frac{\overline{W}}{e}\right)_g = D_g = K_{c,g}^{0,||} (\overline{\mu}_{en})_q^w (\overline{s})_w^g (\prod A)_S, \quad (7.34)$$

where $(\prod A)$ is the product of all the “A” correction factors.

We can can rewrite the above as,

$$K_{c,g}^{0,||} = \frac{\left(\frac{\Delta Q_S}{\Delta m_S}\right) \left(\frac{\overline{W}}{e}\right)_g}{(\overline{\mu}_{en})_g^w (\overline{s})_w^q (\prod A)_S}. \quad (7.35)$$

All the factors on the right hand side are known accurately by the Standards Laboratory, and thus, an internal calibration of the primary chamber provides a measurement of the primary Kerma at the Standard Laboratory.

Now, consider a client’s chamber, subject to a charge measurement in the standard field of the Standards Laboratory, namely,

$$\left(\frac{\Delta Q}{\Delta m}\right)_C \left(\frac{\overline{W}}{e}\right)_g = K_{c,g}^{0,||} (\overline{\mu}_{en})_g^w (\overline{s})_w^g (\prod A)_C, \quad (7.36)$$

This, taken in ratio with a similar measurement of the standard chamber yields,

$$\Delta m_C = \Delta m_S (\Delta Q)_S^C (\overline{\mu}_{en})_{w_C}^{w_S} (\overline{s})_{w_S}^{w_C} (\prod A)_C^S. \quad (7.37)$$

All quantities on the right hand side are measured or calculable. Therefore, the measurement in the Standards Laboratory is tantamount to measuring the active mass of gas in the client’s chamber.

Once the client receives their chamber, they wish to determine the dose to the air cavity of an ion chamber in their beam. Thus, they measure,

$$D_g = \left(\frac{\Delta Q}{\Delta m} \right)_H \left(\frac{\overline{W}}{e} \right)_g, \quad (7.38)$$

back in, for example, their hospital setting. The only unknown in Equation 7.38 is the mass of the gas in their standard chamber, and this is provided by the calibration from the Standards Laboratory. How one goes from dose in the gas to the dose to the medium in the client's laboratory is the subject of various dosimetry protocols which will not be compared here. However, before concluding, it is worthy to note how robust the calibration is. All the factors on the right hand side of Equation 7.37 are very well known, typically to less than several 10'ths of a percent.

Bibliography

Problems

1. Discuss the essential differences among the Bragg-Gray, Spencer-Attix and Burlin cavity theories. Is Spencer-Attix theory an improvement over Bragg-Gray? When should Burlin cavity theory be employed.
2. Two thick-walled cavity chambers, identical in all respects except for the wall material (Lead in one case, Aluminum in the other) are placed in a spatially uniform, monoenergetic 1 MeV photon beam.

Assume that the irradiation conditions are such that you may consider there to exist a state of charged-particle equilibrium (CPE) in the chambers. Two measurements are performed and the dose to the sensitive material is measured for both chambers. What range of values should you expect for a measurement of the ratio of the dose to the sensitive material in the Lead chamber to the dose to the sensitive material in the Aluminum chamber?

You may assume that the charged particle spectrum in the sensitive material is comprised of monoenergetic 500 keV electrons.

3. The ratio of ionization collected in an air gas cavity ionization chamber is $Q_1/Q_2 = 0.95$, for $V_1 = 100$ Volts and $V_2 = 200$ Volts when subject to continuous ionizing radiation.
 - (a) Assuming you know that the chamber is in the "initial" or "columnar" recombination regime between 100 and 200 Volts, what is the recombination correction at 100 and 200 Volts, assuming the ionization in the chamber is nearly all collected?
 - (b) Assuming you know that the chamber is in the "general" or "volume" recombination regime between 100 and 200 Volts, what is the recombination correction at 100 and 200 Volts, assuming the ionization in the chamber is nearly all collected?
 - (c) What if you do not know the saturation characteristics of this chamber between 100 and 200 Volts. How should you proceed?
4. The following expressions were derived for the dose to the sensitive material of a cavity type detector.

$$\begin{aligned}
 D_g &= \frac{1}{V_g} \int dE_e \int d\vec{x} \varphi_g(E_\gamma, S_\gamma, E_e, \vec{x}) R_g(E_e, \vec{x}) \\
 &= \int \varphi_g R_g \quad (\text{compact notational form}) \\
 &= \left(\int \tilde{\varphi}_w^{0,\parallel} R_w \right) \bar{R}_w^g A_{\text{scat}} A_{\text{att}} A_{\text{fl}} A_{\text{an}} \\
 &= K_{c,g} \left(\frac{\bar{L}}{\rho} \right)_g^w \bar{R}_w^g A_{\text{scat}} A_{\text{att}} A_{\text{fl}} A_{\text{an}}
 \end{aligned}$$

- (a) Explain what every symbol in the above equations means, including the domains of the integrations.
- (b) Using the compact notational form, what are the expressions in terms of ratios of integrals for

$$\left(\frac{\bar{\mu}}{\rho}\right)_g^w, \bar{R}_w^g, A_{\text{scat}}, A_{\text{att}}, A_{\text{fl}}, A_{\text{an}}$$

- (c) Under what approximations do the above equations reproduce Bragg-Gray and Spencer-Attix theories?